Katholieke Universiteit Leuven
Faculteit Bio-ingenieurswetenschappen
Departement Aard- en Omgevingswetenschappen
Afdeling Bodem- en Waterbeheer

DISSERTATIONES DE AGRICULTURA

Doctoraatsproefschrift nr. 861 aan de Faculteit Bio-ingenieurswetenschappen van de K.U. Leuven

MODELLING WATER EXCHANGE IN THE HYPORHEIC ZONE BETWEEN RIVER AND AQUIFER BY LABORATORY EXPERIMENT AND NUMERICAL SIMULATIONS



Proefschrift voorgedragen tot het behalen van de graad van Doctor in de Bio-ingenieurswetenschappen
door

Po-Yi CHOU

September 2009

Doctoraatsproefschrift nr. 861 aan de Faculteit Bio-ingenieurswetenschappen van de K.U. Leuven

ISBN: 978-90-8826-113-8
Wettelijk depot: D/2009/11.109/29

Research funded by a PhD scholarship from the Ministry of Education (Taiwan)

Katholieke Universiteit Leuven
Faculteit Bio-ingenieurswetenschappen
Departement Aard- en Omgevingswetenschappen
Afdeling Bodem- en Waterbeheer

DISSERTATIONES DE AGRICULTURA

Doctoraatsproefschrift nr. 861 aan de Faculteit Bio-ingenieurswetenschappen van de K.U. Leuven

MODELLING WATER EXCHANGE IN THE HYPORHEIC ZONE BETWEEN RIVER AND AQUIFER BY LABORATORY EXPERIMENT AND NUMERICAL SIMULATIONS

Promotor:
Prof. dr. ir. Guido Wyseure, K.U. Leuven

Proefschrift voorgedragen tot het behalen van de graad van Doctor in de Bio-ingenieurswetenschappen

door

Po-Yi CHOU

Leden van de examencommissie:
Prof. dr. Martin Hermy, voorzitter
Prof. dr. ir. Jan Diels, K.U. Leuven
Prof. dr. Okke Batelaan, K.U. Leuven
Prof. dr. ir. Marnik Vanclooster, Université catholique de Louvain
Dr. ir. Serge Brouyère, Université de Liège

September 2009

Acknowledgments

I would like to express my personal gratitude to many of you who made the completion of this Ph.D. thesis possible.

First and foremost, my deepest gratitude goes to my promotor, Prof. Guido Wyseure, for his untiring energy to offer guidance and critical comments throughout every stage of the research. I am also grateful for his invaluable encouragement and moral support during the whole period of my studies at the Katholieke Universiteit Leuven.

I would like to express my sincere appreciation to Prof. Jan Diels, Prof. Okke Batelaan, Prof. Marnik Vanclooster (Université catholique de Louvain) and Dr. Serge Brouyère (Université de Liège), for their careful reading and insightful comments to improve the manuscript. My gratitude also goes to Prof. Martin Hermy for accepting to be the chairman of the examination committee.

My gratitude is due to Prof. Jan Feyen, Prof. Seppe Deckers, Prof. Dirk Raes, and Prof. Jan Vanderborght in Division Soil and Water Management, K.U.Leuven, for their encouragements during my studies. Great thanks are due to Mr. Rik Deliever, Mr. René Goeman and especially Mr. Valentijn Tuts, for their professional technical assistance in completing the work of laboratory experiment. I am also grateful to Mrs. Greta Camps, Mrs. Sofie Bruneel and Mrs. Katty Giddelo for their secretarial and administrative assistance.

I would like to thank Prof. Jiang Du-Hsin (retired from Feng China University), Prof. Ting Cheh-Shyh (Pingtung University of Science and Technology), Prof. M.A. Mojid (Bangladesh Agricultural University), Prof. Clyde Munster (Texas A&M University), Dr. Joseph Hsu (Science and Technology Division, Taiwan Representative Office in Belgium) for kindly sharing their experiences and wisdom with me. A special expression of gratitude is due to Mrs. Katrien Lammertyn for her endless patience in reading and correcting the manuscripts before submitting to a journal.

My sincere thanks go to my colleagues and friends in Division Soil and Water Management: Bruno Verbist, Sam Geerts, Lê Anh Tuấn (now at CanTho University, Vietnam), Hamed Rouhani (now at Gorgan University, Iran), Arnoud Cuppens, Bartel Van Nieuwenhuyse, Koen Van Overtveld, Ali Erfani Agah, Theddious Mhizha, and so on for all the emotional and spiritual support they provided.

I greatly appreciate the Ministry of Education (Taiwan) and the Cultural Division of Taiwan Representative Office in Belgium for the financial support in the form of a scholarship during my PhD research in Belgium.

Chou, Po-Yi

謝辭

論文付梓，是理想的實現，也是成果的試煉；是現階段任務的結束，也是下一階段挑戰的開始。

感謝本論文指導教授與審議委員在研究過程中的指導，包括實驗理論和模型的修正、資料分析和結果的批判、數值模擬與驗證的建議，以及許許多多寶貴經驗的分享。感謝系上專業技術人員與秘書在學業期間的幫助，讓實驗器材的架構與操作得以在所需的條件下進行；也感謝研究所的同事與學長在我求學期間的幫助，讓數據分析與論文撰寫更加順利與完整。更感謝過去任職單位的長官所給予的訓練，以及許多教授與專家的指教。

感謝在歐洲求學期間許多旅歐前輩與學長姐的關心，也感謝許多共同在歐洲留學打拼的朋友們在生活與心靈上的扶持。有幸在人生這個階段相遇，分享喜樂與哀愁。比利時漫長的五年，感謝你在我遇到瓶頸的時候提供不同的對策，感謝妳在我失去方向的時候指引可能的路徑，感謝你在我幾乎放棄的時候推我一把，感謝妳在我意志力薄弱的時候給我希望。不論你(妳)來自哪裡，不論你(妳)現在在哪裡，我都要謝謝你(妳) 。

感謝來自台灣教育部與台灣駐歐盟代表處文化組在求學期間所提供的獎助學金之鼓勵，減輕了我在歐洲生活的負擔。

感謝父母，謝謝你們這幾年的體諒與支持，以及無盡的付出；

感謝外婆，謝謝您的期許與耐心等待；

感謝我所有的家人，你們的鼓勵是我決定堅持下去的力量。

周柏儀

Content

Acknowledgments i
Content v
List of Figures vii
List of Tables x
Summary xi
Notation xiii
Chapter 1
Introduction 1
1.1 Preface 1
1.2 Research objectives 2
1.3 Research outline of the study 3
Chapter 2
Hydrological Perspective of Hyporheic Zone: A Review 5
2.1 Definition of hyporheic zone: linkage, exchange and continuum 6
2.2 Significant characteristics of hyporheic zone 8
2.2.1 Ecological contribution 8
2.2.2 Nutrient dynamics and pollutants attenuation 9
2.2.3 Stable thermal regime 9
2.3 Hydrological perspectives and integration 10
2.3.1 A river-centric perspective 10
2.3.2 The conceptual model 11
2.3.3 Conceptual integration with aquifer derived information 13
2.4 Using heat as a tracer for estimating groundwater flow 14
Chapter 3
Hydrodynamic Dispersion Characteristics of Lateral Inflow into a River tested by a Laboratory Model 17
3.1 Introduction 18
3.2 Theory 20
3.3 Material and methodology 23
3.3.1 Experiment setup 23
3.3.2 Pulse-response experiments 25
3.3.3 Data analysis 26
3.3.4 Testing by HYDRUS 2D/3D 26
3.4 Results and discussion 28
3.4.1 Measured and estimated breakthrough data 28
3.4.2 Solute transport parameters by fitting the transfer function on segments 30
3.4.3 Numerical simulation by HYDRUS 2D/3D 35

3.5 Conclusions and recommendations 39
Chapter 4
Can temperature be used as a tracer to estimate fluctuating water fluxes in the riverbed? A laboratory study 41
4.1 Introduction 42
4.2 Theory 44
4.3 Material and methodology 47
4.3.1 Determination of saturated thermal conductivity 47
4.3.2 Experimental setup 48
4.3.3 Simultaneous river-stage and temperature change experiment 49
4.3.4 Application of the numerical model HYDRUS 2D/3D 51
4.4 Results and discussion 51
4.5 Conclusions and recommendation 60
Chapter 5
Numerical simulation by HYDRUS 2D/3D of long- and short-term groundwater flux in the hyporheic zone as influenced by temperature regimes and changing river stage 63
5.1 Introduction 64
5.2 Methodology 65
5.2.1 Numerical model 65
5.2.2 Analytical solution for steady-state heat transfer 66
5.2.3 Numerical modelling approach: HYDRUS 2D/3D 68
5.2.4 Scenarios 69
5.3 Results and discussion 70
5.3.1 The evaluation of thermal regimes under steady state upward water flow 70
5.3.2 The temperature-based estimates of steady groundwater flux 72
5.3.3 The temperature-based estimates of transient penetration of river water 77
5.4 Conclusions and recommendations 82
Chapter 6
Conclusions and Recommendations for Future Research 85
6.1 General conclusions 85
6.2 Recommendations for the future research 90
References 93
Appendix 1: The transfer-function method (Mojid *et al.*, 2004) 105
Appendix 2: R-code used for BTC analysis 107
Appendix 3: Results of the pulse-response BTCs fitting 111
Publications list by Chou Po-Yi (2006-2009) 113

List of Figures

Figure 1 - 1: Dissertation outline 4
Figure 2 - 1: The schematic illustration of hyporheic zone 6
Figure 2 - 2: The schematic representation of hyporheic exchange flows and the associated environmental gradients between river and aquifer 7
Figure 2 - 3: A conceptual diagram of the Transient Storage Model (after Runkel, 1998) 11
Figure 3 - 1: Experimental set-up of J-shaped model 24
Figure 3 - 2: Example of fitting between the measured and estimated response curves in segment 4 from probe No. 4 to 5 in the flux of 0.5cm/hr..... 28
Figure 3 - 3: Average water content (θ_v) along the center of the model in different fluxes..... 30
Figure 3 - 4: Pore-water velocity along the center of the model in different fluxes..... 31
Figure 3 - 5: Dispersivity (λ) as a function of volumetric water content (θ_v)..... 32
Figure 3 - 6: Dispersivity (λ) variation as a function of pore water velocity (V)..... 33
Figure 3 - 7: Log-log relationships between solute dispersion coefficient (D) and ratio of pore water velocity to water content (V/θ_v); two outliers (*) are not included into relation 34
Figure 3 - 8: Comparison of the measured relative EC (open circles) with the simulated results from inverse modelling (full line) ($r^2 = 0.68$) and directly using the equation for dispersion coefficient based on segments (dash line) ($r^2 = 0.72$) in flux of 0.5cm/hr..... 37
Figure 3 - 9: Comparison of the measured relative EC (open circles) with the simulated results from inverse modelling (full line) ($r^2 = 0.86$) and directly using the equation for dispersion coefficient based on segments (dash line) ($r^2 = 0.72$) in flux of 1.0cm/hr..... 37
Figure 3 - 10: Comparison of the measured relative EC (open circles) with the simulated results from inverse modelling (full line) ($r^2 = 0.66$) and directly using the equation for dispersion coefficient based on segments (dash line) ($r^2 = 0.72$) in flux of 1.5cm/hr..... 38
Figure 3 - 11: Comparison of the measured relative EC (open circles) with the simulated results from inverse modelling (full line) ($r^2 = 0.44$) and directly using the equation for dispersion coefficient based on segments (dash line) ($r^2 = 0.50$) in flux of 2.0cm/hr..... 38
Figure 4 - 1: Schematic experimental setup of J-shaped column model and location of the thermocouples..... 48
Figure 4 - 2: The measured temperature profile for a steady-state inflow of 1 cm/hr and a square shape hydrograph with a 15cm river-stage rise 50

Figure 4 - 3: The graphical output of water velocity (in cm/hr) and flow directions (arrows) in the J-shaped model at (a) t = 0 minutes, (b) t = 10 minutes, (c) t = 20 minutes, (d) t = 30 minutes, (e) t = 40 minutes and (f) t = 50 minutes after the rising of river stage as simulated by HYDRUS. Illustration shows the case of 1.5 cm/hr steady-state groundwater inflow on the left and 15cm water level rising on the right. The dark zone on the right represents the penetration of river water, which is generated by the trajectories of flowing particles 52
Figure 4 - 4: Comparison of measured temperature and direct simulation by HYDRUS while the rise of river-stage is (a) 5cm and (b) 15cm with the same groundwater inflow of 2cm/hr 54
Figure 4 - 5: Comparison of the measured temperature with inverse simulation by optimising thermal conductivity while setting hydraulic properties as (a) temperature independent, (b) temperature dependent, and (c) by optimising saturated hydraulic conductivity in the case of river-stage rise of 15cm with groundwater inflow of 2cm/hr 56
Figure 4 - 6: Temperature-based estimates of flux below the riverbed simulated by HYDRUS. The steady-state groundwater flux is (a) 2.0cm/hr, (b) 1.5cm/hr, (c) 1.0cm/hr, (d) 0.5cm/hr and (e) no groundwater inflow 59
Figure 5 - 1: The schematic representation of a river–aquifer interaction model 66
Figure 5 - 2: Simulated temperature-depth profile below the center of sandy-loam riverbed in the summer period under steady-state upward groundwater flow 70
Figure 5 - 3: Comparison of the simulated average temperature-depth profiles in different sediment textures in the (a) winter period and (b) summer period 71
Figure 5 - 4: Comparison of the amplitude of subsurface temperature oscillations versus depth for sandy riverbed in the (a) winter period and (b) summer period 72
Figure 5 - 5: Graphical output of steady groundwater flow patterns surrounding the riverbed. The sediment texture is sandy-loam. Temperature in the aquifer is assigned to 7°C and temperature in the river is assigned to (a) 7°C; (b) 2°C; and (c) 10°C. 73
Figure 5 - 6: Graphical output of steady groundwater flow patterns surrounding the sandy-loam riverbed. The bank slope of river channel is set to H:V = (a) 0, (b) 0.58 and (c) 1.73. Temperature in the aquifer and the river is assigned to 7°C 74
Figure 5 - 7: The estimation of steady volumetric flux at the sides and the bottom of

the river channel by changing the temperature at aquifer–riverbed interface and varying the sediment texture 75
Figure 5 - 8: Comparison of the steady state groundwater fluxes simulated by HYDRUS 2D/3D and calculated by using 1-D analytical solution for sediment textures ranging from (a) sandy-clay, (b) sandy-loam to (c) sand at different seasons 76
Figure 5 - 9: The graphical output of (a) the penetration of river water into a sandy-loam riverbed right after the rise in river stage, (b) the penetration of river water into a sandy-loam riverbed after 1 day and (c) the recovery of baseflow after the recession of river stage. The rise of water level was assigned to be 1m 78
Figure 5 - 10: (a) Travelling distances of the flowing particles in the aquifer during the high river stage event after 0.1 day, 0.2 day, 0.5 day and 1 day; (b) The flow trajectories of particles and the distinction between bank storage zone and hyporheic zone 79
Figure 5 - 11: The estimated vertical versus lateral flow paths of hyporheic zone in (a) sandy-loam sediment during winter; (b) sandy-loam sediment during summer; (c) loamy-sand sediment during winter; (d) loamy-sand sediment during summer in 1 day duration 81

List of Tables

Table 3 - 1: Calibrated length and characteristic impedance of TDR-probes 25
Table 3 - 2: Solute-transport parameters for coarse dune sand with four water flux conditions and with concentration in 1.5g/L of the applied pulse of potassium chloride (KCl) for 30 minutes input. Pore water velocity (*V*) and dispersion coefficient (*D*) are determined by the transfer-function method fitted on individual segments (Mojid *et al*., 2004)..... 29
Table 3 - 3: Optimal parameters of dispersivity by inverse modelling with HYDRUS 2D/3D 36
Table 4 - 1: The heat transport parameters determined by inverse modelling in HYDRUS using the measured temperature data under no-flow conditions..... 47
Table 4 - 2: The estimated optimal hydraulic conductivities at reference temperature 20°C for three levels of square shaped hydrographs and different fluxes while the hydraulic conductivities were scaled in function of simulated temperature according to Equation (4.7) obtained by inverse modelling as in Fig 4-4(c) using measured temperature..... 57
Table 5 - 1: The hydraulic and heat transport parameters of the soils for HYDRUS simulations 69

Summary

River and aquifer are interconnected and viewed as a hydrologic continuum within a catchment. The hyporheic zone is the region in which the exchange of river water and groundwater occurs. Accurate characterization of the flow across the hyporheic zone is important. One challenge is that direct monitoring of water flow between river and aquifer is difficult due to the spatial and temporal variability of flow patterns. In order to develop a systematic framework for quantifying the water exchange in the hyporheic zone, a laboratory experiment and HYDRUS numerical simulations are carried out in this research.

At the first stage, we studied the lateral inflow from the aquifer to the river based on the laboratory J-shaped column model. This model represents a schematic flow line in the succession of unsaturated recharge zone, saturated zone (aquifer) and river. By analysing consecutive column segments with the application of a transfer function method, the relationship between dispersivities and other physical measurement were determined. The dispersivity was found to be flux dependent and increased at lower flux in unsaturated sections (i.e. in vadose zone); in contrast, dispersivity was fairly constant and independent of flux variation in saturated sections (i.e. in riverbed and the adjacent aquifer). The longitudinal dispersion coefficient can best be related to the ratio of pore-water velocity over soil water content. This relation can be performed over the range of saturated and unsaturated conditions.

At the second stage, the experiment has been expanded for the estimation of the transient water fluxes in the riverbed with temperature. A step-wise rise and fall of the water level was induced at the river section simultaneously with a change in water temperature. This square shaped "hydrograph" altered the vertical hydraulic gradient, thus reversing the flow direction in the riverbed. We observed very large changes in water temperature, which in their turn caused important variations in hydraulic conductivity in the riverbed. By inverse modelling on measured temperatures, the numerical model HYDRUS was calibrated to simulate the transient water flow conditions in the riverbed.

At the final stage, the thermal regime and flux variability in the riverbed were investigated by field-scale numerical simulations. This model provided a useful and simple framework for interpreting the flux variability in the riverbed. By respectively analyzing the long-term steady discharge and the transient downwelling groundwater flow patterns surrounding the riverbed, the vertical versus lateral flow paths of the hyporheic zone can be accurately delineated.

論文研究摘要

伏流水帶(Hyporheic zone)是意指表面河川與地下水含水層之間相當重要的連接區塊，雙向水流交換受到河川動態、河川幾何特徵、河床底質特性、集水區基流量的影響，在河床底形成不同的物理性、化學性以及能量梯度，也塑造伏流水帶成為一個相當重要的生態交會區。然而，由於目前技術尚無法明確在現場標定雙向水流動態交換的範圍，因此本研究嘗試建立一實驗室尺度的地下含水層與河川水文連續體模型，並搭配數學傳輸方程與數值模擬來進行雙向水流動態的量化。

本論文首先提出模擬河川伏流區水文連續性的創新試驗。理論建立在以土壤含水率進行河濱地質單元的切割，將達西實驗進行概念延伸，從而建立伏流水區試驗模型。試驗構想首先以脈衝響應實驗搭配時域反射儀(Time Domain Reflectometry)，同步量測土壤含水率與電導度，在穩定流況下換算分區之溶質傳輸參數變化。最後再以統計軟體進行一維傳輸方程和觀測值的擬合，比較分區示蹤劑的延散度、孔隙水流速、平均含水量之間的關係。初步推導出解延散係數的冪次關係式，做為下一階段數值模擬和野外試驗之銜接。

第二階段實驗進行河川入滲模擬，由於傳統化學性、放射性甚至生物性示蹤劑無法標定此暫態厘米維度的水文變化，本研究因此嘗試以熱能配合數值模式來進行觀測。實驗的設計首先將實驗模型包覆絕熱，在穩定流況下使河川水位與溫度同步進行改變，透過植入的熱電偶紀錄河床底的溫度變化，再以數值模式中進行水力傳導係數之逆推。如此，便可以在設計河川水位變化與不同基流量狀態下，透過顆粒追蹤功能來標定河川入滲的範圍與通量。

最後階段的研究主要在於建立大尺度地下水與表面水交換的數值概念模式(HYDRUS)，模擬包括不同河床質、不同環境溫度之改變、不同河川渠道斷面積、表面河川溫度振盪等參數對於河床水文通量和溫度變化的影響，並比較河床側向與底部水文通量之差異，明確標定地表水與地下水雙向水文交換量與範圍，以做為往後野外觀測的參考。

Notation

Latin symbols

Symbol	*Definition*	*Units*
A	Cross-sectional area of river channel	L^2
A_S	Cross-sectional area of subsurface transient storage zone	L^2
a_1, a_2	Constants determined by the heat transport parameters of riverbed for the Stallman equation	-
b_1, b_2, b_3	Soil specific empirical parameters for thermal conductivity	$M\,L\,T^{-3}\,K^{-1}$
C	Solute concentration	$M\,L^{-3}$
c	Specific heat	$L^2\,T^{-2}\,K^{-1}$
C^*	Volumetric heat capacity	$M\,L^{-1}T^{-2}\,K^{-1}$
C^*_B	Volumetric heat capacity of bulk sediment matrix	$M\,L^{-1}T^{-2}\,K^{-1}$
C^*_s	Volumetric heat capacity of soil	$M\,L^{-1}T^{-2}\,K^{-1}$
C^*_w	Volumetric heat capacity of water	$M\,L^{-1}T^{-2}\,K^{-1}$
C_i	Initial solute concentration	$M\,L^{-3}$
C_L	Solute concentration returning flow from the riverbed	$M\,L^{-3}$
C_o	Solute concentration applied to the upper boundary of system	$M\,L^{-3}$
C_R	Solute concentration in the river	$M\,L^{-3}$
$C_{r.est}$	Time-dependent estimated response solute concentration	$M\,L^{-3}$
C_S	Solute concentration in the subsurface transient storage zone	$M\,L^{-3}$
D	Coefficient of hydrodynamic dispersion	$L^2\,T^{-1}$
d_{50}	Median grain diameter	L
D_B	Thickness of aquifer	L
D_d	Depth of river channel	L
D_e	Coefficient of molecular diffusion	$L^2\,T^{-1}$
D_T	Effective thermal diffusivity	$L^2\,T^{-1}$
D_w	Width of river channel	L
$DLin$	Lateral extent of the hyporheic zone	L
$DVin$	Vertical extent of the hyporheic zone	L
g	Acceleration of gravity	$L\,T^{-2}$
h	Pressure head	L
h_B	Base flow level of river	L
h_F	Risen stage of river	L
k_i	Intrinsic permeability of the porous medium	L^2

$\boldsymbol{Ks}$	Saturated hydraulic conductivity of soil	$L\ T^{-1}$
$\boldsymbol{L}$	Length	L
$\boldsymbol{l}$	Vertical distance between adjacent TCR probes	L
$\boldsymbol{L_P}$	TDR probe length	L
$\boldsymbol{N}$	Mass-dispersion number	-
$\boldsymbol{n}$	Empirical constant ranging between 1 and 2	-
$\boldsymbol{n^*}$	Pore size distribution index/ parameter for van Genuchten hydraulic function	-
$\boldsymbol{n_e}$	Porosity	$L^3\ L^{-3}$
$\boldsymbol{P_e}$	Thermal grain Péclet number	-
$\boldsymbol{P_L}$	Column Péclet number	-
$\boldsymbol{Q}$	Volumetric flow rate of the river	$L^3\ T^{-1}$
$\boldsymbol{QLin}$	Cumulative flux across the side of the river channel	$L^3\ T^{-1}$
$\boldsymbol{QVin}$	Cumulative flux across the bottom of the river channel	$L^3\ T^{-1}$
$\boldsymbol{q}$	Water flux (discharge per unit area)	$L\ T^{-1}$
$\boldsymbol{q_{Lin}}$	Volumetric flow rate entering from the storage zone	$L^3\ T^{-1}$
$\boldsymbol{R}$	Constant rate of precipitation per unit area	$L\ T^{-1}$
$\boldsymbol{R_f}$	Retardation factor	-
$\boldsymbol{S_e}$	Effective water content	$L^3\ L^{-3}$
$\boldsymbol{T}$	Temperature	K
$\boldsymbol{t}$	Time	T
$\boldsymbol{T_A}$	Amplitude of temperature oscillation	K
$\boldsymbol{T_L}$	Temperature at the lower boundary of the heat transfer domain below the riverbed	K
$\boldsymbol{T_o}$	Temperature at the uppermost position ($\boldsymbol{z} = 0$) of riverbed	K
$\boldsymbol{T_z}$	Temperature at a depth $\boldsymbol{z}$ below the riverbed	K
$\boldsymbol{V}$	Pore water velocity	$L\ T^{-1}$
$\boldsymbol{\omega}$	Angular frequency of diurnal temperature oscillation	T^{-1}
$\boldsymbol{Z_d}$	Temperature damping depth	L
$\boldsymbol{Z_0}$	Impedance	Ω
$\boldsymbol{z}$	Vertical coordinate (depth)	L

Greek symbols

Symbol	*Definition*	*Units*
α	Inverse of the air-entry value/ parameter for van Genuchten hydraulic function	L^{-1}
α^*	Exchange coefficient	T^{-1}
θ	Volumetric water content/ volumetric fraction of bulk porous medium	$L^3 L^{-3}$
θ_r	Residual volumetric water content	$L^3 L^{-3}$
θ_s	Saturated volumetric water content	$L^3 L^{-3}$
θ_v	Average soil water content (measured by TDR)	$L^3 L^{-3}$
κ	Thermal conductivity	$M L T^{-3} K^{-1}$
λ	Longitudinal solute dispersivity	L
λ_T	Thermal dispersivity	L
μ_w	Dynamic viscosity of water	$M L^{-1}T^{-1}$
ρ_w	Density of water	$M L^{-3}$
τ	Mean travel time of the tracer	L
τ_p	Period	L

Acronyms

Symbol	*Definition*
BTC	Break Through Curve
CDE	Convective-Dispersion Equation
EC	Electrical Conductivity
GPL	General Public License
KCl	Potassium chloride
PDE	Partial Differential Equation
PMMA	Polymethyl methacrylate
PVC	Polyvinyl chloride
TC	Thermocouple sensors
TDR	Time Domain Reflectometry
TSM	Transient Storage Model

Mathematical symbols

Symbol	*Definition*
C_{in}	Input
C_r	Response
C_V	Coefficient of variation
$F(s)$	Transfer function of a column
R^2	Coefficient of determination
r^2	Coefficient of correlation
$RMSE$	Root-mean-square error
s	Laplace operator
β	Time integration variable

Chapter 1
Introduction

1.1 Preface

River and aquifer are interconnected. The study of the hydrological connectivity between river and aquifer is of essential importance for the land and water management activities. It is necessary to recognize that aquifer and river are the hydrologic continuum within a catchment (Holmes, 2000).

The concept of hydrological connectivity is emerging as an important theme in integrating hydrological and ecological perspectives in the catchment science (Tetzlaff *et al*., 2007). Different aspects of the hydrological connectivity have been discussed in greater detail by many studies (e.g., Tockner *et al*., 2000; Ocampo *et al*., 2006; Bracken and Croke, 2007; Nadeau and Rains, 2007; Tetzlaff *et al*., 2007; Borselli *et al*., 2008). Hydrological connectivity refers to the physical linkage of water among different landscape components in the catchment. Hydrological connectivity is a transient phenomenon that closely relates to the catchment rainfall-runoff processes. Hydrological connectivity controls the transport of sediment, solute, energy, and organisms between the river and the surrounding aquifer. Such linkages play a determining role in riverine ecosystems (Boulton *et al*., 1993; Pusch *et al*., 1998; Ward *et al*., 1999; Hein *et al*., 2003; Thorp *et al*., 2006; Boulton *et al*., 2007; Roach *et al*., 2009). As indicated by Sear *et al*. (1999) the scientific recognition of the aquifer-river "boundary" has begun to blur. Therefore quantification of water flow dynamics across the interface between the river and the surrounding aquifer has received increasing attention in research. Stanley and Jones (2000) pointed out that understanding the interaction of groundwater and surface water is one of the fastest growing research directions in the science of river ecology. It was also concluded in the UNESCO Integrated Science Initiative Workshop (held in Oxford, UK, 2005)…"*more interdisciplinary research and environmental management practices are needed to better understand, predict and manage processes at the interface of environmental compartments*" (Smith *et al*., 2008).

The hyporheic zone is the region composed by sand, gravel, sediments and/or other permeable material where mixing of shallow groundwater and surface water occurs. It combines features of rivers and aquifers (Cleven, 2004). The significance of the hyporheic zone has been well recognized (Bencala, 2005 and chapter 2 herein). In this zone there is not only a bidirectional exchange of water but also a diffusion of oxygen and carbon dioxide along with a transport and transformation of nutrients. It is also a major rooting zone for many riparian plants (Dahm *et al*., 1998), where much of the natural water purification occurs due to the high surface areas and retention times. Contaminants may undergo attenuation or transformation in this zone (Cirone and Duncan, 2000). The research of the hyporheic zone is certainly a cross-disciplinary science with relevance to ecology and water quality.

The extent of the hyporheic zone is highly variable in time and space. The existing delineation is usually somewhat arbitrary due to the difficulty in accessing the hyporheic zone in situ. Stanley and Jones (2000) pointed out that there is still substantial research in the examination of interface dynamics remained. It is the goal of this research to contribute to a better understanding of the hydrological linkage and flux exchange between the river and the surrounding aquifer.

1.2 Research objectives

The general objective of this doctoral research is to develop a systematic framework for the quantification of water exchange in the hyporheic zone between river and aquifer. A laboratory J-shaped column experiment and HYDRUS numerical simulations are carried out. The experiment attempts to combine a flow-line within the continuum of vadose zone, aquifer and river. It is hypothesized that this experimental set up allows the hydrological processes in hyporheic zone in conjunction with the adjacent aquifer to be systematically identified. The application of a numerical model allows at a later stage to incorporate the findings of the laboratory model into a real-life complex geometry and layering. The specific objectives of this PhD research are as follows:

1. To provide a broader perspective and integration of hyporheic exchange flows by literature review;
2. To characterize the transport of dissolved material by hydrodynamic dispersion in the hyporheic zone in conjunction with the adjacent aquifer;
3. To determine a relation for the dispersion parameters that can be implemented in a realistic model;

4. To investigate whether temperature can be used as a tracer to estimate transient water fluxes in the riverbed;
5. To determine the penetrated fluxes of river water according to different scenarios of river-stage rising and groundwater inflow by numerical simulation;
6. To investigate the potential influence of temperature on water flux variability in shallow aquifers by numerical simulation;
7. To provide a useful framework for the analysis of both steady-state and transient water flow conditions in the hyporheic zone.

1.3 Research outline of the study

Chapter 2 provides a review of the literature on the key functional description of the hyporheic zone, including the ecological function, nutrient dynamics and thermal gradient variation. An overview of hydrological perspectives and integration of hyporheic exchange flows is presented. The potential of temperature measurements on quantifying hyporheic exchange flows is discussed.

Chapter 3 investigates the impact of lateral inflow processes by groundwater into the hyporheic zone. A laboratory J-shaped column experiment was designed. This J-shaped column represents a schematic flow line in the succession of unsaturated recharge zone, saturated zone (aquifer) and river. This experimental set up allowed to identify the hydrological processes in hyporheic zone in conjunction with the adjacent aquifer. We determined the physical transport parameters in this model by fitting an analytical convective-dispersion equation to the observed breakthrough curves. Transport parameters including pore water velocity and dispersion coefficient were determined and compared for the consecutive segments in the model. The observed relationship among dispersion coefficient, pore water velocity and soil water content was tested by means of the numerical model HYDRUS 2D/3D.

Chapter 4 investigated whether temperature measurements can be used to estimate water flux fluctuations in the riverbed. The same laboratory model was used to explore this technique. A step-wise rise and fall of the water level was induced in the river section along with a simultaneous change in water temperature. This square shaped "hydrograph" altered the vertical hydraulic gradient and reverses the flow direction in the riverbed. As no analytical solutions are available for transient heat transfer in transient water flow conditions the numerical model HYDRUS 2D/3D was used. The

measured temperatures were used for inverse modelling and to validate the simulations.

Chapter 5 reported the application of HYDRUS 2D/3D on temperature-based estimation of groundwater flux in the hyporheic zone. A two-dimensional river–aquifer interaction model has been composed in HYDRUS. The temperature dependence of soil hydraulic properties was considered. Simulations were first performed under steady-state water flow conditions. The vertical temperature gradients, the attenuation of temperature oscillations, and the groundwater fluxes in different sediment textures were determined. The simulation results were then compared with calculations using a 1-D steady-state analytical solution proposed by Schmidt *et al*. (2007). Subsequently, simulations were performed to quantify the extent and volume of water flux exchange in the riverbed induced by the rising flood stage.

Chapter 6 summarizes in short this research and draws the general conclusions based on the conclusions of each prior chapter. It provides answers to the objectives stated in this chapter. In addition, it identifies the limitations of the current study. Recommendations are provided for ongoing research, including the improvements for the laboratory scale experiment, potentials for the HYDRUS simulation and strategies for the field scale measurements.

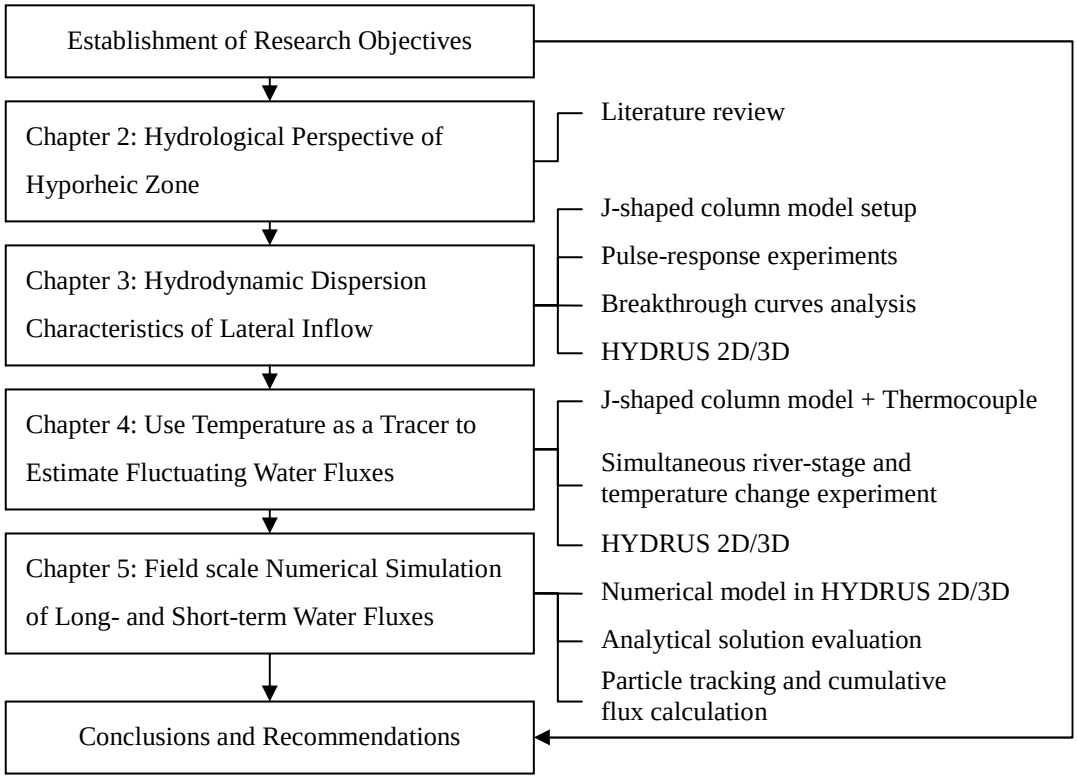


Figure 1 - 1: Dissertation outline

Chapter 2

Hydrological Perspective of Hyporheic Zone: A Review

Abstract

Growing research attention has been devoted to the hydrological linkages between aquifer and river. These linkages are closely related to the biological processes and chemical transformations in a river environment. The hyporheic zone is a critical landscape component connecting the river and the underlying aquifer. It is important to properly quantify the direction and magnitude of groundwater flux across the hyporheic zone.

The hydrological dynamics and sediment heterogeneity below the riverbed establish the role of the hyporheic zone as a unique and active ecotone. However, the actual extent and temporal variability of the hyporheic zone has not been well quantified. Direct in situ measurements by chemical tracer studies are not able to determine lateral and vertical exchanges of water across the aquifer–riverbed interface. Challenges and knowledge gaps remain in regard to how the extent of fluxes exchange varies with different river-derived and aquifer-derived variables.

This chapter provides a review of the literature on the key functional description of hyporheic zone, including the ecological function, nutrient dynamics and thermal gradient variation. An overview of hydrological perspectives and integration of hyporheic exchange flows is presented. Finally, the potential of temperature measurements on quantifying hyporheic exchange patterns is discussed.

2.1 Definition of hyporheic zone: linkage, exchange and continuum

The investigation of hydrological processes at the aquifer-riverbed interface has received growing research attention. The stability and variability of a river ecosystem is largely a function of the physical constraints on surface-subsurface water exchange through the aquifer-riverbed interface (Findlay, 1995). The hydrological connectivity across the aquifer-riverbed interface in different scales and types have been reviewed and discussed in several previous studies (Brunke and Gonser, 1997; Boulton *et al*., 1998; Woessner, 2000; Malard *et al*., 2002; Sophocleous, 2002; Fox and Durnford, 2003). The hyporheic zone has increasingly been recognized as an important component in the aquifer. The research of river–aquifer interaction in the hyporheic zone not only opens door for studying linkage and heterogeneity within the river subsystems (Stanley and Jones, 2000; Hayashi and Rosenberry, 2002; Bencala, 2005), but also facilitates the bridging of knowledge gaps existing in river ecosystems.

The literal derivation of the term "hyporheic" can be understood from the prefix "hypo" (Greek: υπο), representing "*beneath or diminished*", and the term "rheo" (Greek: ρεω), indicating "*the flow of a river*". Findlay (1995) considered the hyporheic zone as the sediment hydrologically linked to the open river channel. The linkage involves the continuous bidirectional exchange of water, nutrients and fauna between the river and alluvial aquifer (Triska *et al*., 1993). Bencala (2000) indicated that the hyporheic zone, at whatever scale, is part of the hydrological continuum between rivers and various subsurface water components in the catchment. Figure 2-1 illustrates a schematic illustration of the hyporheic zone.

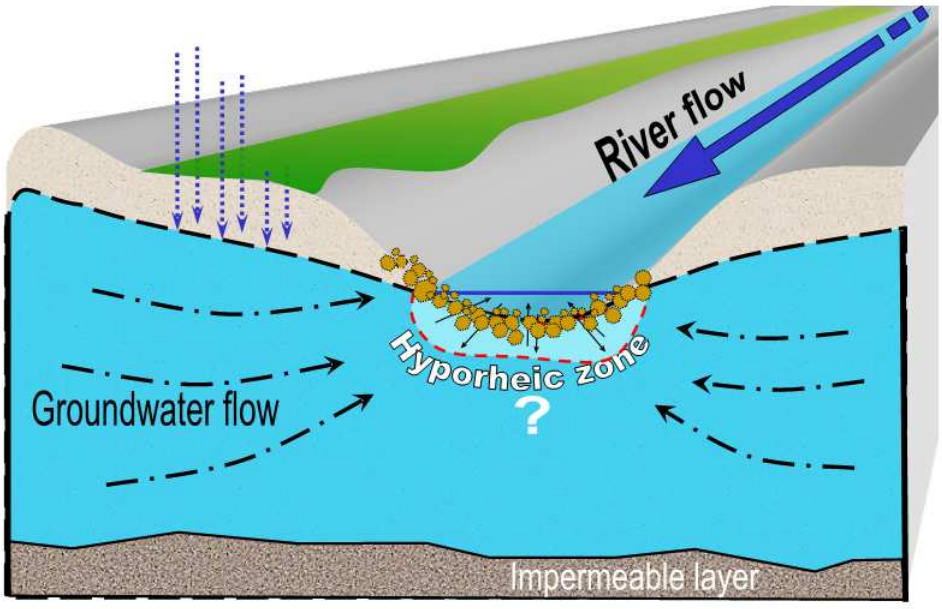


Figure 2 - 1: The schematic illustration of hyporheic zone

Krause *et al*. (2009) indicated that the hyporheic zone can be described in terms of different research questions that resulting in different spatial and temporal scales of investigation. A variety of specific descriptions can be found associated with different scientific disciplines in the literatures:

1. The hyporheic zone is an important habitat that supports a diverse fauna of invertebrates.
2. The hyporheic zone is a geochemical active region in which steep chemical gradients and long solute residence times can be observed.
3. The hyporheic zone acts as the thermal buffer layer where a considerable amount of thermal energy from the river is retained and transferred.
4. The hyporheic zone is a dynamic landscape corridor, which controls the flow of materials between the adjacent riverine patches.

As illustrated in Figure 2-2, groundwater is usually low in dissolved oxygen and high in nutrients as compared to river water. Diurnal and seasonal temperature fluctuations in river water are typical, while groundwater has a relatively stable thermal regime. The hyporheic zone is thus a transition zone (i.e. an ecotone) which subjected to rapid physical, chemical and biological transitions between the river and the aquifer (Gibert *et al*., 1994). Since the extent of the hyporheic zone is highly variable in time and space, its quantitative defining criteria is difficult to find (Hancock 2002). Wroblicky *et al*. (1998) indicated that the extent of the hyporheic zone varied not only with the river flow conditions, but also with the hydraulic conductivity of aquifer and riverbed sediments. The fluctuation in the volume of hyporheic zone thus strongly influences the composition of nutrients or pollutions both in the river and the aquifer.

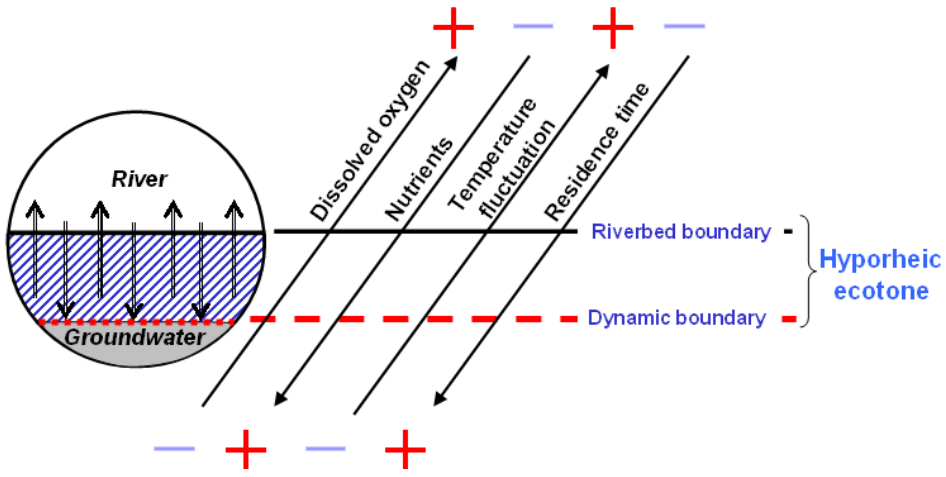


Figure 2 - 2: The schematic representation of hyporheic exchange flows and the associated environmental gradients between river and aquifer

2.2 Significant characteristics of hyporheic zone

2.2.1 Ecological contribution

The ecological research on hyporheic zone has evolved since the last two decades (Runkel *et al*., 2003; Storey and Williams, 2004). The hyporheic zone is usually characterized by permanent darkness, low current velocities and high substrate stability. Studies have shown that hyporheic zone serves as a habitat for a variety of fauna, nursery for fish spawning and incubation, and refugia for invertebrates during times of floods. Consequently, the hyporheic zone is an important ecological hotspot (Boulton *et al*., 1998; Biksey and Gross, 2001; McClain *et al*., 2003).

Gibert *et al*. (1997) mentioned that an ecotone must accommodate a great variety of permeability and connectivity in order to provide local biota with sufficient nutrient income. Boulton *et al*. (1998) indicated that the connection between hyporheic zone and river determines the ecological processes in the hyporheic zone. On the contrary, Winkelmann *et al*. (2003) indicated that the hyporheic zone can not be viewed as an ecotone if it is missing the connection to the groundwater. Belaidi *et al*. (2004) described the hyporheic biotope as a mosaic of microcosms relying on localized fluctuating conditions. Kincanon and McAnally (2004) pointed out the lack of consideration of hyporheic processes is a source of uncertainty in predicting the ecosystem response.

It was mentioned in the study of Fraser and Williams (1998) that the distribution of organisms in the riverbed was used as an indicator to describe the spatial extent of a hyporheic zone. The vertical distribution of organisms was reported to reach a peak a few centimetres below the riverbed (Stanford and Ward, 1988; Ricci and Balsamo, 2000; Swan and Palmer, 2000; Winkelmann *et al*., 2003; Cleven, 2004). The pattern of fauna distribution in the hyporheic zone was reported correlating to sediment physical characteristics (Fowler and Scarsbrook, 2002; Gayraud and Philippe, 2003; Winkelmann *et al*., 2003; Weigelhofer and Waringer, 2003) and the supply of organic carbon (Battin *et al*., 2003; Hahn, 2006). Clearly, the hyporheic exchange flows appear to be one of the most important factors in determining the distribution of interstitial fauna.

Soulsby *et al*. (2001) indicated that the process of hyporheic exchange flows should be well considered in the restoration projects of degraded aquatic ecosystems. Datry *et al*. (2007) reported that the diversity and density of invertebrate increase with

increasing flow permanence. They also found higher taxonomic richness at groundwater-dominated sites than that at the river runoff-dominated sites.

2.2.2 Nutrient dynamics and pollutants attenuation

The hyporheic zone is a geochemical focal point for nutrients loading, transforming and transporting. It is the major pathway of nutrients transport between riparian area and river (Cirmo and McDonnell, 1997). Schindler and Krabbenhoft (1998) argued that the geochemical focus of the hyporheic zone should be limited in the last few centimetres below the riverbed.

The change of redox condition is strongly regulated by the dynamics of hyporheic exchange flows (Dahm *et al*., 1998; Baker *et al*., 2000; Hinkle *et al*., 2001; Greig *et al*., 2007). As summarized by Duff and Triska (2000), the fluxes exchange in the hyporheic zone increases the contact opportunity of sediment with river water, enhances microbial activity rates, reduces nutrient cycling distances and alters the chemical form of elements in the sediment. Researches have also discussed the close linkage between hyporheic exchange flows and the dissolved organic carbon (Schindler and Krabbenhoft, 1998; Battin, 1999; Kaplan and Newbold, 2000), nitrogen (Cirmo and McDonnell, 1997; Fernald *et al*., 2006; Schilling *et al*., 2006), phosphorous (Hendricks and White, 2000) and microbial biofilm activity (Battin, 2000; Rulík and Spáčil, 2004; Fischer *et al*., 2005; Mermillod-Blondin *et al*., 2005). As a consequence, hyporheic exchange flows have great potential in influencing the river water quality (Hancock *et al*., 2005; Pretty *et al*., 2006; Gandy *et al*., 2007). Ellis *et al*. (2007) commented that hyporheic zone is influential in controlling the attenuation of contaminants especially during the low flow periods.

2.2.3 Stable thermal regime

Previous researches have also indicated the potential influence of hyporheic exchange flows on river thermal dynamics. Evans *et al*. (1998) concluded that up to one-quarter of daily heat exchange in the river occurred through the riverbed. Similar results were also reported by Moore *et al*. (2005) and Cozzetto *et al*. (2006). Ozaki *et al*. (2008) concluded that subsurface flow dynamics play an important role in determining seasonal variations in river water temperature. As a result, the hyporheic zone can also

be identified as an important source and sink of heat within a river environment.

Hunt *et al*. (2006) indicated that the temperature/chemical variation in the hyporheic zone is related to the amount of groundwater discharge. The influence of groundwater flow on the thermal regimes in the riverbed has been discussed by previous studies (Malard *et al*., 2001; Conant Jr., 2004; Hannah *et al*., 2004; Caissie, 2006; Hoehn and Cirpka, 2006). The alternation of temperature associated with hydrologic exchange in the hyporheic zone is also relevant to the river ecosystem. River temperature is directly influenced by meteorological conditions and by human activities, while groundwater has a relatively stable thermal regime in comparison to the river water. Poole and Berman (2001) indicated that the hyporheic zone acts as a thermal buffer for the interstitial organisms against the river temperature fluctuations. Stable thermal regime in the hyporheic zone is considered to be the essential requirement for the development and survival of aquatic vertebrates (Malcolm *et al*., 2002; Alexander and Caissie, 2003; Ebersole, 2003; Malcolm *et al*., 2004; Boxall *et al*., 2007).

2.3 Hydrological perspectives and integration

2.3.1 A river-centric perspective

As described in many previous studies, the hyporheic zone was conceptualized as an arbitrarily fixed volume adjacent to the water in the main river channel. Based on the river-centric perspective (Newman *et al*., 2006) the hydrological process of hyporheic exchange flows was denoted as the movement of near-bed river water entering and re-emerging out of the riverbed (Wroblicky *et al*., 1998; Harvey and Wagner, 2000; Jonsson *et al*., 2003; Fernald *et al*., 2006). The principal control of the hyporheic exchange flows is the spatial pressure variation over the riverbed that drives the acceleration and penetration of the near-bed flow (Harvey and Bencala, 1993; Mutz and Rohde, 2003).

Low order and high gradient rivers were most commonly chosen for field investigation due to the frequent appearance of gravel bedform and riffle-pool sequences. Numerous techniques have been proposed for the in situ measurements of groundwater flux including by using seepage meters and piezometers, performing tracer tests and fitting the measured breakthrough curves with analytical or numerical models (Marion *et al*., 2003; Zaramella *et al*., 2006), as well as indirect approaches like water balance or heat budget calculation. Landon *et al*. (2001) compared different

techniques of estimating hydraulic conductivity in sandy riverbed, including slug tests, permeameter measurements, seepage meter measurements and grain-size analysis. They concluded that making multiple measurements to characterize the spatial variability of hydraulic conductivity in the field is more significant than the selection of techniques.

Well-defined laboratory flume experiments with contrived riverbed deployment were also applied in many studies (Elliott and Brooks, 1997a, b; Packman and MacKay, 2003; Rehg *et al*., 2005; Tonina and Buffington, 2007). By using dye or salt as a tracer, the penetrating depth and flowing path of surface inflow toward the riverbed can be quantified. The influence of individual parameters on hyporheic exchange flows can be tested in a relatively idealized condition. However, in most laboratory or tracer experiments the lateral groundwater inflow and outflow were not considered.

2.3.2 The conceptual model

Many studies applied the Transient Storage Model (TSM) (Bencala and Walters, 1983) to analyze the effect of solute exchange between the main river channel and the subsurface storage zone in the longitudinal sections of rivers (e.g. Gooseff *et al*., 2003a, b; Lin and Medina, 2003; Jonsson *et al*., 2003; Cozzetto *et al*., 2006; Ge and Boufadel, 2006; Kazezyilmaz-Alhan and Medina, 2006; Zaramella *et al*., 2006). Figure 2-3 illustrates a conceptual diagram of TSM (Runkel, 1998).

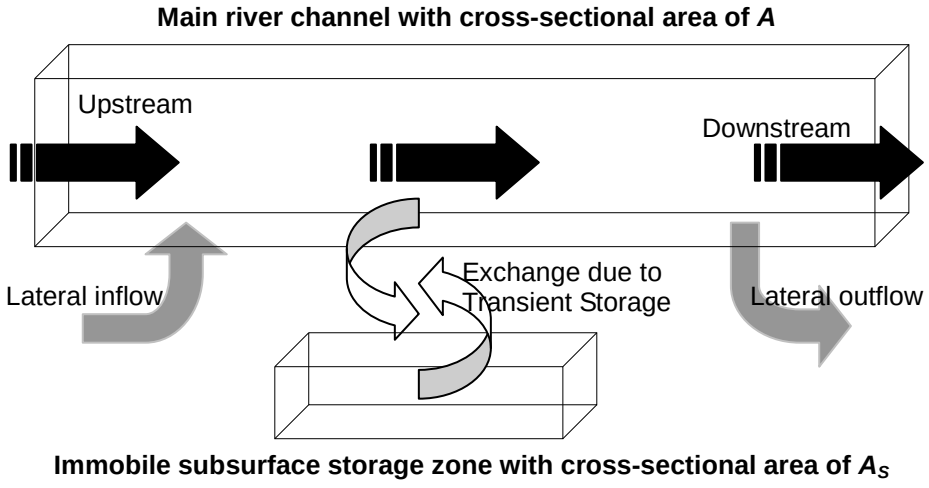


Figure 2 - 3: A conceptual diagram of the Transient Storage Model (after Runkel, 1998)

The TSM is composed of two partial differential equations:

$$\frac{\partial C_R}{\partial t} = -\frac{Q}{A}\frac{\partial C_R}{\partial x} + \frac{1}{A}\frac{\partial}{\partial x}\left(AD\frac{\partial C_R}{\partial x} \right) + \frac{q_{Lin}}{A}(C_L - C_R) + \alpha^*(C_S - C_R) \quad (2.1)$$

$$\frac{dC_S}{dt} = \alpha^* \frac{A}{A_S}(C_R - C_S) \quad (2.2)$$

where $\boldsymbol{C_R}$ represents the solute concentration ($M\,L^{-3}$) in the river, $\boldsymbol{C_L}$ represents the solute concentration returning flow from the riverbed, and $\boldsymbol{C_S}$ represents the solute concentration in the subsurface transient storage zone; $\boldsymbol{Q}$ represents the volumetric flow rate of the river ($L^3\,T^{-1}$); $\boldsymbol{q_{Lin}}$ represents the volumetric flow rate entering from the storage zone ($L^3\,T^{-1}$); $\boldsymbol{x}$ represents the longitudinal distance (L) in the river channel; $\boldsymbol{D}$ represents the dispersion coefficient ($L^2\ T^{-1}$); $\boldsymbol{A}$ and $\boldsymbol{A_S}$ represents the cross-sectional area (L^2) of the river channel and the subsurface transient storage zone, respectively; $\boldsymbol{\alpha}^*$ represents the exchange coefficient between river and the subsurface (T^{-1}). $\boldsymbol{A_S}$ and $\boldsymbol{\alpha}^*$ were usually chosen as the parameters for fitting tracer breakthrough curves.

In the TSM the physical mechanics of transient storage are conceptually lumped into a single storage zone (Packman and Bencala, 2000; Runkel *et al*., 2003). As discussed by Kalbus *et al*. (2006), this implies that water entered the river from the subsurface can either be groundwater from the aquifer, or re-emerging river water from the upstream, or a mixture of both. The study of Zaramella *et al*. (2003, 2006) thus concluded that the TSM did not explicitly represent the process of surface-subsurface water exchange and cannot be used to assess reactive transport in pore waters.

Studies have also focused on the localized fine-scale advective nature of exchange processes (Marion, 2005). The process of the interstitial pore-water circulation below the riverbed is predominately driven by the river flow-induced sinusoidal head variation over the riverbed. Elliott and Brooks (1997a, b) presented a theoretical and laboratory analysis for passive solute exchange between riverbed sediments and the overlying water. The mechanism of exchange can be due to the effect of “pumping” (i.e. the movement of river water through the riverbed driven by pressure variations over a stationary bed form) or “turnover” (i.e. the pore water release caused by moving bed forms). Their analysis was based on predicting the residence time of solute within the riverbed then calculating the net mass transfer between the riverbed and the river. However, one major limitation is that the spatial and temporal dynamics

of lateral groundwater inflow and the wide range of solute residence times are not considered.

2.3.3 Conceptual integration with aquifer derived information

Several studies argued that groundwater flow is dominating the hyporheic flow regimes (Sear *et al*., 1999; Holmes, 2000; Malcolm *et al*., 2004). A conceptual integration with the focus on aquifer contributes to a better insight for the whole hydrologic pattern in the hyporheic zone. Both river-derived and aquifer-derived hydrodynamics have to be described in an appropriate manner.

The study of Butturini *et al*. (2002) concluded that catchment rainfall-runoff models should include the near-stream compartment. By using the groundwater flow model MODFLOW Storey *et al*. (2003) indicated that exchange flows are up to twice as strong at the sides of the river than near the centre. Howard *et al*. (2006) found that the volume of hyporheic zone was inversely proportional to the lateral groundwater inflow towards the river. The study of Wondzell (2006) summarized that hyporheic exchange flows were highly influenced by the hydraulic gradients between the river and the floodplain. By applying three different numerical models (HEC-RAS, MODFLOW, MODPATH), Hester and Doyle (2008) concluded that the most crucial factors determining the magnitude of water exchange through the hyporheic zone appear to be the size of in-stream geomorphic structures, the groundwater discharge to the river baseflow and the hydraulic conductivity of the alluvial deposits.

Kalbus *et al*. (2006) provided an overview of the methods that are currently applied for quantifying the flux across the riverbed, including direct measurements by seepage meters, analysis by riverbed temperature profiles, measurement based on Darcy's Law (corresponding to the review by Landon *et al*., 2001), and mass balance analysis of tracers. They indicated that the choice of methods relies on the trade-off between the resolution of heterogeneity and the available measuring scale. In addition, they suggested for the localized or small scale exchange processes, the qualitative methods like temperature monitoring are more feasible than others.

2.4 Using heat as a tracer for estimating groundwater flow

Numerous studies have demonstrated that temperature can be used to characterize the river–aquifer interaction (Johnson, 2003; Anderson, 2005; Webb *et al*., 2008). Diurnal and seasonal temperature fluctuations of river water have been documented to drive the continuous change of temperature in the riverbed (Silliman *et al*., 1995; Ronan *et al*., 1998; Keery *et al*., 2007). Thermal stratification develops as the surface temperature fluctuations are damped with depth. The thermal profile of a riverbed in a losing portion of river would primarily reflect the temperature fluctuation of the river water; in contrast, the thermal profile of the riverbed in a gaining portion of river is reflecting the water temperature from the surrounding aquifer (Evans and Petts, 1997; Alexander and Caissie, 2003). Observations of temperature variations with depth therefore give qualitative indications of the direction and the intensity of flux across the riverbed (Essaid *et al*., 2008).

By considering sinusoidal temperature fluctuations of river water as upper boundary, the analytical solution derived by Stallman (1965) was widely accepted in literature (Anderson, 2005; Weeks, 2006). This solution considered one-dimensional heat transfer through the saturated sediment with vertical water flow. A sinusoidal temperature fluctuation was assumed on the top of riverbed. The temperature oscillation was attenuated with depth and time in the riverbed. The amplitude difference of temperature oscillation between river and aquifer is generally expressed as an exponential function of depth (Blasch *et al*., 2004). The temperature $\boldsymbol{T_z}$ at a specific depth below the riverbed is expressed as:

$$T_z = \overline{T_Z} + T_A(0)\cdot\exp(-a_1 z)\cdot\sin\left(\frac{2\pi t}{\tau_P} - a_2 z\right) \qquad (2.3)$$

where $\boldsymbol{\overline{T_Z}}$ is diurnal average temperature at depth $\boldsymbol{z}$; $\boldsymbol{T_A}(0)$ is the amplitude of temperature oscillation at the uppermost position ($\boldsymbol{z}$ = 0) of the riverbed; $\boldsymbol{\tau_p}$ is the period; $\boldsymbol{a_1}$ and $\boldsymbol{a_2}$ are constants determined by the heat transport parameters of riverbed (Taniguchi, 1993; Keery *et al*., 2007). Silliman *et al*. (1995) proposed an extension of Stallman's solution by combining riverbed temperature records. The extended solution was also widely applied in subsequent studies. Becker *et al*. (2004) argued that Silliman's solution is useful when the river is dominated by diffuse groundwater discharge. The study of Blasch *et al*. (2004) applied the moving-standard-deviation method to identify the variation of river stage from sediment temperature. Hoehn and

Cirpka (2006) evaluated the residence times of groundwater by interpreting the seasonal and diurnal temperature variations in wells. Keery *et al*. (2007) applied a harmonic regression model to calculate the lag of the temperature signal at different depth below the riverbed.

By focusing on the spatial variability of temperature below the riverbed, another analytical solution derived by Bredehoeft and Papadopulos (1965) has also been applied in the interpretation of groundwater flow. The solution assumes the vertical temperature profile below the riverbed is only a function of vertical flow. It is written as Equation (2.4):

$$\frac{T_z - T_o}{T_L - T_o} = \frac{exp\left(\frac{qC^*_B}{\kappa} z\right) - 1}{exp\left(\frac{qC^*_B}{\kappa} L\right) - 1} \tag{2.4}$$

where $\boldsymbol{q}$ is the vertical groundwater velocity (L T^{-1}); $\boldsymbol{C^*_B}$ is the volumetric heat capacity of bulk sediment matrix (M L^{-1} T^{-2} K^{-1}); $\boldsymbol{T_o}$ is the temperature at the uppermost position ($\boldsymbol{z}$ = 0) of riverbed, $\boldsymbol{T_L}$ is the temperature at the lower boundary of the heat transfer domain ($\boldsymbol{z}$ = $\boldsymbol{L}$) below the riverbed. The lower boundary can be regarded as the utmost depth of heat-transfer, while the temperature for deeper layers is assumed to remain constant. The temperature $\boldsymbol{T_z}$ at a specific intermediate depth $\boldsymbol{z}$ in the riverbed always lies in between the constant temperature boundaries $\boldsymbol{T_o}$ and $\boldsymbol{T_L}$.

The primary merit of this approach is that both magnitude and direction of groundwater flux can be determined (Dim *et al*., 2002). But the lower boundary of heat transfer domain in the riverbed may not be easily defined. Taniguchi (1993) integrated the pattern of temperature fluctuation into the type-curve method. Lu and Ge (1996) proposed an extension by including the horizontal groundwater flux. Ge (1998) applied the type-curve method to interpret the abrupt temperature changes in fractured rocks and to estimate the groundwater velocity. More recently, Ferguson and Woodbury (2005) pointed out that climatic variability may influence the estimates of groundwater discharge calculated from subsurface temperature profiles.

The majority of studies using heat as a tracer for interpreting groundwater flow tried to estimate longer-term (i.e. months) average fluxes based on time series temperature measurements. They used a steady-state water flux approximation. However, the

localized short-time flux variations in the hyporheic zone are rarely evaluated. More research is certainly required to explore the possibility of estimating transient groundwater fluxes by temperature.

2.5 Conclusions

River and aquifer should be considered as a whole entity with a dynamic connection. The hyporheic zone is an important linkage between the river and the underlying aquifer. The bidirectional exchange of water in the hyporheic zone dominates the physical, chemical and biological transitions between the river and the aquifer, which establishes the role of hyporheic zone as an active ecotone.

The extent of the hyporheic zone is highly variable in time and space. A river-centric perspective on hyporheic exchange flows only emphasizes the movement of river water entering and re-emerging out of the riverbed. The spatial and temporal dynamics of the lateral groundwater inflow from the aquifer are often disregarded or seen as a time-invariant constant. As a result, the actual extent and temporal variability of the hyporheic zone has been seen as a lumped storage without explicit dynamic interaction with the aquifer. It is difficult to measure in situ by chemical tracer studies inside the riverbed. Therefore, there is little quantitative information on the lateral and vertical exchanges of water across the riverbed at short temporal and spatial scales. As a consequence the range of hydrodynamic processes in the hyporheic zone is not fully specified (Gandy *et al*., 2007). Challenges and knowledge gaps remain concerning the extent of the hyporheic zone in function of river-derived and aquifer-derived variables. The equal attention the river and the aquifer will contribute to a better insight into the hyporheic zone.

The application of temperature measurements in the study of river–aquifer interaction also has received growing research interest in recent years. Most studies assume a steady-state water-flux or an approximation by quasi steady-state. They try to estimate the longer term average fluxes between the river and the underlying aquifer. Little attention has been paid to the effects of ambient temperature change on the hyporheic exchange patterns. The thermal effects on temporal variability of hydraulic conductivity should not be ignored during elaboration of field studies regarding the river-aquifer interaction. More studies have to be conducted on the estimation of transient groundwater fluxes by temperature.

Chapter 3

Hydrodynamic Dispersion Characteristics of Lateral Inflow into a River tested by a Laboratory Model*

Abstract

Groundwater and river water have a different composition and interact in and below the riverbed. The riverbed-aquifer flux interactions have received growing interest because of their role in the exchange and transformation of nutrients and pollutants between rivers and the aquifer. In this research our main purpose is to identify the physical processes and characteristics needed for a numerical transport model, which includes the unsaturated recharge zone, the aquifer and the riverbed. In order to investigate such lateral groundwater inflow processes, a laboratory J-shaped column experiment was designed. This study determined the transport parameters of the J-shaped column by fitting an analytical solution of the convective-dispersion equation for individual segments to the observed breakthrough curves of the resident concentration, and by inverse modelling for different flux conditions simultaneously over the entire flow domain. The obtained transport-parameter relation was tested by numerical simulation using HYDRUS 2D/3D.

Four steady-state flux conditions (i.e. 0.5cm/hr, 1cm/hr, 1.5cm/hr and 2cm/hr) were applied, transport parameters including pore water velocity and dispersivity were determined for the consecutive segments along the column. Results showed that the dispersivities for the segments under the saturated conditions were fairly constant and independent of the flux. In contrast, the dispersivities for the segments under unsaturated conditions were flux dependent and decreased at higher flux. For our porous medium the dispersion coefficient related best to the quotient of the pore water velocity divided by the water content. A simulation model of riverbed-aquifer flux interaction should take this into account.

* Adapted from Chou PY, Wyseure G. 2009. Hydrodynamic dispersion characteristics of lateral inflow into a river tested by a laboratory model. *Hydrology and Earth System Sciences* 13: 217-228

3.1 Introduction

Knowledge of the river–aquifer interaction is important for understanding the continuum of groundwater and surface water hydrology. The significance of river–aquifer interaction is however difficult to quantify (Valett *et al*., 1994) and commonly ignored in water-management considerations or policies.

Groundwater has different dissolved minerals, it usually contains less oxygen, and it has a more constant temperature as compared to river water. On the one hand, riverbed-aquifer flux interactions result in specific dissolved minerals from the aquifer moving into the riverbed, on the other hand down penetrating flow from the river moves oxygen and organic matter into the riverbed and the surrounding aquifer. The part of the riverbed subject to exchange of fluxes is called the hyporheic zone, which also acts as an important heat source and sink that affects river water temperatures (Brown *et al*., 2005; Moore *et al*., 2005; Cozzetto *et al*., 2006) and the solubility of oxygen (Ricci and Balsamo, 2000; Hahn, 2006).

Many studies analyzed the river–aquifer interaction by comparing the difference of tracer concentrations between river water and subsurface flowpaths as reviewed by Marion *et al*. (2003) and Zaramella *et al*. (2006). Conceptual models of the river solute advection dispersion model, such as the Transient Storage Model (TSM) (Bencala and Walters, 1983), are widely adopted in previous research to analyze and predict the solute exchange between river water and bed sediment in the longitudinal section of a river (e.g. Gooseff *et al*., 2003a, b; Lin and Medina, 2003; Jonsson *et al*., 2003; Cozzetto *et al*., 2006; Ge and Boufadel, 2006; Kazezyilmaz-Alhan and Medina, 2006; Zaramella *et al*., 2006). The transient storage and exchange of water in the riverbed sediment is assumed to be governed by flow-induced pressure differences over the riverbed (Wörman *et al*., 2002; Harvey *et al*., 2003; Rehg *et al*., 2005). The flow-induced pressure differences can be due to riverbed irregularities and associated waves or flood hydrographs. The waves in river flow generally have small amplitude and high frequency, while the flood hydrographs have a rapid increase associated with high pressures and slower recession. Many studies have also investigated the river–aquifer interaction resulting from different topographical features of the riverbed (Harvey and Bencala, 1993; Wroblicky *et al*., 1998; Anderson *et al*., 2005; Gooseff *et al*., 2005; Wondzell, 2006; Boano *et al*., 2007).

In the TSM the physical mechanics of transient storage are conceptually lumped into a single storage zone (Packman and Bencala, 2000; Runkel *et al*., 2003).

Kazezyilmaz-Alhan and Medina (2006) assumed in their version of the TSM that the solute concentration in the river and in the storage zone varies only along the longitudinal direction of river. The study of Zaramella *et al*. (2003, 2006) concluded that TSM did not explicitly represent the surface-subsurface water exchange. One major limitation of the TSM approach is the fact that the spatial and temporal dynamics of lateral groundwater inflow and the wide range of solute residence times are not considered.

More insights are needed into our understanding of the hydrodynamic transport in a vadose zone-aquifer-river system. Several studies show that in ephemeral rivers the groundwater flow dominates the river-subsurface flow regimes. Storey *et al*. (2003) used a three-dimensional groundwater flow model (MODFLOW) and concluded that the exchange flows are stronger, but more variable in time, at the side of a river than near the middle. Also, they revealed that vertical exchange flows below the river channel occurred more consistently than lateral flows into the banks. This study reinforced the need to represent the subsurface in a spatially distributed way. The study of Malcolm *et al*. (2004) concluded that the differences in concentrations between river and subsurface water increased with depth into the hyporheic zone, and that during low flow periods, lateral groundwater input has an increasingly dominant effect on hyporheic hydrochemistry. The study of Wondzell (2006) found that hyporheic exchange flows were little affected by river discharge, but rather influenced by the hydraulic gradients between the river and the floodplain. Consequently, there is a need for distributed modelling of the flow exchanges below the river bed and in conjunction with the lateral groundwater inflow.

To contribute to a better understanding of the linkage between the river and the surrounding aquifer, the overall goal of this study is to characterize the mass transport by hydrodynamic dispersion from the vadose zone via the hyporheic zone into the river. The specific objective is to determine a relation for the dispersion parameters so that it can be implemented in a more field-realistic model which can be applied under a wide range of spatial and temporal variable saturation and fluxes.

3.2 Theory

Transport of material conveyed by the water flow in porous media can be described by the convective-dispersion equation (CDE). The CDE in one dimension is expressed by the following partial differential equation:

$$R_f \frac{\partial C}{\partial t} = D \frac{\partial^2 C}{\partial z^2} - V \frac{\partial C}{\partial z} \qquad (3.1)$$

where $\boldsymbol{D}$ is the dispersion coefficient ($L^2\ T^{-1}$); $\boldsymbol{V}$ is the pore water velocity ($L\ T^{-1}$); $\boldsymbol{C}$ is the concentration of solute ($M\ L^{-3}$); $\boldsymbol{t}$ (T) and $\boldsymbol{z}$ (L) is the time and space coordinates; $\boldsymbol{R_f}$ is the retardation factor (dimensionless). Equation (3.1) can be solved analytically (e.g. Lindstrom *et al*., 1976) for simple geometries and numerically for more complex cases in two and three dimensions. In addition this equation can be expanded for mobile-immobile water in the soil (e.g. Šimůnek *et al*., 2003) and by sink/source terms representing local *in situ* degradation or generation. The analytical solution of CDE allows a more straightforward and parsimonious estimation for the underlying physical mechanisms for column-like situations. Alternatively, the parameters can be determined by inverse modelling using more comprehensive numerical models like HYDRUS 2D/3D (Šimůnek *et al*., 2006), which allows a more complex geometry and soil layering. At this stage it was preferred to consider only homogeneous sand and using conservative solute.

The pore water velocity refers to the average velocity of the solute plume over the travel path. It is usually expressed as the ratio between the flow rate and the volumetric water content. The hydrodynamic dispersion coefficient is often calculated as a combination of mechanical dispersion and molecular diffusion by:

$$D = V^n \lambda + D_e \qquad (3.2)$$

where $\boldsymbol{\lambda}$ represents the dispersivity (L); $\boldsymbol{n}$ is an empirical coefficient ranging between 1 and 2; $\boldsymbol{D_e}$ is the molecular diffusion ($L^2\ T^{-1}$). At usual flow conditions the mechanical dispersion is much higher than the diffusion, therefore the molecular diffusion is often disregarded and the coefficient $\boldsymbol{n}$ equals to 1 (Bear, 1972). Since a linear relation between $\boldsymbol{D}$ and $\boldsymbol{V}$ is obtained, the dispersion coefficient is primarily influenced by the pore water velocity and the dispersivity.

The dispersivity is an important parameter for determining the spreading of a definite fluid portion in porous media (Bear, 1972); it is usually described as a function of medium characteristics and water content (Nützmann *et al*., 2002; Hutchison *et al*., 2003; Toride *et al*., 2003; Costa and Prunty, 2006). Previous studies assumed that the dispersivity was a constant or an intrinsic property of soils. The study of Maraqa *et al*. (1997) reported that the dispersivity of a soil under unsaturated conditions was higher than when the soil was fully or nearly saturated. A similar result was concluded by Fesch *et al*. (1998). Padilla *et al*. (1999) concluded in their study that the dispersivity was inversely proportional to water content. Pang and Close (1999) suggested that dispersivity was a property determined by both aquifer medium and fluid dynamics. The study of Vanderborght *et al*. (2001) indicated that the dispersivity was not an intrinsic soil characteristic but depended on the flow rate and the water content in the soil profile. They also indicated that the vertical scale of experiment was influential to the solute dispersion in the soil. In contrast to other studies, Javaux and Vanclooster (2003) found in their experiment an insignificant difference in the dispersivity for different flow rates. They emphasized that the influence of non-uniform layering in the soil sample on the formation of preferential flows should not be ignored. A recent review of dispersivity given by Vanderborght and Vereecken (2007) concluded that for short vertical travel distance (0 to 30cm) that corresponds with the length of the soil column, a clear increase in dispersivity with increasing flow rate was present, however, this increase was not apparent for long travel distance (>30cm); moreover they found that the dispersivity increased when the lateral scale of the experiment increased. Their study also discussed the impact of texture and structure, but little information was given on the influence of soil water content.

The unsaturated soil water content is often characterized by the soil-water retention curve. One commonly used parameterization is by the van Genuchten (1980) curve:

$$\theta(h)=\begin{cases}\theta_r+\dfrac{\theta_s-\theta_r}{\left[1+\left|\alpha h\right|^{n^*}\right]^m} & h<0\\ \theta_s & h\geq 0\end{cases}, \qquad m=1-1/n^* \tag{3.3}$$

where $\boldsymbol{\theta}(\boldsymbol{h})$ is the soil water retention ($L^3\ L^{-3}$); $\boldsymbol{\theta_r}$ and $\boldsymbol{\theta_s}$ represent the residual and the saturated water content ($L^3\ L^{-3}$) respectively; $\boldsymbol{\alpha}$ is the inverse of the air-entry value (L^{-1}), it indicates the capacity of soil to hold water against external pressure (Patgiri and Baruah, 1995); $\boldsymbol{n}^*$ is a pore size distribution index (>1), both values are considered as empirical coefficients affecting the shape of the hydraulic functions; $\boldsymbol{h}$ is the pressure

head (L). The hydraulic conductivity in relation to the soil water retention based on the van Genuchten-Mualem model is given by:

$$K(h) = K_s S_e^{0.5}[1-(1-S_e^{1/m})^m]^2, \qquad S_e = \frac{\theta-\theta_r}{\theta_s-\theta_r} \tag{3.4}$$

where $\boldsymbol{K(h)}$ is the unsaturated hydraulic conductivity (L T^{-1}); $\boldsymbol{K_s}$ is the saturated hydraulic conductivity of soil; $\boldsymbol{S_e}$ is the effective water content ($L^3 L^{-3}$). The numerical model HYDRUS 2D/3D uses Equation (3.3) and (3.4) to specify the soil hydraulic properties (Šimůnek *et al*., 2006).

Correct interpretation of initial and boundary conditions is required for the analysis of tracer experiments. The prescribed concentration or Dirichlet boundary condition is adopted by measuring a time-dependent input concentration inside the column provided the flow is fully developed. The dimensionless column Péclet number $\boldsymbol{P_L}$, a ratio between solute convection and molecular diffusion (Bear, 1972), for a given column segment with length $\boldsymbol{L}$, is defined as:

$$P_L = \frac{VL}{D} \tag{3.5}$$

At larger column Péclet numbers (>5) the flow and transport is well developed and the choice of analytical solutions linked to boundary conditions is less critical (van Genuchten and Parker, 1984). As a result, at sufficiently high column Péclet numbers the electrical conductivity (EC) measured by Time Domain Reflectometry (TDR) can be used as a prescribed concentration at the upper boundary, and it allows the elimination of uncertainty of the nature of the inlet condition. Thus the initial and boundary condition can be set as:

Initial condition $C(z \geq 0, t)\big|_{t=0} = C_i$ (3.6)

Upper boundary condition $C(0,t) = C_0$ (3.7)

End boundary condition $\frac{\partial C}{\partial z}(\infty, t) = 0$ (3.8)

where $\boldsymbol{C_i}$ is the initial concentration; $\boldsymbol{C_0}$ is the given concentration applied to the system;

both C_i and C_0 are assumed as constant.

Mojid *et al*. (2004) developed an efficient transfer-function method based on the Wakao and Kaguei (1982) solution. A short description of the transfer-function method is given in **Appendix 1**. The impulse response in the time-domain becomes:

$$f(t) = \exp\left[-\left(1 - \frac{t}{\tau R_f}\right)^2 \Big/ 4N\left(\frac{t}{\tau R_f}\right)\right] \Big/ \left[2\tau R_f \left\{ \pi N \left(\frac{t}{\tau R_f}\right)^3 \right\}^{0.5} \right] \qquad (3.9)$$

where t is total variable time (T); τ is average travel time of the tracer, which is determined by dividing the length of travel by V; N is mass-dispersion number (dimensionless), which is the reciprocal of the column Péclet number P_L. The time-dependent estimated normalized response concentration ($C_{r.est}$) can be predicted by convoluting the input with Equation (3.9). Mojid *et al*. (2006) showed that this transfer-function method is not sensitive to the tail of the pulse and the response. Thus it is capable of accurately estimating solute-transport parameters by this method from partial breakthrough data that contains the peak of the response concentration. The detection of the end-point is therefore not as critical as that of the start point.

3.3 Material and methodology

3.3.1 Experiment setup

Soil water content and bulk electrical conductivity was monitored simultaneously by TDR. Three-rod stainless steel probes, with length of 10cm, 0.2cm in diameter, spaced 1cm apart and attached to a 200cm coaxial cable were used. Six TDR probes were connected to a Tektronix 1502B metallic cable tester via a Campbell Scientific multiplexer for consecutive scanning. During the experiments the bulk EC (S/m) and the soil moisture content (cm^3/cm^3) were continuously measured by using the WinTDR-software, Version 6.1, developed by the Soil Physics Group at Utah State University (Jones *et al*., 2002; Or *et al*., 2004).

The laboratory model focuses on studying the continuum of unsaturated zone, aquifer and river. The experimental set-up is shown in Figure 3-1. This J-shaped column model was assembled by two vertical columns in transparent Perspex (Polymethyl-methacrylate, PMMA) with two 90° elbow PVC tubes. The inner diameter

of the column was 20cm, and the height of the left and right column was 100cm and 50cm respectively. The laboratory model was supported in a frame.

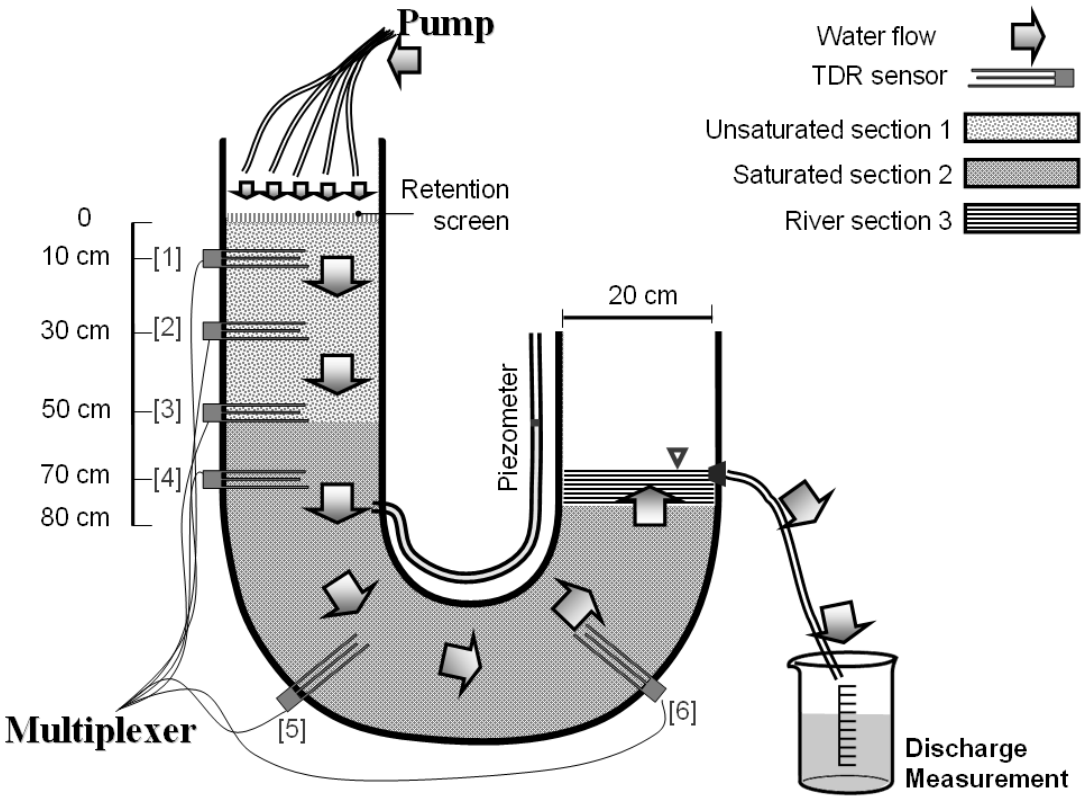


Figure 3 - 1: Experimental set-up of J-shaped model

The J-shaped model was filled with dune sand with bulk density of 1.55g/cm^3. Clean washed dune sand was preferred for this experiment as higher fluxes can be used and different flux rates can be tested within a reasonable timeframe. Additionally, homogeneous sand allows the fast attainment of steady flow conditions in the experiment. Texture analysis by sieving gave an average of 100.0%, 97.0%, 51.7%, 7.4% and 1.4% pass-rates through the 2, 0.5, 0.25, 0.1, 0.05mm sieves respectively.

Section 1 at the left hand, represents the vadose zone, which remained unsaturated. Section 2 represents the riverbed in conjunction with the adjacent aquifer, which contained the dynamic interface between the unsaturated section 1 and the constantly saturated part. A piezometer was inserted into the top of the saturated section and was connected to a flexible tube. The water levels in the piezometer were compared to the levels in section 3, which stands for the head loss along the saturated zone in section 2. The water level in section 3 at the right hand side was kept constant using an overspill

that was connected with a flexible tube.

Before the pulse-response experiment, the exact length and the impedance of all TDR-probes were calibrated by the WinTDR procedure. Information on the six probes after calibration is shown in Table 3-1.

Table 3 - 1: Calibrated length and characteristic impedance of TDR-probes

	Probe number					
	1	**2**	**3**	**4**	**5**	**6**
Length (cm), L_p	8.55	8.61	8.91	8.6	8.52	8.59
Impedance (Ω), Z_0	202.06	200.85	199.65	199.9	195.85	200.29

Three TDR-probes were inserted in the section 1 and three in section 2. The TDR-probes were numbered from 1 to 6, starting from the top of the unsaturated section and were separated by distances of 20cm, 20cm, 20cm, 30cm and 40cm respectively. Each 10 minutes, a cycle of consecutive measurements for the TDR-probes at all locations and data storage was performed.

3.3.2 Pulse-response experiments

Firstly, a steady-state water inflow was maintained by a peristaltic pump. The steady-state flux condition was also checked by observing the constant water content by TDR. The coefficient of variation (C_V) for the water content was between 0.08% and 1%. Ordinary tap water was used as “tracer-free” but had a small background EC. On top of section 1 a paper filter was placed in order to spread water uniformly over the sand. The salt tracer pulse was applied by changing the water source to the pump from tap water to the potassium chloride (KCl) solution, which was equivalent to a surface application rate of 1.5×10^{-3}g/cm^2. The pulse duration was 30 minutes while maintaining the same pumping speed before, during and after the pulse application to ensure a constant pore water velocity. Four different flux conditions (i.e. 0.5cm/hr, 1cm/hr, 1.5cm/hr and 2cm/hr) were applied. The transport of the solute per segment, 5 in total, was characterized by monitoring the change in EC at the inlet and outlet of each segment.

3.3.3 Data analysis

The EC of the soil solution was calculated from the TDR-measured bulk soil EC via a physically based model developed by Mojid *et al*. (2007). The background EC was firstly subtracted from the measured EC responses in order to obtain the increase in EC due to the tracer. The start and the end of a response were determined by a simple and automatic algorithm. The slopes of adjacent EC data over the time step were calculated. The start of rising slope was identified by exceeding a specified minimum value. The slope was taken sufficiently high and the start was set 3 time intervals before the exceedance of the minimum slope. The EC-level just before the start was also set as the background EC. In this way the algorithm was robust and avoided the false start of a response caused by fluctuation in background EC. The end of a response was set either when the background EC was reached or after a specified maximum duration. Whichever came first was taken as the end, and in most cases the end of a response was determined because the background EC had been reached. The EC values after subtraction of the background were summed over the duration. By dividing the EC values by this sum, normalized relative EC values were obtained with sum equal to 1. The normalization also avoided problems due to variation in water content. Imposing the same sum to all response ensures a conservation of the tracer.

Equation (3.9) was fitted to the pulse-response normalized EC-data. For every segment the signal at the upstream inlet was taken as the input ($\boldsymbol{C_{in}}$) while the signal at the downstream outlet was taken as the response ($\boldsymbol{C_r}$). Pore water velocity and dispersion coefficient were determined for each segment. The method was implemented in the R software, which is a flexible open source and analysis free software under General Public License (GPL). Although R is meant as a language and environment for statistical computing and graphics, it is flexible and allows writing tailor-fitted analysis so that it can be extended through desired packages for specific purposes (Dalgaard, 2004). The automatic calibration was executed by parameter search algorithms available in R. The code is given in **Appendix 2**.

3.3.4 Testing by HYDRUS 2D/3D

HYDRUS 2D/3D provides a numerical multi-dimensional solution to the transport equations under variable saturated conditions. It solves the Richard's equation for water flow and solves the CDE for solute and heat transport. The simulation can be displayed

graphically and animation can be shown. The HYDRUS program uses Marquardt-Levenberg optimization algorithm for the inverse estimation of soil hydraulic and solute transport parameters. The simulation results for nodes of the mesh can be stored for comparison to the measurements.

A 2-D vertical plane was created to represent the geometry of the J-shaped model in Figure 3-1. The initial and boundary conditions were set according to the experimental set-up and pulse-response experiment procedures. Each TDR probe was compared to a node in the finite element mesh corresponding to the middle of the probe that represents an average in space. For probe No. 5 and 6 in the bend we also checked extra nodes between the start and the end of the probe.

The simulation started with the establishment of steady state water flux condition with a low background concentration. Then during the pulse-time of 30 minutes the tracer concentration was supplied, after which the water inflow with the same low background concentration as before the pulse was used. The simulated concentrations were normalized after subtraction of the background level in the same way as the EC-measurements.

Inverse modelling was performed by using the measured relative EC data from the pulse-response experiment to estimate the soil longitudinal dispersivity. Subsequently the result by inverse modelling was compared with direct simulation using the longitudinal dispersivity on segments derived from the obtained transport parameters relation. Pore water velocity was calculated by HYDRUS and then the longitudinal dispersivity at each segment was specified according to Equation (3.2) with dispersion coefficient determined from the obtained transport parameters relation. Equation (3.2) was used while neglecting the molecular diffusion and setting the empirical coefficient $n = 1$. The value of the transversal dispersivity in this simulation was set as 1/10 of the longitudinal dispersivity. Setting transversal dispersivity at 1/20 of the longitudinal dispersivity and zero transversal dispersivity were also tested for checking the parameter sensitivity.

3.4 Results and discussion

3.4.1 Measured and estimated breakthrough data

The majority of the measured and estimated response curves ($\boldsymbol{C_r}$ and $\boldsymbol{C_{r.est}}$) at each segment under different flux conditions indicated a good fit. Coefficients of determination R^2 are very high for almost all segment calculations (majority shows from 0.97 to 0.99). Except to the experiment with water flux of 1cm/hr from probe No. 3 to 4 the response had a shorter duration than the input, which is inconsistent with the dispersion process. Figure 3-2 shows an example of the fitting between the measured and estimated response curves in segment 4 from probe No. 4 to 5 in flux of 0.5cm/hr. The results of the pulse-response curves fitting in different segments and different flux conditions are illustrated in **Appendix 3**.

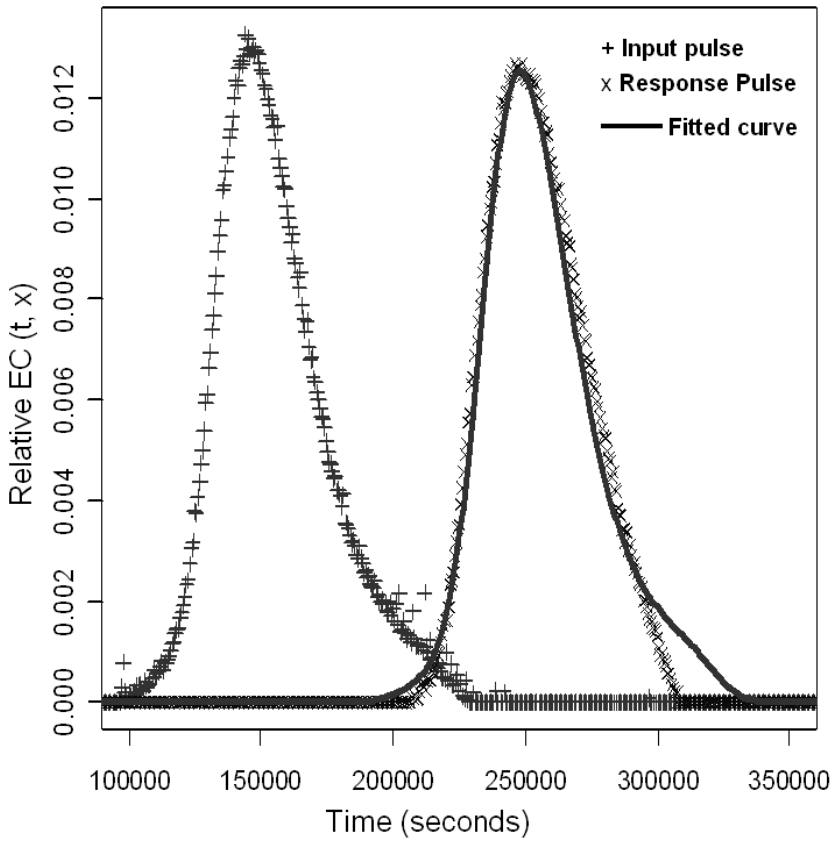


Figure 3 - 2: Example of fitting between the measured and estimated response curves in segment 4 from probe No. 4 to 5 in the flux of 0.5cm/hr

Table 3-2 summarizes the transport parameters obtained from analysing the laboratory experiments by the transfer-function on the segments between probes.

Table 3 - 2: Solute-transport parameters for coarse dune sand with four water flux conditions and with concentration in 1.5g/L of the applied pulse of potassium chloride (KCl) for 30 minutes input. Pore water velocity (*V*) and dispersion coefficient (*D*) are determined by the transfer-function method fitted on individual segments (Mojid *et al*., 2004)

Flux					**Estimated transport parameters**			
q	***Segment***	***l***	θ_v	τ	***V***	***D***	P_L	λ
cm/hr	-	cm	cm^3/cm^3	hr	cm/hr	cm^2/hr	-	cm
0.5	No.1 to 2	20	0.207	4.47	4.478	9.211	9.72E+00	2.06E+00
	No.2 to 3	20	0.278	19.02	1.050	0.398	5.27E+01	3.79E-01
	No.3 to 4	20	0.378	10.27	1.885	0.500	7.54E+01	2.65E-01
	No.4 to 5	30	0.433	28.26	1.061	0.017	1.90E+03	1.58E-02
	No.5 to 6	40	0.420	55.45	0.718	0.007	3.93E+03	1.02E-02
1	No.1 to 2	20	0.200	2.61	7.676	7.254	2.12E+01	9.45E-01
	No.2 to 3	20	0.251	10.43	1.903	1.266	3.01E+01	6.65E-01
	No.3 to 4	20	0.379	6.83	2.958	0.182	3.25E+02	6.16E-02
	No.4 to 5	30	0.437	15.57	1.927	0.176	3.28E+02	9.14E-02
	No.5 to 6	40	0.419	31.45	1.272	0.069	7.42E+02	5.39E-02
1.5	No.1 to 2	20	0.217	2.10	9.530	8.403	2.27E+01	8.82E-01
	No.2 to 3	20	0.264	7.45	2.669	0.198	2.69E+02	7.43E-02
	No.3 to 4	20	0.382	4.73	4.151	0.366	2.27E+02	8.81E-02
	No.4 to 5	30	0.438	9.35	3.375	0.224	4.53E+02	6.62E-02
	No.5 to 6	40	0.419	20.78	1.925	0.071	1.08E+03	3.70E-02
2	No.1 to 2	20	0.208	1.20	16.719	1.390	2.41E+02	8.31E-02
	No.2 to 3	20	0.256	6.52	3.067	0.509	1.20E+02	1.66E-01
	No.3 to 4	20	0.386	3.50	5.722	0.008	1.38E+04	1.44E-03
	No.4 to 5	30	0.441	8.89	3.375	0.311	3.26E+02	9.20E-02
	No.5 to 6	40	0.421	18.15	2.206	0.070	1.26E+03	3.18E-02

q, water flux (cm/hr); *l*, vertical distance between adjacent probes (cm); θ_v, average soil water content (measured by TDR) (cm^3/cm^3); τ, mean travel time of solute (hr); *V*, pore water velocity (cm/hr); *D*, dispersion coefficient (cm^2/hr); P_L, column Péclet number (dimensionless) for each segment; λ, dispersivity (cm).

3.4.2 Solute transport parameters by fitting the transfer function on segments

As shown in Table 3-2, the average water content between adjacent probes for each segment was different. In addition, water content varied as expected with the flux imposed. The elevation of the piezometric surface as measured by the piezometer increased in function of the flux and was located between the probes No. 3 and 4. The section delineated above the probe No. 3 was always unsaturated. All segments downstream of probe No. 4 were always saturated. As shown in Figure 3-3 at the unsaturated vertical section (probe No. 1 to 3) the average water contents were less than 30%, and the water contents in the saturated section (probe No. 3 to 6) varied between 37 and 44%, in accordance to the porosity range of the coarse sand (35% to 40%).

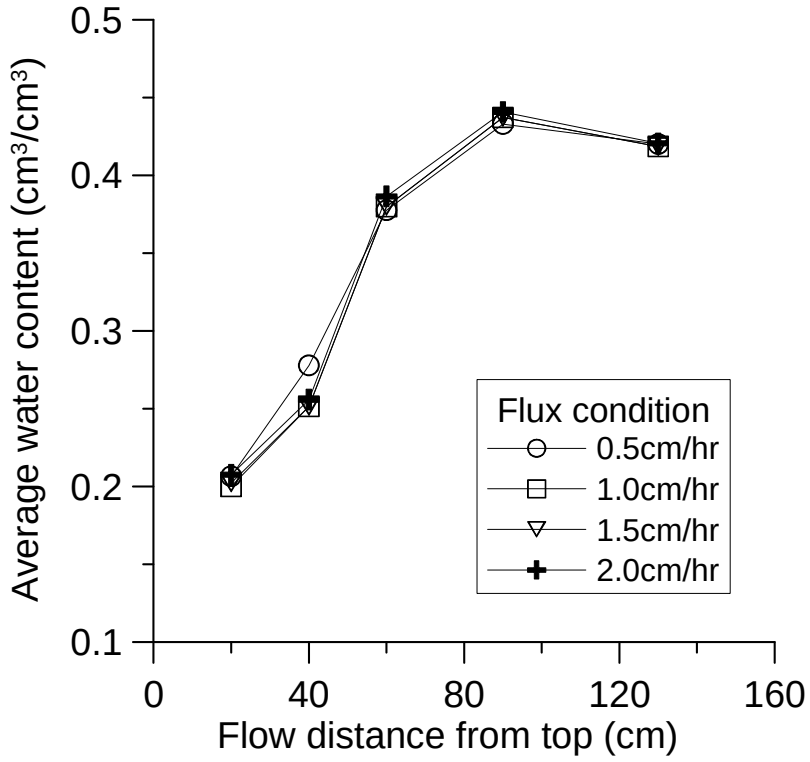


Figure 3 - 3: Average water content (θ_v) along the center of the model in different fluxes

Figure 3-4 illustrates the distribution of the estimated pore water velocity along the model in different flux conditions. As expected the measured pore velocities were much higher in the unsaturated segment of probe No. 1 to 2 (at 20cm depth) and resulted in faster breakthrough, as the water content is lower and hence the water filled pore space is less. The lower values in the segment of probe No. 2 to 3 (at 40cm depth) were possibly related to the layering of the soil sample. This is likely to be caused by a different packing of the sand in that segment. The pore-water velocity decreased dramatically in the saturated section, and the measured dispersion coefficients varied accordingly (Bear, 1972; Perfect *et al*., 2002).

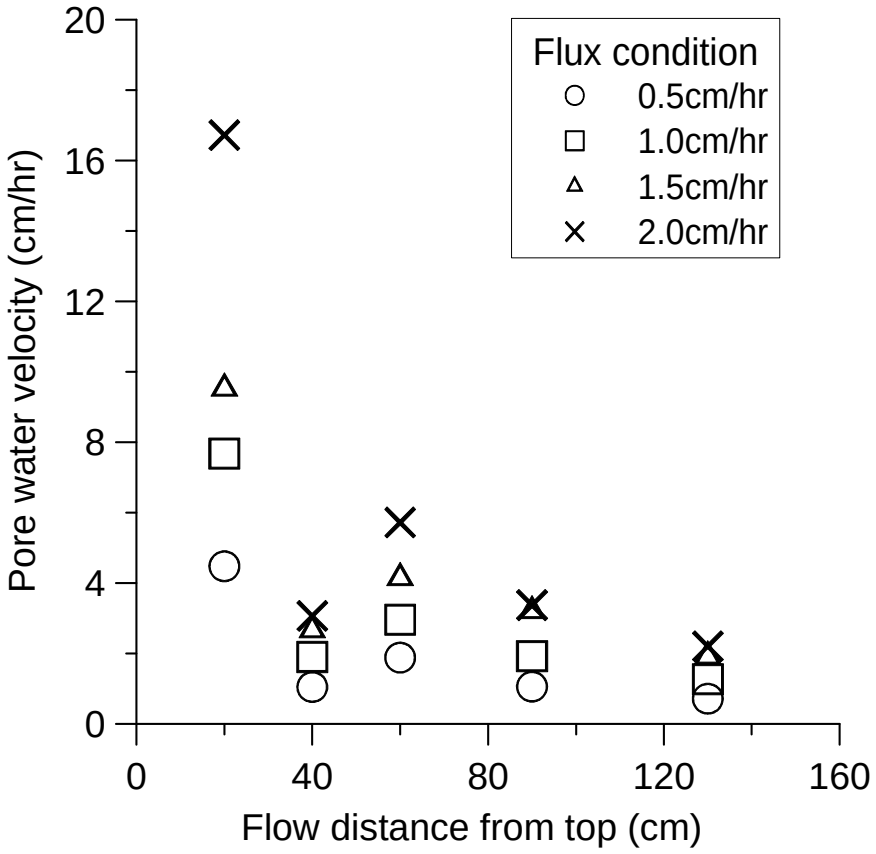


Figure 3 - 4: Pore-water velocity along the center of the model in different fluxes

As defined by Equation (3.2), dispersivity was calculated as the dispersion coefficient divided by the pore water velocity, hereby neglecting the molecular diffusion effect and taking empirical coefficient n = 1. Most calculated dispersivities in our experiments were smaller than 1cm, except for the extreme high value measured at the beginning of

the experiment. The values of dispersivity are shown as a function of the volumetric water content in Figure 3-5. It was observed that the variation in dispersivity as a consequence of the different applied flux conditions decreased as the soil water content increases. Similar result was also reported by Maraqa *et al*. (1997) and Hutchison *et al*. (2003). For lower flux conditions the flow path in the unsaturated section was more tortuous and solute transport was restricted to a smaller part of the soil matrix. Consequently, the dispersivity in the unsaturated section was much greater than that in the saturated section. When increasing the water flux a reduction of tortuosity occurred and the mean travel time of solute reduced. In this case, a lower dispersivity in the unsaturated section was observed. The dispersivities for the segments under the saturated conditions were fairly constant and independent of the water flux.

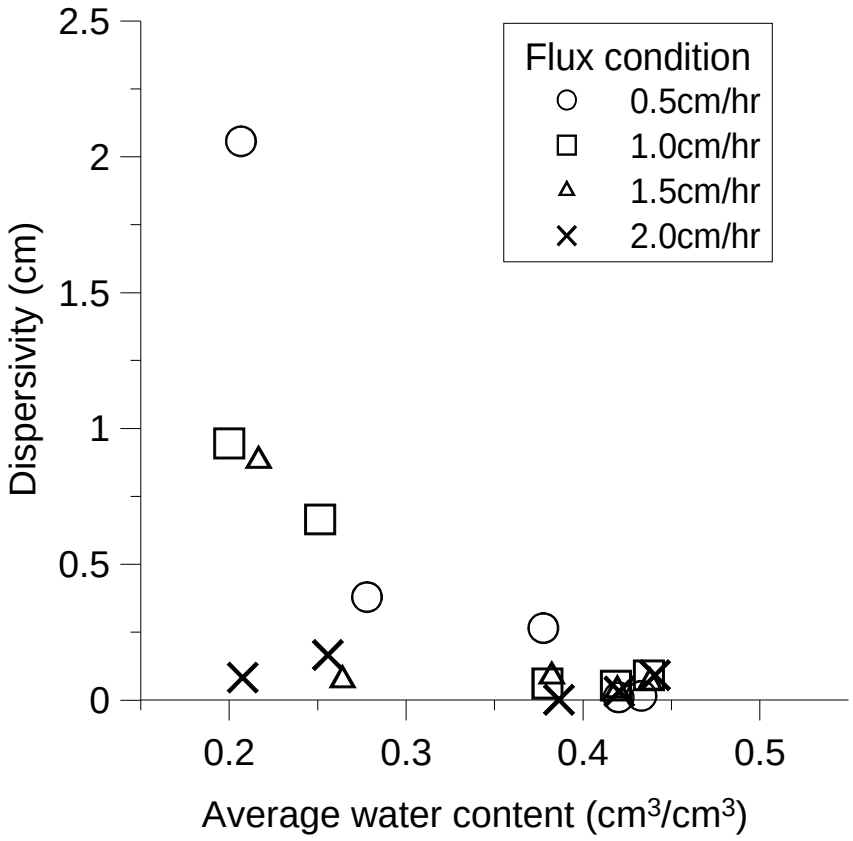


Figure 3 - 5: Dispersivity (λ) as a function of volumetric water content (θ_v)

Figure 3-6 shows the values of dispersivity as a function of pore-water velocity. It shows that in the unsaturated section of probe No. 1 to 2 dispersivity decreased as pore water velocity increased, and in the saturated sections of probe No. 4 to 5 and No. 5 to

6 the dispersivity did not respond to a change in pore water velocity. This situation was also reported by Toride *et al*. (2003). Their study observed the occurrence of considerable tailing of breakthrough curves (BTC) for unsaturated flow. Similarly in our experiment larger dispersivities were observed in the unsaturated soil section as compared to the saturated soil section. For lower fluxes condition the tailing effect of breakthrough curve was not distinct. For higher fluxes the tailing was much more pronounced, especially in the unsaturated section (i.e. at probe No. 1 to 2). The measurements for the unsaturated section of probe No. 2 to 3 did not perform similarly to the probe No. 1 to 2. This could be again attributed to the effect of layering caused by different packing of the sand in that segment.

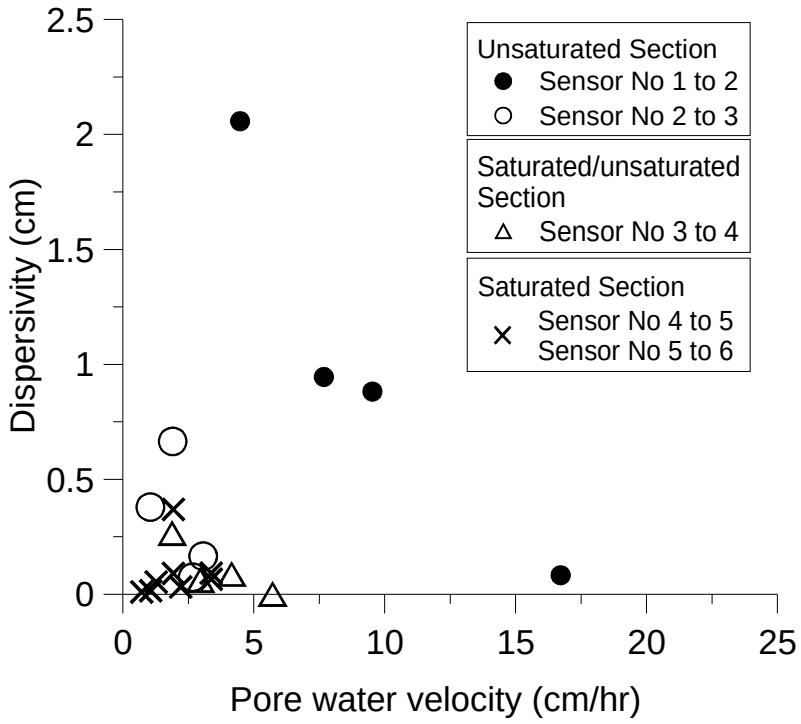


Figure 3 - 6: Dispersivity (λ) variation as a function of pore water velocity (*V*)

In order to simulate over the entire range of fluxes and water contents as present in the continuum of unsaturated zone, aquifer and river, a more general relationship was identified. After exploring several possibilities the best result was obtained by plotting a log-log scale the solute dispersion coefficient against the ratio of pore water velocity over water content as shown in Figure 3-7.

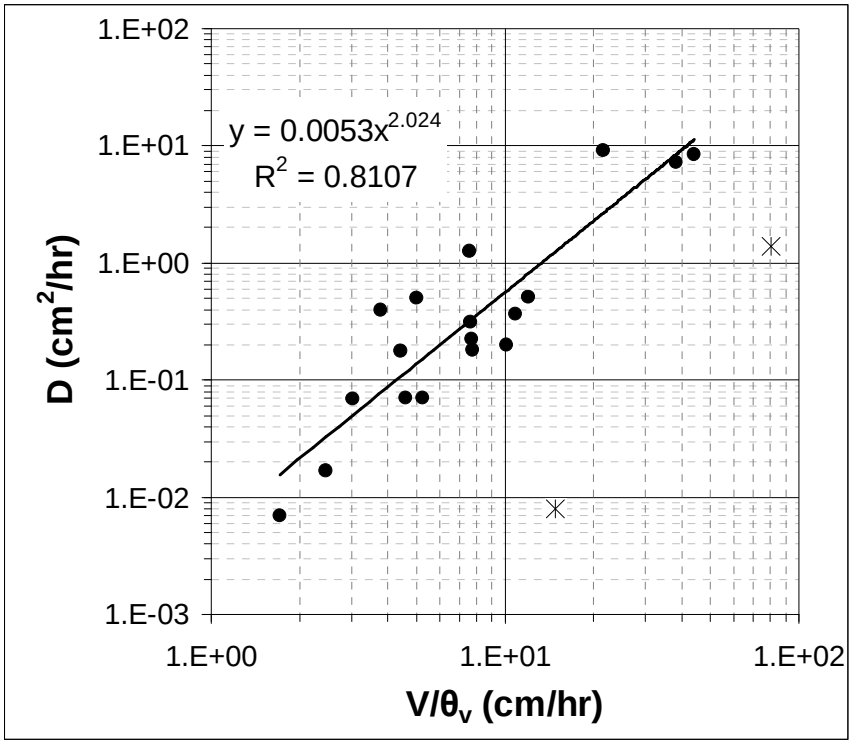


Figure 3 - 7: Log-log relationships between solute dispersion coefficient (*D*) and ratio of pore water velocity to water content (V/θ_v); two outliers (*) are not included into relation

This relation was similar to the empirical power law shown by Padilla *et al*. (1999). They compared their data to earlier findings (e.g. those by De Smedt and Wierenga, 1984) and also proposed a log-log relation between the dispersion coefficient and the ratio of pore water velocity over water content. The following equation fitted the data of our study:

$$D = 0.0053\left(V/\theta_v\right)^{2.02} \tag{3.10}$$

The coefficients in Equation (3.10) are soil specific. During the fitting we excluded 2 outliers. The two outlier data are in the unsaturated section of segment between probe No. 1 and 2 and segment between probe No. 3 and 4 of flux = 2cm/hr. The measured dispersivities are relatively low when compared with the data of the same segment in other fluxes. The study of Padilla *et al*. (1999) used silica sand as material and they found 1.99 as the power coefficient for their data, which is very close to our value of 2.02. This equation accounts for the fact that the dispersivity of the porous medium depends on both pore water velocity and soil water content. A relation between the dispersion parameter, water flux and the soil water content is required for simulating

the transport of solutes and other substances in the environment which is imbedded by saturated and unsaturated zones.

3.4.3 Numerical simulation by HYDRUS 2D/3D

To the numerical simulation by using HYDRUS 2D/3D, inverse modelling was first performed by using the measured relative EC data from the pulse-response experiment to estimate the soil longitudinal dispersivity. Initial results showed an anomaly due to different packing of sand in the segment between probe No. 2 and 3, in which the transport was much slower than the adjacent segments. This anomaly can be improved by changing the parameter α in the soil water retention function for segment between probe No. 2 and 3, the shape of the soil water retention curve according to van Genuchten (1980) and the hydraulic conductivity was modified in that segment, which made it possible to simulate this phenomenon. This result indicated that the parameter α in the soil water retention function has a very important effect on the solute transport. The use of "default characteristics" and pedotransfer functions in HYDRUS should therefore be used with caution when comparing to real soils or porous media.

The inverse modelling was therefore performed by optimizing two parameters: λ_1, the longitudinal dispersivity for the region before probe No. 2 and after No. 3 with α = 0.145, and λ_2, the longitudinal dispersivity for the segment between probe No. 2 to 3, in which α was set as 0.03. Results of parameters optimization in different fluxes are summarized in Table 3-3. The comparison of the measured relative EC (open circles) and the simulated results from inverse modelling (full line) is given in Figure 3-8, 3-9, 3-10 and 3-11. Initial runs by HYDRUS 2D/3D suffered instabilities leading to negative concentrations and oscillating tails of the responses. Also the simulation of the last probes showed initially a slow increase and a fast recession followed by numerical oscillation. The discretization was therefore reduced to 0.5cm for the vertical section and 0.3cm for the bend section as finite element size. However, this led to excessive long computational times. For inverse modelling, which requires iteration, this resulted in several days on a PC for one flux condition only.

The decrease of longitudinal dispersivity for the region before and after probe No. 2 and 3 (λ_1) was found as flux increased from 0.5cm/hr to 1cm/hr, subsequently an increase was found as flux increased from 1cm/hr to 2cm/hr. The variation of dispersivity (λ_2) in the segment where the layering of soil occurred followed a different pattern. The inverse modelling showed that longitudinal dispersivity is a variable in function of water flux, which is especially important for the porous media under

variably saturated conditions.

Table 3 - 3: Optimal parameters of dispersivity by inverse modelling with HYDRUS 2D/3D

Flux	**Information about the fitted parameters**			
q	λ_1	λ_2	r^2	**Mass balance error**
cm/hr	cm	cm	-	%
0.5	1.54	0.23	0.86	0.590
1.0	1.19	1.43	0.68	0.342
1.5	1.61	0.51	0.66	0.252
2.0	4.69	1.04	0.44	0.191

q, water flux (cm/hr)

λ_1, longitudinal dispersivity (cm) for the region before and after probe No. 2 and 3 with $\alpha = 0.145$;

λ_2, longitudinal dispersivity (cm) for the segment between probe No. 2 to 3 with $\alpha = 0.03$.

r^2, coefficient of correlation

Subsequently the result by inverse modelling was compared with direct simulation using the longitudinal dispersivity on segments derived from the obtained transport parameters relation. To the simulation by using the power relationship among dispersion coefficient, pore water velocity and water content (Equation 3.10 in this study), different longitudinal dispersivities were specified for each segment between adjacent probes. The timing of the resulting simulated responses corresponds well with the measured ones. In the bend different velocities were simulated: slower at the outer side and faster at the inner side. One hypothesis was that this was due to transversal dispersivity between layers with different convective velocities. A sensitivity analysis using different values for relative transversal dispersivity, including zero transversal dispersivity did not show any visible difference between the simulations.

The comparison of the simulated results from inverse modelling (full line) and directly using Equation (3.10) on individual segment (dash line) can be seen in Figure 3-8, 3-9, 3-10 and 3-11. Three over four simulations by using the equation for dispersion coefficient based on segments presented better correlation than the simulation by fitting dispersivities. For the lowest flux the inverse modelling delivered better results.

The fact that inverse modelling delivered a range of dispersivities in function of the flux illustrates that the classical Equation (3.2) should be used with caution in circumstances with variably saturated conditions. The fitting of dispersion coefficients on individual segments was lot more straightforward and allows a generalization after exploratory study of the possible relations.

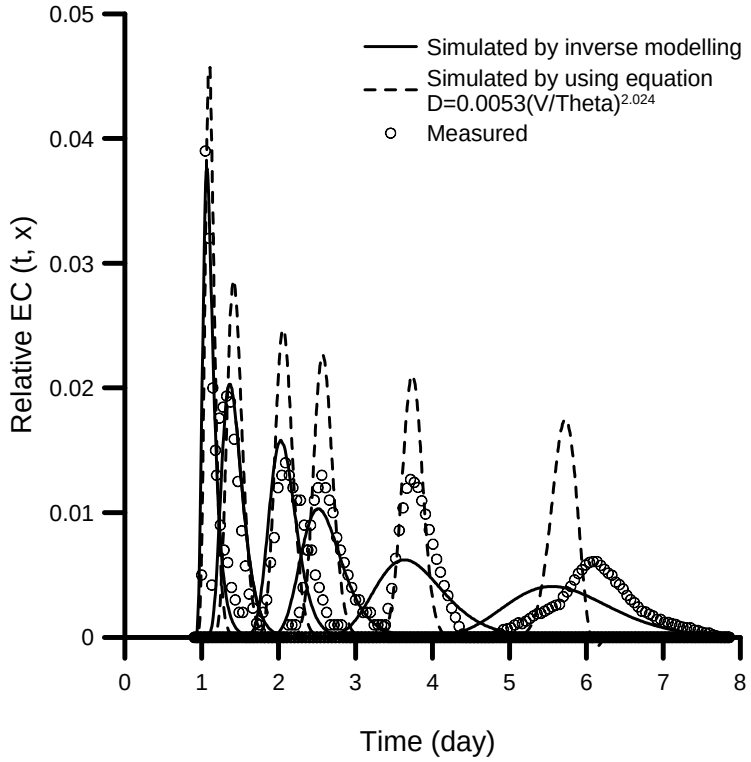


Figure 3 - 8: Comparison of the measured relative EC (open circles) with the simulated results from inverse modelling (full line) (r^2 = 0.68) and directly using the equation for dispersion coefficient based on segments (dash line) (r^2 = 0.72) in flux of 0.5cm/hr

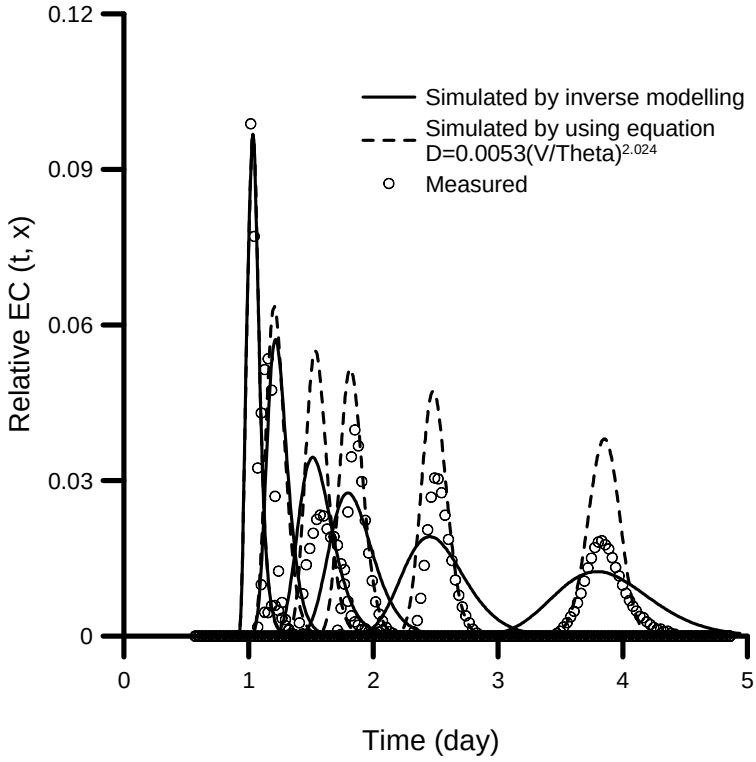


Figure 3 - 9: Comparison of the measured relative EC (open circles) with the simulated results from inverse modelling (full line) (r^2 = 0.86) and directly using the equation for dispersion coefficient based on segments (dash line) (r^2 = 0.72) in flux of 1.0cm/hr

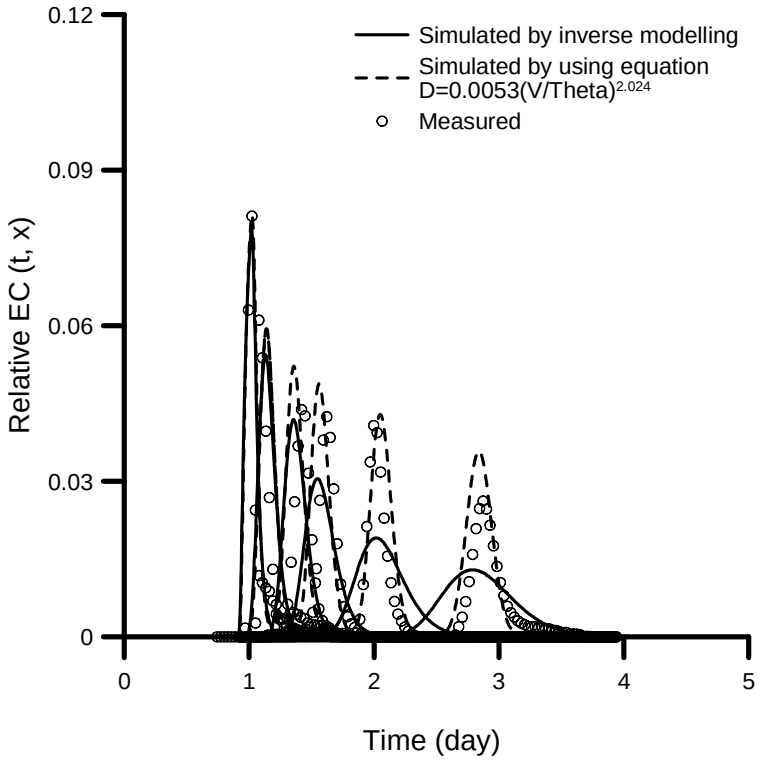


Figure 3 - 10: Comparison of the measured relative EC (open circles) with the simulated results from inverse modelling (full line) (r^2 = 0.66) and directly using the equation for dispersion coefficient based on segments (dash line) (r^2 = 0.72) in flux of 1.5cm/hr

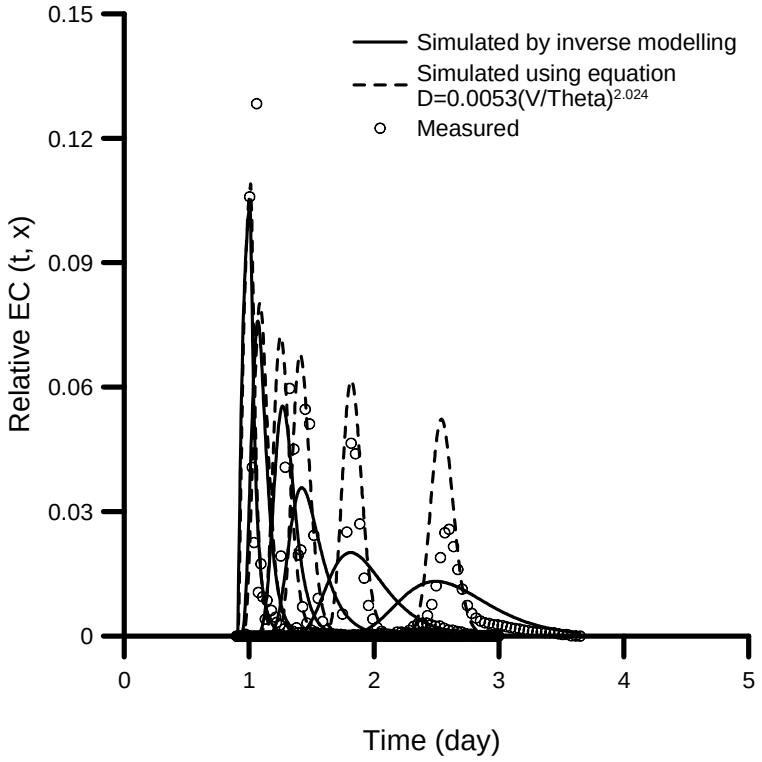


Figure 3 - 11: Comparison of the measured relative EC (open circles) with the simulated results from inverse modelling (full line) (r^2 = 0.44) and directly using the equation for dispersion coefficient based on segments (dash line) (r^2 = 0.50) in flux of 2.0cm/hr

3.5 Conclusions and recommendations

The characterization of the lateral groundwater inflow from the aquifer to the river contributes to a better insight of riverbed-aquifer flux interactions. In order to investigate the physical processes and characteristics of lateral groundwater inflow, a laboratory J-shaped column experiment was designed in this study. This J-shaped column model represents a schematic flow line in the succession of unsaturated recharge zone, saturated zone (aquifer) and river. Soil moisture contents along the model were determined by time domain reflectometry (TDR). The hydrodynamic dispersion transport parameters in consecutive column segments were determined via the transfer function method proposed by Mojid *et al*. (2004) by performing pulse-response experiments. The relationship between dispersivities and other physical measurement were determined.

The conclusions and recommendations from this experiment are:

1. The dispersivity is flux dependent and increases at lower flux in unsaturated section (i.e. in vadose zone); in contrast, dispersivity is fairly constant and independent of flux variations in saturated sections (i.e. in riverbed in conjunction with the adjacent aquifer).

2. The longitudinal dispersion coefficient can best be related to the ratio of pore-water velocity over soil water content. This obtained relation can be performed over the range of saturated and unsaturated conditions, and it appears similar to the earlier findings. This relation was tested by numerical simulation using HYDRUS 2D/3D and it presented a better correlation than the inverse modelling by fitting dispersivities.

3. The shape of the soil water retention curve has an important impact on the pore water velocity, and has consequence on the dispersion coefficient. The parameter $\boldsymbol{\alpha}$ controlling the shape of the soil water retention curve should be given sufficient attention when evaluating the hydrodynamic dispersion transport parameters in a variably saturated environment.

4. More systematic research and sensitivity analysis is needed to formulate relationships for longitudinal dispersivity with real soils or porous media under the variably saturated conditions.

Chapter 4

Can temperature be used as a tracer to estimate fluctuating water fluxes in the riverbed? A laboratory study*

Abstract

Temperature differences have been widely applied as a tracer in the study of groundwater-surface water interaction. Measuring temperature with thermocouples is cheap, easy to log with a high time resolution and can be installed with great precision in a small volume of the flow domain. Most studies using temperature as a groundwater tracer have been carried out based on the assumption of a steady-state water-flux, or an approximation as quasi steady-state, but the transient hyporheic exchange patterns have not been studied to the same extent. There are no analytical solutions available for transient heat transfer in transient water flow conditions.

A laboratory J-shaped column experiment has been developed in this study to explore the possibility of estimating the transient water fluxes in the riverbed with temperature. This laboratorial model schematises a stratified succession from the vadose zone over the aquifer to the river. A steady state water flow through the model was first established by a peristaltic pump, then a step-wise rise and fall of the water level was induced at the river section simultaneously with a change in water temperature. The square shaped "hydrograph" altered the vertical hydraulic gradient, thus reversing the flow direction in the riverbed. Changes in water temperature caused variations in hydraulic conductivity of the riverbed. By validation with measured temperatures, the numerical model HYDRUS was calibrated to simulate the transient water flow conditions in the riverbed.

* Adapted from Chou PY, Van Nieuwenhuyse BHJ, Wyseure G. 2009. Can temperature be used as a tracer to estimate fluctuating water fluxes in the riverbed? A laboratory study. *Submitted to Hydrological Processes*

4.1 Introduction

The hyporheic zone is the part of a riverbed where river water and groundwater are exchanged. The exchange of fluxes influences the transport of nutrients, oxygen and other important elements between river and aquifer. Hence, the hyporheic zone plays an important role in the water quality and diversity of aquatic ecosystem (Brunke and Gonser, 1997; Dent *et al*., 2000; Hancock *et al*., 2005).

The accurate characterisation of the extent of the hyporheic zone is important but challenging. Use of tracers is an option; however, sampling inside the riverbed is labour-intensive, destructive and hard to execute within small distances. The water flux's dynamics in the hyporheic zone are driven by water-level changes and associated pressure differences over the riverbed. It is a transient phenomenon that closely relates to the catchment's rainfall-runoff processes. Biksey and Gross (2001) indicated that the extent of flux exchange in the riverbed is a function of the river-stage fluctuations and the groundwater flow towards the river. The fundamental hydraulic mechanisms which drive the transient exchange of fluxes in the hyporheic zone have been tested in laboratory scale experiments (Elliott and Brooks, 1997; Marion *et al*., 2003; Tonina *et al*., 2007) and also in the field (Harvey and Bencala, 1993; Rodgers *et al*., 2004; Cardenas and Wilson, 2007; Stofleth *et al*., 2008). However, in most experiments the lateral groundwater inflow and outflow were not reckoned with.

Temperature is an important ecological variable (Hayashi and Rosenberry, 2002; Hahn, 2006; Barlocher *et al*., 2008). Groundwater usually has a relatively stable thermal regime in comparison with the regime of surface water which is influenced by meteorological conditions and human activities resulting in a diurnal and seasonal temperature oscillation. This drives a continuous change of temperature in the riverbed (Silliman *et al*., 1995; Ronan *et al*., 1998; Keery *et al*., 2007). The study of Constantz and Thomas (1996) demonstrated that the dynamics of surface runoff are reflected in the variation of temperature gradients in the riverbed. As reviewed by Constantz and Stonestrom (2003), different subsurface temperature-depth profiles were found depending on whether the river is influent or effluent to the surrounding. In general, the riverbed's thermal profile in a water losing portion of the river reflects the pattern of temperature fluctuation in the river, in contrast to a gaining portion where the groundwater temperature is dominated by the riverbed temperature. Accordingly, zones of groundwater recharge and discharge can be distinguished by the investigation of riverbed thermal profiles.

Numerous methods were developed to characterise temperature profiles across riverbeds (Anderson, 2005). Measuring temperature with thermocouples is relatively easy, cost-effective and allows a high spatial and temporal resolution. Hence, the

application of temperature monitoring as a natural tracer in environmental research is a logical and economic choice (Taniguchi *et al*., 2003a, b; Burow *et al*., 2005; Ferguson and Woodbury, 2005). A comparison between heat and conservative tracers in groundwater studies was discussed by Constantz *et al*. (2003a) and Cox *et al*. (2007). They recommended to combine analyses of heat and conservative tracers in order to provide more hydrologic insight into the interaction of groundwater and river water.

Most studies using temperature as a groundwater tracer try to estimate long-term average fluxes, which are based on diurnal or seasonal temperature measurements, but transient hyporheic exchange flows which are difficult to interpret by analysis of diurnal or seasonal temperature measurements, have not been studied to the same extent. The study of Constantz *et al*. (2003b) revealed that the transient water fluxes in the riverbed caused by ephemeral surface flow events lead to a rapid temperature decline in the riverbed. Hoehn and Cirpka (2006) also suggested that the assessment of rapid temperature fluctuations induced by flash floods could provide more accurate evaluation of the penetration of river water into the riverbed and the surrounding aquifer. In this study, we aim to investigate whether temperature measurements can be used to estimate transient hyporheic exchange flows in the riverbed. A laboratory model is used to explore the technique. As there are no analytical solutions available for transient heat transfer in transient water flow conditions, the numerical model HYDRUS was used to simulate the penetrating fluxes of river water for different scenarios of river-stage rising and groundwater inflow.

4.2 Theory

The thermal profile in the riverbed is determined by the combination of conduction due to thermal gradients and convection associated with water flux. The governing partial differential equation (PDE) expressing one-dimensional heat transfer through saturated sediment with vertical water flow is:

$$\frac{\partial T}{\partial t} = D_T \frac{\partial^2 T}{\partial z^2} - q \frac{C^*_w}{C^*_B} \frac{\partial T}{\partial z} \tag{4.1}$$

where $\boldsymbol{T}$ is temperature (K); $\boldsymbol{t}$ is time (T); $\boldsymbol{z}$ is the vertical depth (L) below the riverbed surface, the latter defined as $\boldsymbol{z} = 0$; $\boldsymbol{q}$ is the specific discharge ($L\,T^{-1}$) in the $\boldsymbol{z}$ direction; $\boldsymbol{D_T}$ is the effective thermal diffusivity ($L^2\,T^{-1}$); $\boldsymbol{C^*}$ is the volumetric heat capacity ($M\,L^{-1}T^{-2}\,K^{-1}$), which can also be defined as the product of density, $\boldsymbol{\rho}$ ($M\,L^{-3}$), and specific heat, $\boldsymbol{c}$ ($L^2\,T^{-2}\,K^{-1}$); the subscripts $\boldsymbol{B}$ and $\boldsymbol{w}$ denote the bulk sediment matrix and its liquid phase, respectively. The first term at the right hand side of Equation (4.1) represents the transport of heat by conduction and the second term by convection, associated with the flux of water at different temperatures. Solving this PDE requires boundary and initial conditions.

The riverbed is a saturated porous medium in which the volumetric heat capacity can be estimated as:

$$C^*_B = \theta C^*_w + (1-n_e) C^*_s \tag{4.2}$$

where $\boldsymbol{\theta}$ represents the volumetric fraction of bulk porous medium ($L^3\,L^{-3}$); $\boldsymbol{n_e}$ is the porosity ($L^3\,L^{-3}$); and the subscript $\boldsymbol{s}$ denotes the solid phase of the porous medium.

The effective thermal diffusivity in Equation (4.1) incorporates the effects of heat conduction by random molecular motion through the solid and liquid phase of the sediment, as well as the hydrodynamic dispersion of temperature caused by microscopic velocity variation within the pore spaces (Anderson, 2005; Hoehn and Cirpka, 2006; Mortensen *et al.*, 2006). The effective thermal diffusivity can further be described by:

$$D_T(\theta) = \frac{\kappa(\theta)}{C^*_B} + q\lambda_T \frac{C^*_w}{C^*_B} \tag{4.3}$$

where $\boldsymbol{\kappa}$ is the thermal conductivity (M L $T^{-3}K^{-1}$) of the porous medium and $\boldsymbol{\lambda_T}$ the thermal dispersivity (L). It can be seen from Equation (4.3) that the effective thermal diffusivity $\boldsymbol{D_T}$ is compounded of the effect of thermal conduction in the sediment matrix and the effect of thermal dispersion caused by velocity variation. The second term at the right hand side of Equation (4.3) becomes negligible when the water flux is minimal or zero when absent. The thermal grain Peclet number ***Pe*** gives an indication of the relative importance of these two terms.

$$Pe = \frac{C^*_w qL}{\kappa(\theta)} \tag{4.4}$$

where ***L*** represents the characteristic length. The thermal conductivity $\boldsymbol{\kappa}$ in a porous medium partially saturated with water is a function of mineral type, geometrical arrangement, as well as water content (Hopmans *et al*., 2002; Šimůnek *et al*., 2006) and can be estimated by:

$$\kappa(\theta) = b_1 + b_2\theta + b_3\theta^{0.5} \tag{4.5}$$

where $\boldsymbol{b_1}$, $\boldsymbol{b_2}$ and $\boldsymbol{b_3}$ are soil specific empirical parameters (M L $T^{-3}K^{-1}$).

If a PDE like Equation (4.1) has constant coefficients, then superposing in analytical solutions is possible for some geometries and boundary conditions. For steady-state water flux, i.e. for constant ***q***, the analytical solution derived by Stallman (1965) is widely accepted in literature. As a top boundary condition a regular sinusoidal fluctuation of the temperature at the top of the riverbed is then assumed.

For varying flux ***q***, the solution of the PDE requires a numerical scheme. A widely used numerical model in variably saturated porous media is HYDRUS (Šimůnek *et al*., 2006). This finite element model solves the Richard's equation for water flow simultaneously with the convection-dispersion equations for solute and heat transfer. The 2D/3D version has a finite element mesh generator for irregular flow domains and can handle a wide variety of boundary and initial conditions. HYDRUS provides default empirical parameters for the expression of the thermal conductivity function (Equation 4.5) and for the volumetric heat capacity of the solid phase, organic matter and liquid phase or they can be specified by the user. In addition, transport parameters

can be estimated from measured variables by inverse modelling.

The hydraulic conductivity is a function of the intrinsic permeability of the porous medium and of the density and viscosity of water:

$$K_s = \frac{k_i \times g \times \rho_w}{\mu_w} \tag{4.6}$$

where $\boldsymbol{K_s}$ represents the saturated hydraulic conductivity (L T^{-1}); $\boldsymbol{k_i}$ the intrinsic permeability of the porous medium (L^2); $\boldsymbol{g}$ the acceleration of gravity (L T^{-2}); $\boldsymbol{\rho_w}$ the density of water (M L^{-3}); and $\boldsymbol{\mu_w}$ the dynamic viscosity of water (M $L^{-1}T^{-1}$). The density of water is relatively constant, the cause of a change in hydraulic conductivity should therefore be sought in a change of the viscosity of water.

The scaling method used in HYDRUS to describe the temperature dependency of soil hydraulic functions is expressed as (Šimůnek *et al*., 2006):

$$K_s(T) = \frac{\mu_{ref}}{\mu_T}\frac{\rho_T}{\rho_{ref}} K_s\left(T_{ref}\right) \tag{4.7}$$

where the subscript ***ref*** represents the reference temperature and often set at a room temperature of 20°C.

Though HYDRUS has the capacity of coupling water flow, solute transport and heat transfer (Šimůnek *et al*., 2008), the amount of HYDRUS applications in literature with coupled water flow and heat transport are limited. Mortensen *et al*. (2006) evaluated the capability of a multi-functional heat pulse probe (MFHPP) technique by using HYDRUS 2D/3D. Saito *et al*. (2006) studied the dynamics of soil moisture associated with meteorological information. Dahiya *et al*. (2007) studied the effect of mulching and tillage on soil moisture and thermal regimes using HYDRUS-1D, the one-dimensional version.

4.3 Material and methodology

4.3.1 Determination of saturated thermal conductivity

The heat transport parameters of the soil material under no-flow conditions were first determined in a vertical column (30cm height × 20cm diameter) which was uniformly filled with sand identical to the experiment's and with a bulk density of 1.55g/cm^3. The texture analysis showed an average of 100.0%, 97.0%, 51.7%, 7.4% and 1.4% pass-rates through the 2mm, 0.5mm, 0.25mm, 0.1mm and 0.05mm sieves respectively. The value of median grain diameter (d_{50} = 0.24mm) was determined by interpolation. The value of saturated hydraulic conductivity (K_s = 0.679cm/min) was determined by the constant head method.

Ten stainless steel K-type (Chromel-Alumel) thermocouple sensors (TC), with a length of 15cm each, were horizontally inserted at intervals of 3cm. The water-saturated column with a water layer on top was kept at constant room-temperature during a sufficient long time. The steady initial conditions were ascertained by the thermocouple measurements. The temperature of the water layer at the top was then instantaneously lowered by adding crushed ice. The saturated thermal conductivity was determined by inverse modelling in HYDRUS based on the measured temperature data.

Equation (4.5) was adopted in HYDRUS for the calculation of thermal conductivity. As the water content in the column was constant, only the empirical parameter b_1 was optimised while b_2 and b_3 were kept at their default values. The heat transport parameters used in this study are shown in Table 4-1.

Table 4 - 1: The heat transport parameters determined by inverse modelling in HYDRUS using the measured temperature data under no-flow conditions

κ	$b1$	$b2$	$b3$	C^*_s	C^*_w	C^*_B	D_T
W/m·K	W/m·K	W/m·K	W/m·K	J/m^{3}K	J/m^{3}K	J/m^{3}K	m^2/s
3.05E+00	8.67E-01	-2.41E+00	4.91E+00	1.92E+06	4.18E+06	2.89E+06	1.06E-06

κ, thermal conductivity (W/m·K); $b1$, $b2$, $b3$, soil specific empirical parameters (W/m·K) for calculating thermal conductivity; C^*_s, volumetric heat capacity of solid phase (J/m^{3}K); C^*_w, volumetric heat capacity of liquid phase(J/m^{3}K); C^*_B, volumetric heat capacity of bulk sediment matrix (J/m^{3}K); D_T, thermal diffusivity (m^2/s).

With the obtained thermal conductivity for the expected range of water fluxes inserted in Equation (4.4), the thermal grain Péclet number was evaluated. Considering the flux $\boldsymbol{q}$ at 2cm/hr together with the median grain diameter $\boldsymbol{d_{50}}$ as characteristic length, the thermal grain Péclet number was estimated to be in the order of magnitude of 2×10^{-3}. It was therefore concluded that the contribution of convection in the effective thermal diffusivity could be neglected. This has the advantage that the thermal diffusivity is purely caused by conduction and is not confounded by microscopic velocity variations associated with water flux. The letter is the quantity to be measured

4.3.2 Experimental setup

The experimental setup consisted of a J-shaped column as shown in Figure 4-1. This laboratory model schematises a stratified succession from the vadose zone (unsaturated section 1) over the aquifer and riverbed (saturated section 2) into the river (section 3). A J-shaped column was preferred above a vertical tank in this study as it reduced the pattern of lateral groundwater inflow from the aquifer to the river to one dimension, and at the same time allowed the classical identification techniques for columns to be applied. More information about the setup of the J-shaped column model is available in the previous chapter.

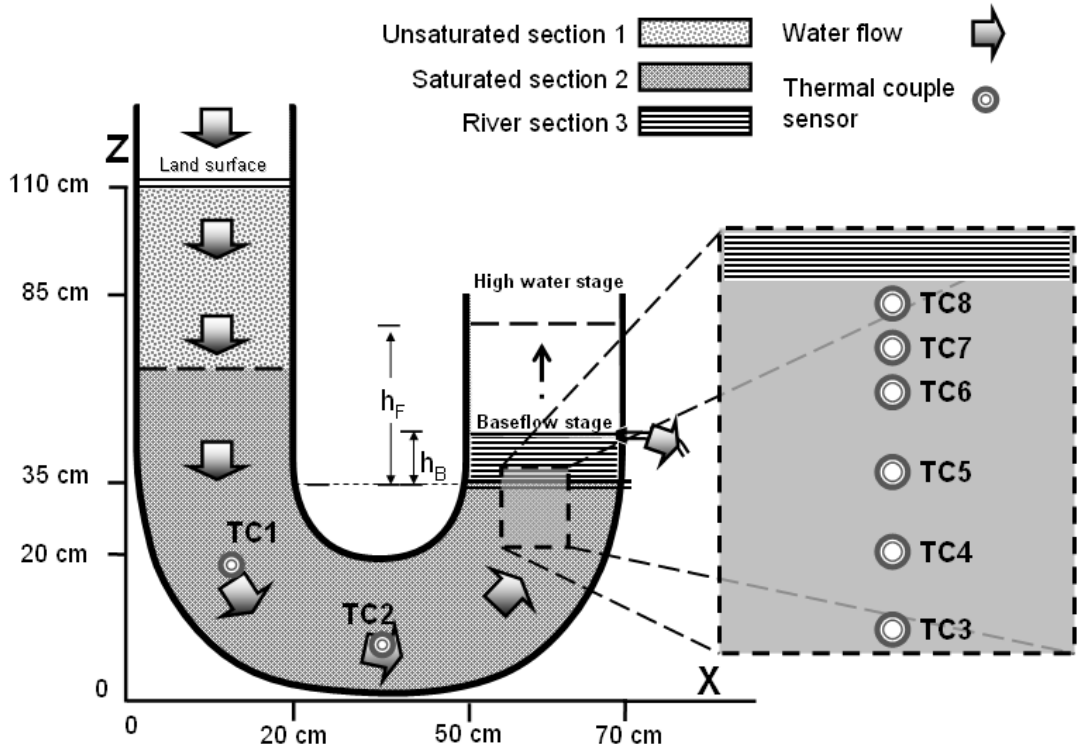


Figure 4 - 1: Schematic experimental setup of J-shaped column model and location of the thermocouples

The column was uniformly filled with the same dune sand. A constant water flux was pumped by a peristaltic pump into the unsaturated section on the left. The pumping rate was kept constant throughout each experiment. A filter paper was used to spread the water uniformly over the sand. This inflow represented the long term recharge of the aquifer surrounding the river. The flow was maintained during a sufficient time to create a steady-state flow throughout the whole column. The steady-state flow condition was monitored by observing the water content in the unsaturated part with time domain reflectometry, and by the establishment of a steady outflow at the overspill on the right. The water level on the right $\boldsymbol{h_B}$ was maintained at 10cm above the sand surface, which represented the river at baseflow conditions.

The entire column was wrapped into 10cm thick rockwool for insulation. Ten thermocouple sensors, numbered 1 to 10, were inserted. TC1 was inserted in the saturated section at the left hand side, which represented the temperature of groundwater entering from the vadose zone. TC2 was inserted at the bottom of the saturated section. TC3 to TC8 were inserted at 16cm, 12cm, 8cm, 4cm, 2cm and 1cm respectively below the riverbed. TC9 was inserted in the water 5cm above the riverbed representing the river section. TC10 measured the air temperature in the laboratory. The thermocouple sensors were connected to a 21X-Micrologger (Campbell Scientific Inc., USA).

4.3.3 Simultaneous river-stage and temperature change experiment

After the establishment of steady state throughout the whole column, a square shaped hydrograph (representing a simplified flood event) was created by instantaneously raising the water level of the river section and changing its temperature simultaneously. This was achieved by replacing the original water at room temperature by water mixed with crushed-ice.

The change of water level coming with this step function reversed the flow direction in the riverbed. At time t = 0, the water level was instantly raised from $\boldsymbol{h_B}$ (10cm above the riverbed) to a higher stage $\boldsymbol{h_F}$ and the overflow adjusted to this new level. The water stage was held at $\boldsymbol{h_F}$ for 30 minutes. The hydrograph was ended by a similar step function and the cold water replaced at the same time by water of 50°C. The overflow level was lowered to the original water level. In this way the river-stage was lowered instantaneously to the original level accompanied with a simultaneous temperature change.

Four steady-state inflow fluxes ($\boldsymbol{q}$ = 0.5cm/hr, 1cm/hr, 1.5cm/hr and 2cm/hr) and a zero inflow condition were applied, each time combined with three levels of the square shaped hydrograph ($\boldsymbol{h_F}$ - $\boldsymbol{h_B}$ = 5cm, 10cm and 15cm). Every minute, all the thermocouple sensors were scanned. Figure 4-2 shows an example of the measured temperature profile in the riverbed for a steady-state inflow of 1cm/hr.

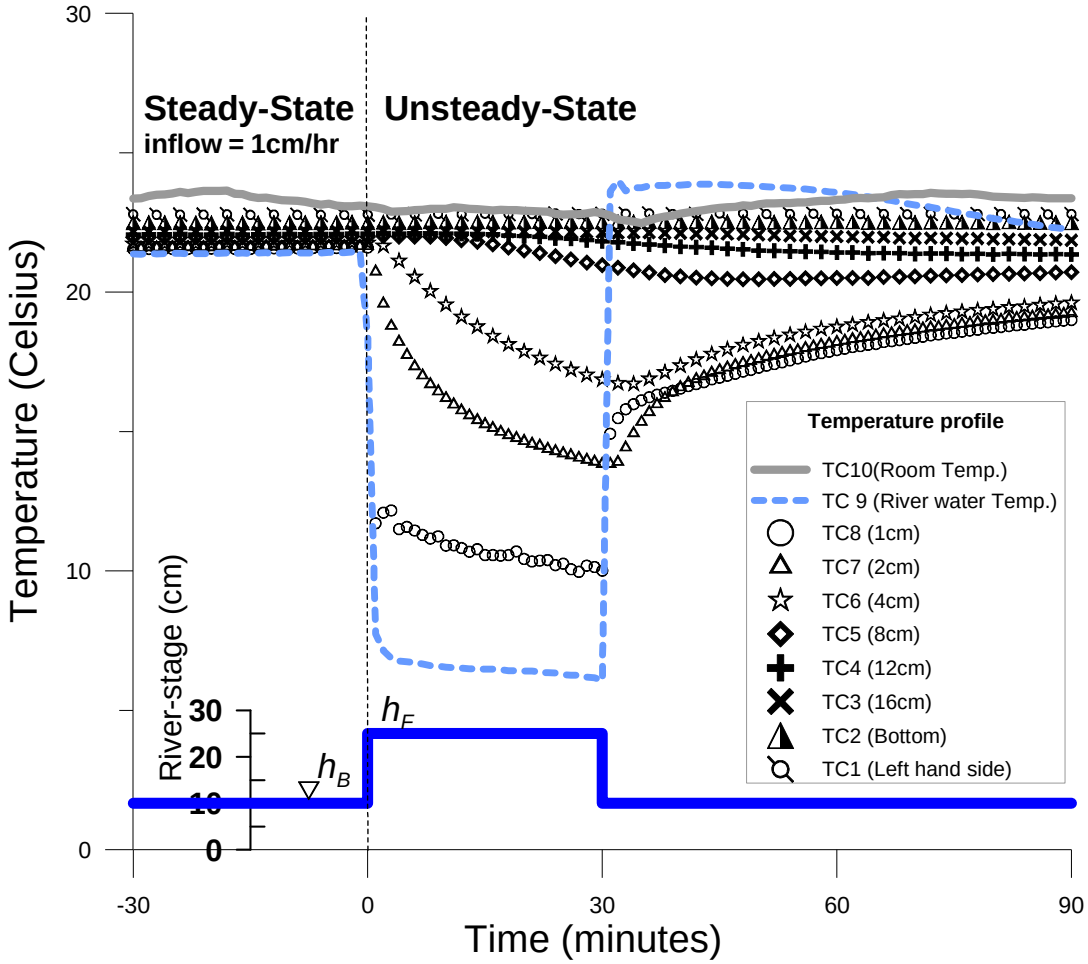


Figure 4 - 2: The measured temperature profile for a steady-state inflow of 1 cm/hr and a square shape hydrograph with a 15cm river-stage rise

Throughout the experiments the measured temperatures at the bottom (TC2) and left hand side (TC1) of the saturated section remained constant over time. The temperature variation below the riverbed (from TC3 to TC8) lagged behind the river water temperature change (TC9), and was attenuated in function of depth. The average room temperature (TC10) was close to 23°C with a small diurnal fluctuation. The water temperature in the tank supplying the peristaltic pump fluctuated slower and less as compared to the variation in the room. As TC2 was constant and never influenced by

the hydrograph, it was taken as a constant boundary condition. This temperature represented the condition of the surrounding aquifer.

4.3.4 Application of the numerical model HYDRUS 2D/3D

For the simulation of transient river water penetration and temperature variation in the riverbed, a finite element mesh in the numerical model HYDRUS 2D/3D was generated to mimic the 2D vertical cross-section of the J-shaped model (shown in Figure 4-1). Heat transport parameters were specified according to Table 4-1. The temperatures of the thermocouple sensors were compared to values at nodes with identical positions in the finite element mesh.

The initial measured temperature and water content were inputted as initial conditions. The boundary conditions of water flow were set according to the experimental set-up: steady-state flow condition on the left and the specified water level on the right. The heat transfer boundary condition at the inlet and outlet were specified as appropriate temperatures using the measurements of TC2 and TC8, respectively. The use of TC8 (1cm below the surface) eliminated the uncertainty of the convection boundary condition between the river water and the riverbed surface. The simulation started with a “warming-up” period in order to establish an equilibrium steady-state. Then the squared hydrograph was simulated by changing the boundary conditions on the right (simultaneous change in water level and temperature) while maintaining constant conditions on the left (steady water influx and temperature).

4.4 Results and discussion

Figures 4-3(a) to 4-3(f) demonstrate the velocity contours (cm/hr) and flow directions (arrows) in the J-shaped model simulated by HYDRUS. The simulation illustrated coincides with the scenario of 1.5cm/hr steady-state groundwater inflow on the left and a water level rising of 15cm on the right. The positive flux represents the groundwater flow towards the river and the negative the reversed direction of water flow in the aquifer. The dark zone on the right represents the extent of river water penetration, which is generated by the moving trajectories of flowing particles.

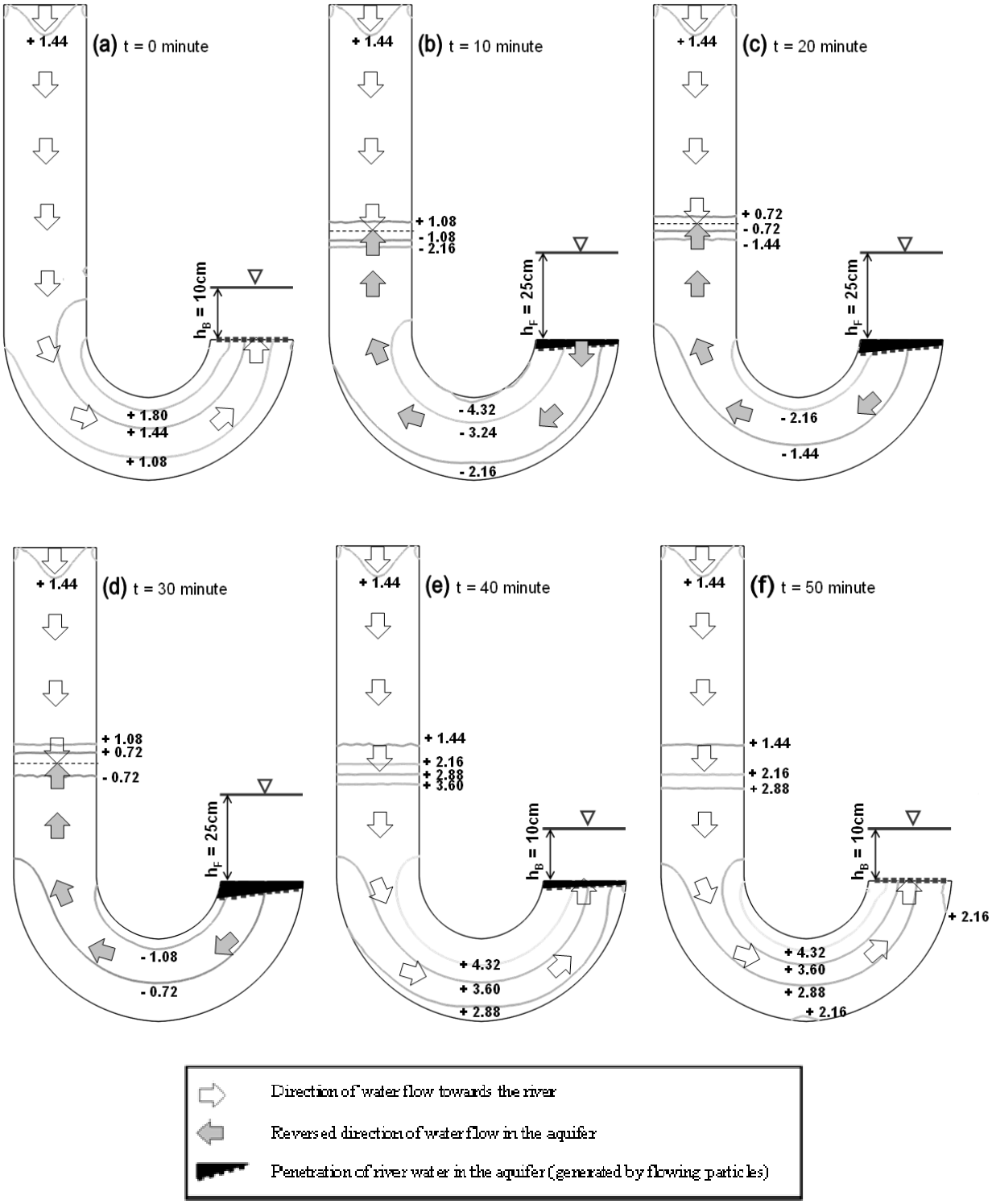


Figure 4 - 3: The graphical output of water velocity (in cm/hr) and flow directions (arrows) in the J-shaped model at (a) t = 0 minutes, (b) t = 10 minutes, (c) t = 20 minutes, (d) t = 30 minutes, (e) t = 40 minutes and (f) t = 50 minutes after the rising of river stage as simulated by HYDRUS. Illustration shows the case of 1.5 cm/hr steady-state groundwater inflow on the left and 15cm water level rising on the right. The dark zone on the right represents the penetration of river water, which is generated by the trajectories of flowing particles

Figure 4-3(a) shows that a steady-state flow condition was established throughout the entire column before the hydrograph was introduced to the river section. Concerning the water flowing through the bend of the saturated section, faster water velocities were simulated at the inner side and slower at the outer side. Afterwards, the river water level was instantly raised to a higher stage, as shown in Figure 4-3(b), 4-3(c) and 4-3(d). The change in vertical hydraulic gradient reversed the groundwater flow direction in the saturated section. The reversal tends to be moderated by the steady groundwater inflow from the unsaturated section.

As can be seen when comparing Figure 4-3(b), 4-3(c) and 4-3(d), a zero-flux interface was formed at the upstream part of the saturated section, where the groundwater flow was stagnant. The zero-flux interface was found to be slowly advancing over time. Figure 4-3(e) and 4-3(f) show the pattern of flow recession in the saturated section after the hydrograph.

The penetration of river water was simulated in HYDRUS by the tracking particles in the numerical model. The resulting trajectories are shown in Figure 4-3 and only reached relatively shallow depths below the river section. This penetration depth represented the extent of the hyporheic zone in which river water and groundwater exchange. The bend with higher velocities also showed deeper penetration. The prediction coincided with the observed rapid temperature decline from thermocouple TC8, TC7 and TC6, i.e. 1~4cm below the riverbed, after the rising stage of the hydrograph. A comparison between measured temperature profiles and direct simulation by HYDRUS is illustrated in Figure 4-4(a) and 4-4(b), where the rising level was set to 5cm and 15cm respectively and for the same groundwater inflow of 2cm/hr. The sharper rise in river-stage resulted in a relatively steeper gradient of temperature at shallow depth; while at deeper depths, temperature profiles did not show substantial changes.

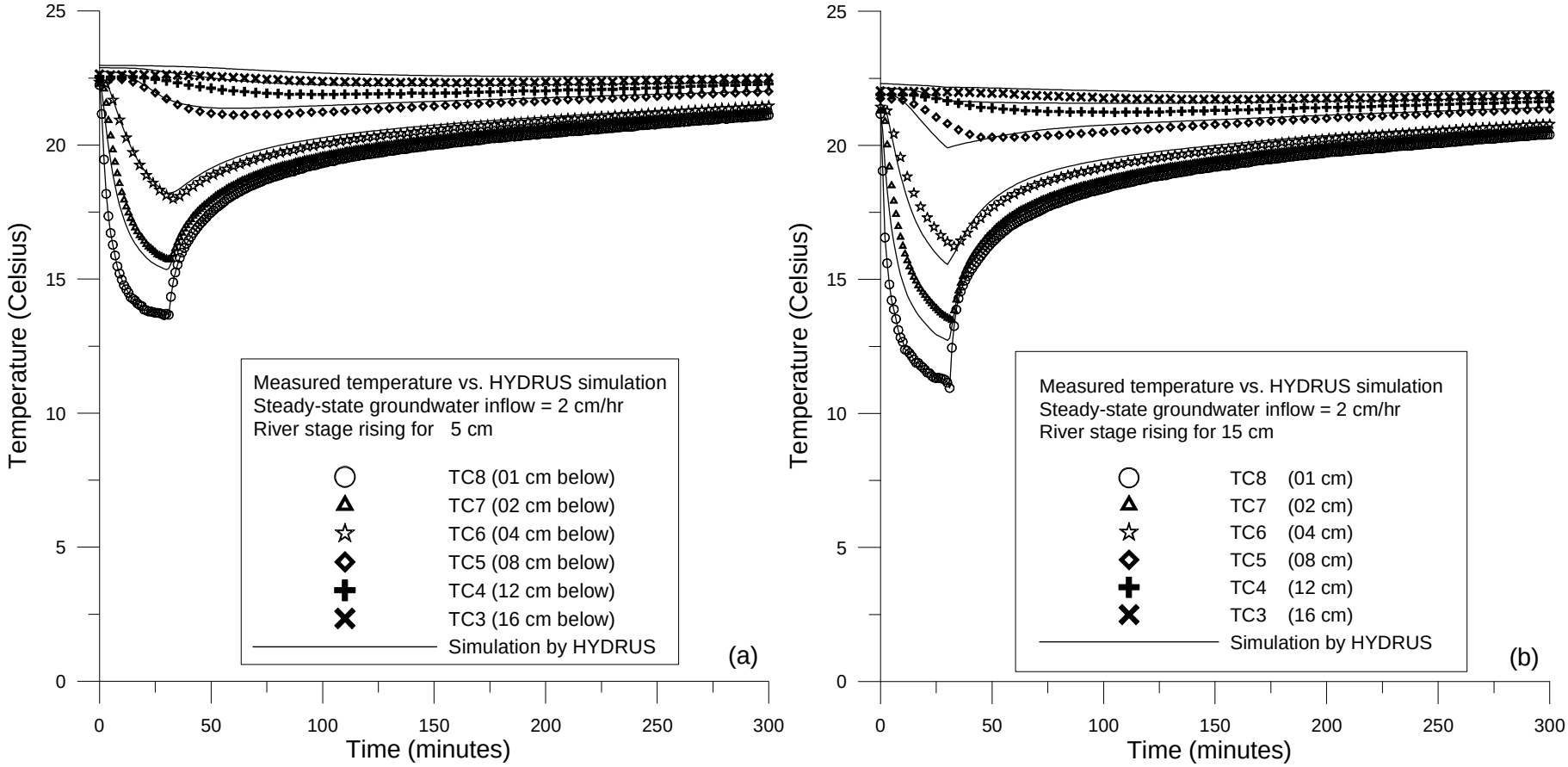


Figure 4 - 4: Comparison of measured temperature and direct simulation by HYDRUS while the rise of river-stage is (a) 5cm and (b) 15cm with the same groundwater inflow of 2cm/hr

Figure 4-4(a) reveals that the simulation and the measured temperature profile in the riverbed showed a good fit for low rise in river-stage ($\boldsymbol{h_F}$ - $\boldsymbol{h_B}$ = 5cm). For the experiment of higher rise ($\boldsymbol{h_F}$ - $\boldsymbol{h_B}$ = 15cm), as shown in Figure 4-4(b), the temperature as simulated by HYDRUS at shallow depths penetrated faster in comparison with the measured temperatures. During the recession stage all simulated temperatures were close to the measured ones.

In order to evaluate the impact of rapid temperature fluctuations induced by river stage rising, temperature sensitivities of thermal and hydraulic conductivity were investigated in a systematic way and evaluated each time by the improvement in fit of the simulations. A comparison of the measured temperatures in the experiment of river-stage rise of 15cm with groundwater inflow of 2cm/hr and the inverse simulation by HYDRUS is shown in Figure 4-5(a) to 4-5(c). Firstly, the thermal conductivity was optimised by inverse modelling while the hydraulic conductivity was kept as temperature independent. As shown in Figure 4-5(a), the improvements were limited. Secondly, the thermal conductivity was optimised while changing the viscosity in function of temperature and thus making the hydraulic properties temperature dependent according to Equation (4.7). As shown in Figure 4-5(b), the fit improved. In a third step, the saturated hydraulic conductivity was optimised for each separate experiment with a temperature dependent conductivity. The variation of conductivity in function of temperature is accounted for by scaling viscosity and density. As shown in Figure 4-5(c), further substantial improvements were observed. Important is that the hydraulic conductivity at reference temperature was no longer a constant.

Comparing Figure 4-5(a), 4-5(b) and 4-5(c) showed an improved fit by turning hydraulic properties temperature dependent and optimising the value of hydraulic conductivity. It is obvious that a rapid change of water temperature has more effect on hydraulic conductivity than on thermal conductivity. The review by Constantz *et al.* (2003b) and Anderson (2005) also indicated that thermal conductivity is less subjected to uncertainty than the hydraulic conductivity in regard to the sediment texture.

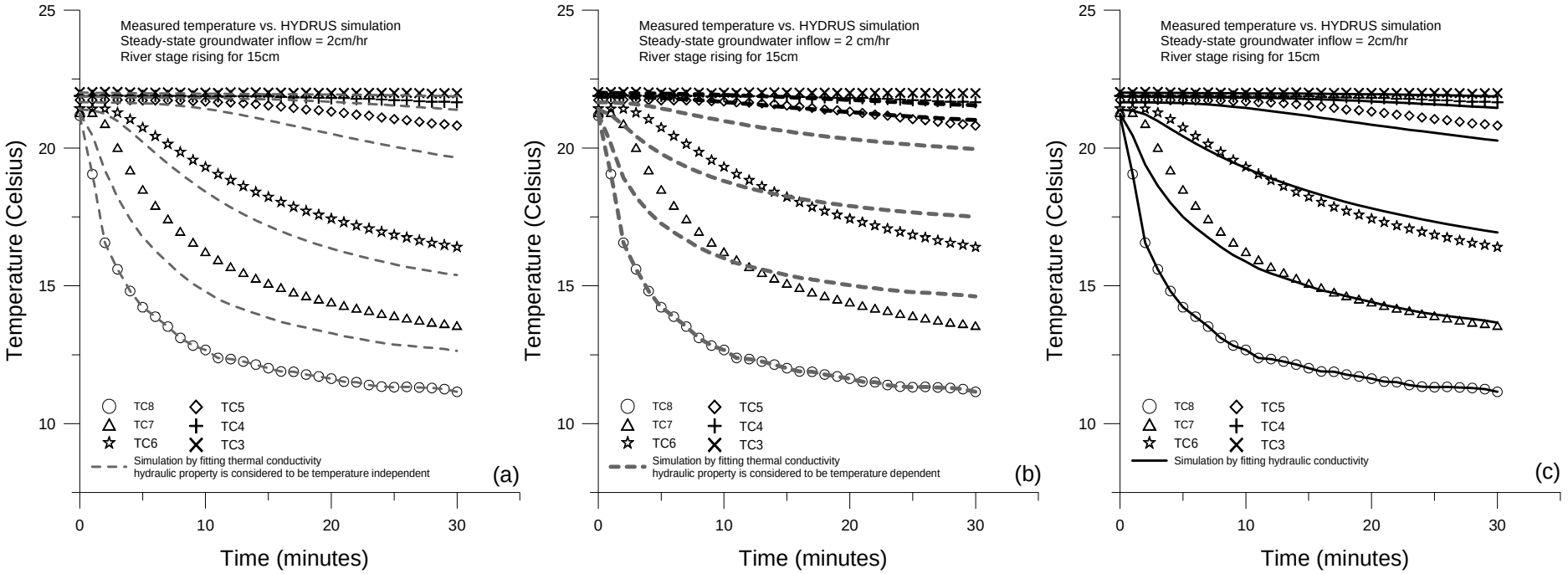


Figure 4 - 5: Comparison of the measured temperature with inverse simulation by optimising thermal conductivity while setting hydraulic properties as (a) temperature independent, (b) temperature dependent, and (c) by optimising saturated hydraulic conductivity in the case of river-stage rise of 15cm with groundwater inflow of 2cm/hr

The estimated optimal hydraulic conductivity at reference temperature (20°C) for three levels of the square shaped hydrographs and different groundwater fluxes are shown in Table 4-2, the decrease in hydraulic conductivity caused by a decline of water temperature is accounted for. One would expect the same hydraulic conductivity at 20°C. As there is a large range in different hydraulic conductivities it can be concluded that temperature scaling by Equation (4.7) is not satisfactory. The increase in the viscosity is relatively larger as compared to changes in density. A lower hydraulic conductivity at reference temperature is obtained when the rising of river water level is sharper. This is counteracted by the lateral groundwater flux. One possible explanation could be that during transient temperature conditions both the water and the grains are not at the same temperature and not homogenous. The cold intruding water in the pores is much colder than the average temperature of the porous medium. The scaling equation assumes a homogeneous temperature.

Table 4 - 2: The estimated optimal hydraulic conductivities at reference temperature 20°C for three levels of square shaped hydrographs and different fluxes while the hydraulic conductivities were scaled in function of simulated temperature according to Equation (4.7) obtained by inverse modelling as in Fig 4-4(c) using measured temperature

Steady-state groundwater flux	***Levels of square shaped hydrograph***		
	5cm	10cm	15cm
cm/hr	**Estimated optimal hydraulic conductivities, *Ks* (cm/min)**		
2.0	0.468	0.374	0.320
1.5	0.501	0.487	0.355
1.0	0.653	0.482	0.335
0.5	0.504	0.289	0.248
0	0.442	0.162	0.111

The estimated hydraulic conductivity at reference temperatures of 20°C in Table 4-2 were used in HYDRUS for each scenario and the fluxes at each observation node below the river section were determined. Figure 4-6(a) to 4-6(e) show the temperature-based estimates of the flux in the riverbed as simulated by HYDRUS. The negative flux is a downwelling flow (i.e. river water penetration into the surrounding aquifer), while the positive flux represents an upwelling flow (i.e. groundwater flow towards the river). The simulated fluxes at two depths are shown (1cm and 16cm below the riverbed). The first 30 minutes in the graph represent the square shaped hydrograph and the last 30 minutes the recession. The horizontal dashed line shows the flux pumped into the left column. This flux was a steady-state flux throughout the entire experiment and the same as before the hydrograph. After the recession, the flux gradually converged on the same steady state as before the hydrograph.

As shown in Figure 4-6(a) to 4-6(e), the instantaneous change of river water level caused the largest flux change in the riverbed, i.e. at t = 0 min. and t = 30 min. respectively. The sharper the rising of river water level, the larger the river water penetrating flux, but also the greater fluxes differed between shallow and deep aquifer. The effect of steady-state groundwater inflow on flux changes in the riverbed can also be seen by comparing Figures 4-6(a) to 4-6(e). A smaller downwelling water flux was found at larger steady-state groundwater inflow. This is consistent with the study of Hester and Doyle (2008) which concluded that hyporheic exchange flows would be less prevalent if stronger gaining conditions were present.

The duration of downwelling flow was influenced by the level of river-stage rising as well as by the magnitude of groundwater inflow. As illustrated in Figure 4-6(a), the duration of downwelling flow induced by low river-stage rising (5cm) for a steady-state groundwater inflow of 2cm/hr was relatively short as compared to high river-stage rising (15cm) for the same lateral inflow. The duration was getting longer when lower steady-state groundwater inflow was applied.

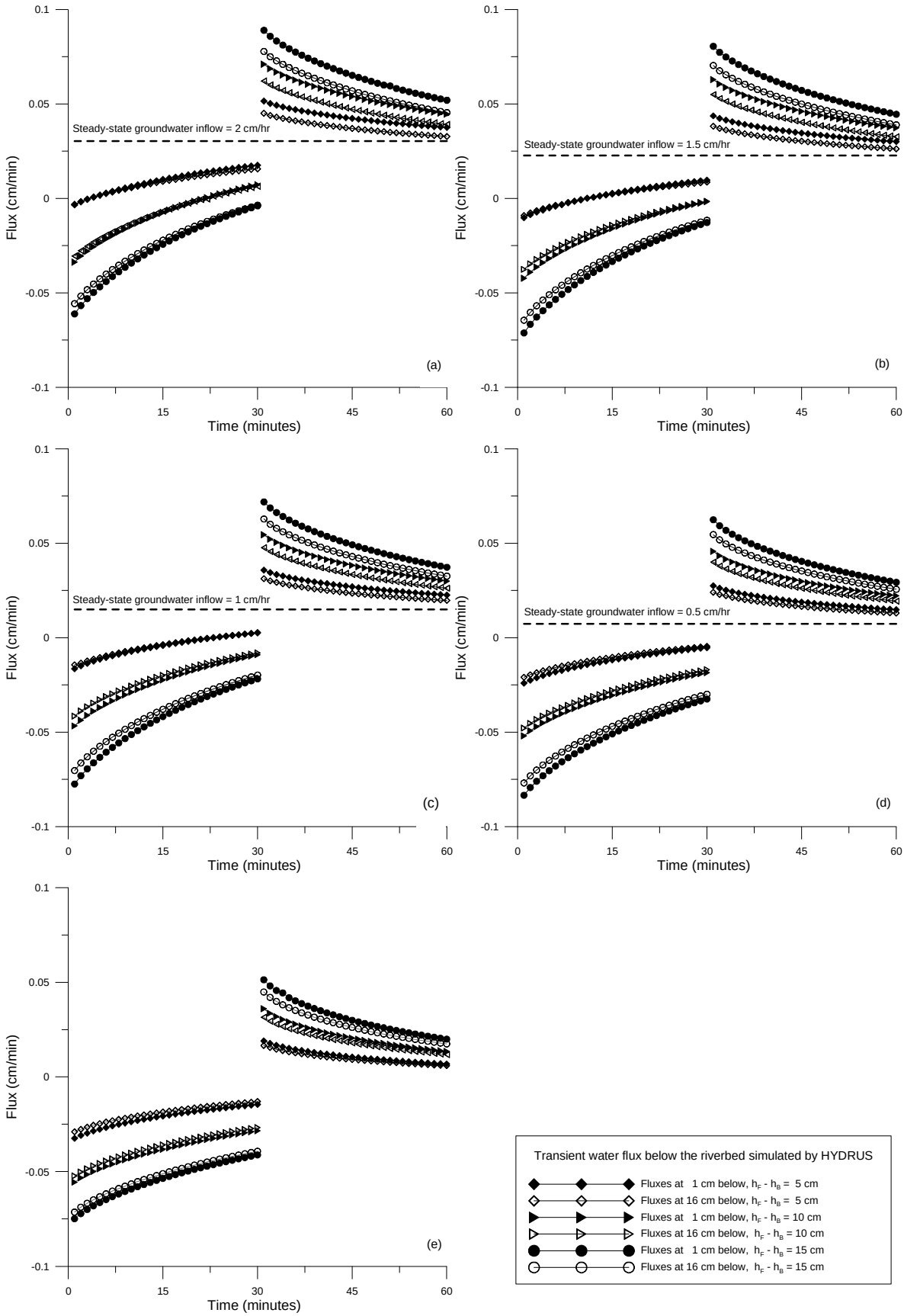


Figure 4 - 6: Temperature-based estimates of flux below the riverbed simulated by HYDRUS. The steady-state groundwater flux is (a) 2.0cm/hr, (b) 1.5cm/hr, (c) 1.0cm/hr, (d) 0.5cm/hr and (e) no groundwater inflow

4.5 Conclusions and recommendation

A laboratory J-shaped column has been developed in this study to explore the possibility of estimating the transient water fluxes in the riverbed with temperature. This J-shaped column schematises a stratified succession from the vadose zone over the aquifer to the river. The numerical model HYDRUS was used to simulate water flow and heat transfer. During each experiment, a square shaped hydrograph accompanied with a simultaneous change in water temperature was created in the river section. The change in vertical hydraulic gradient induced the penetration of river water and reversed the groundwater flow direction in the riverbed. By using the flowing particle tracking options in HYDRUS, the simulated extent of river water penetration was found to be limited to shallow depths in the riverbed only. The corresponding temperature change measured by the thermocouple during experiments also revealed the same trend. Sharper rise in river-stage resulted in a relatively steeper gradient of temperature at shallow depth; while temperature profiles at deeper depths did not show substantial changes.

From this study we found that a rapid change in groundwater temperature has an important effect on hydraulic conductivity. However, the simple scaling of the viscosity in function of temperature is not able to predict the hydraulic conductivity. We propose that temperature can be used as an indirect tracer to assist the estimation of fluctuating water fluxes in the field. This is important for accurately characterising the extent of the hyporheic zone. As a first step, temperature data at shallow depth below the riverbed are used in order to determine the optimal hydraulic conductivity through inverse modelling. The thermal conductivity could be taken as temperature invariant. The objective function in this step is the minimum sum of squared deviations between observed and simulated temperatures. As the most prominent temperature changes were detected at shallow depth below the riverbed the majority of sensors should consequently be placed close to the riverbed and at short distances from each other. After determination of the optimal conductivity, the fluctuating water fluxes below the riverbed can be estimated by a numerical model, such as HYDRUS.

Furthermore, more research is required to establish the relation between hydraulic conductivity and temperature. The existing relations appear not to be valid under transient conditions because of the fact that the porous medium is composed of grains and water, which are at different and heterogeneous temperatures. In the mean time, a pragmatic optimisation of hydraulic conductivity by inverse modelling in function of temperature is needed. The study of the most appropriate updating scheme for hydraulic

conductivity under transient heat transfer in transient water flow conditions is recommended.

Chapter 5

Numerical simulation by HYDRUS 2D/3D of long- and short-term groundwater flux in the hyporheic zone as influenced by temperature regimes and changing river stage*

Abstract

Temperature has been used as a tracer for exploring long-term water fluxes between aquifer and river. The use of temperature was encouraged by the easy low-cost data-logging and installation in the field of thermocouple sensors with a narrow time and space resolution. The majority of studies focused on exploring long-term and large-scale groundwater flow regimes in the aquifer based on analytical solutions for simplified flow domains and boundary conditions. Less attention has been given to the hydrodynamics and thermal regimes inside the riverbed, i.e. the hyporheic zone, as a 2-dimensional flow domain and under changes of river stage.

A numerical model of river–aquifer interaction has been built in HYDRUS 2D/3D. The temperature dependence of soil hydraulic properties was included in HYDRUS. Simulations were first performed under steady-state water flow conditions. The vertical temperature gradients, the attenuation of temperature oscillations, and the groundwater fluxes in different sediment textures were determined. The simulation results were compared with calculations using a 1-D steady-state analytical solution proposed by Schmidt *et al*. (2007). Subsequently, simulations were executed to quantify the extent and volume of water flux exchange in the riverbed induced by the rising flood stage. This study revealed that the long-term steady groundwater discharge at the banks of a river channel is stronger than the flux close at the river-bottom. The change in ambient temperatures has a substantial effect on water flux variability in shallow aquifers. For identical river stage changes the hyporheic exchange fluxes are more intense in summer than in winter. The lateral infiltration of river water into the aquifer during larger flood events was also found to be stronger than the downwelling flow across the bottom of the river channel. The lateral extent of the hyporheic zone would be 2 to 3.5 times longer than its vertical extent.

* Adapted from Chou PY, Cuppens A, Wyseure G. 2009. Numerical simulation by HYDRUS 2D/3D of long- and short-term groundwater flux in the hyporheic zone influenced by temperature regimes and changing river stage. *In preparation to be submitted to Ground Water*

5.1 Introduction

The water flux across the aquifer–riverbed interface has received growing attention. The hyporheic zone is the part of riverbed where river water and groundwater exchange. The biogeochemical importance of hyporheic exchange flows has long been recognized (Findlay, 1995; Cirmo and McDonnell, 1997; Hinkle *et al*., 2001; Runkel *et al*., 2003; Storey and Williams, 2004). The flow induced pressure-differences over the riverbed lead to downwelling of river water into the aquifer, which facilitates the exchange of substances like oxygen and organic matter between the river and the aquifer. The adequate quantification of riverbed–aquifer flux interactions through the hyporheic zone is essential for the management and protection of the river basin environment.

Many advances have been made in the understanding the surface-subsurface water exchange through the hyporheic zone. The interactions between various river geomorphological features and the water exchange patterns have been examined at various scales (Harvey and Bencala, 1993; Wroblicky *et al*., 1998; Harvey and Wagner, 2000; Jonsson *et al*., 2003; Mutz and Rohde, 2003; Packman and MacKay, 2003; Storey *et al*., 2003; Rehg *et al*., 2005; Boano *et al*., 2007; Tonina and Buffington, 2007). Hester and Doyle (2008) concluded that the most crucial factors determining the magnitude of water exchange through the hyporheic zone appear to be the size of in-stream geomorphic structures, the groundwater discharge to the river baseflow and the hydraulic conductivity of the alluvial deposits. The majority of previous studies, however, mainly focused on quantifying vertical exchange of water across the riverbed based on tracer studies in the river-flow. The lateral groundwater inflow from the aquifer was usually not considered or at best taken as constant steady state inflow into the river. One difficulty has been that chemical tracer studies were not able to distinguish the difference between lateral and vertical exchange of water across the aquifer–riverbed interface. It was therefore not feasible to delineate the spatial variability of the hyporheic zone. Howard *et al*. (2006) indicated that the extent of the hyporheic zone is inversely proportional to the lateral groundwater inflow towards the river. In addition, little attention has been paid to the effects of ambient temperature change on the hyporheic exchange patterns. Few studies noticed that the effect of temperature dependence of the hydraulic conductivity would also be influential (Cozzetto *et al*., 2006; Kollet and Zlotnik, 2007). The ambient temperature of river water is easily influenced by meteorological conditions and human activities. The thermal effects on temporal variability of hydraulic conductivity should not be ignored during elaboration of field studies regarding the river-aquifer interaction.

There are a variety of techniques that can be implemented in the field to quantify river-aquifer interactions. The use of temperature as a natural tracer has proven to be promising from the earlier studies (Johnson, 2003; Anderson, 2005; Webb *et al*., 2008). Thermocouple sensors with high spatial and temporal resolution can be easily installed in the field at a low cost. Different analytical methods for estimating long term fluxes based on temperature profiles have been derived previously (Stallman, 1965; Bredehoeft and Papadopulos, 1965; Turcotte and Schubert, 1982; Taniguchi, 1993; Silliman *et al*., 1995). The majority of these studies used multi-depth time-series temperatures below the riverbed to quantify long-term and large-scale groundwater flow pattern in the aquifer. The evaluation by using uniform depth temperatures were proposed by Conant Jr. (2004) and Schmidt *et al*. (2007). However, the feasibility of using temperature to quantify the localized short-term fluxes exchange in the hyporheic zone has not been studied in detail.

To provide more insights into the understanding of hydrodynamics and thermal regimes at the aquifer–riverbed interface, we performed in this study numerical simulations to interpret the flux variability and thermal regime in the riverbed. A coupled groundwater flow and heat transport model, HYDRUS 2D/3D, is used for the numerical simulation. This type of model can provide a useful and simple framework for the temperature-based analysis of both steady-state and transient water flow conditions in the field. In this study the gaining river condition was considered. Different scenarios were defined. The simulated long-term groundwater fluxes below the riverbed were compared with calculations using a 1-D steady-state analytical solution proposed by Schmidt *et al*. (2007). The specific objective is to investigate the potential influence of temperature on the spatial variability of the hyporheic zone. The spatial and temporal variability of hyporheic zone can then be quantified by using the flowing particle tracking option in HYDRUS.

5.2 Methodology

5.2.1 Numerical model

A two-dimensional river–aquifer interaction model has been composed in HYDRUS as shown in Figure 5-1. This model represents a schematic cross-sectional view of an aquifer system, which is underlain by a horizontal layer of impervious bedrock. Let $\boldsymbol{R}$ ($L\,T^{-1}$) denote a constant rate of recharge per unit area, which percolates from the soil into the aquifer. The groundwater flow is driven by the hydraulic gradient of the

phreatic water table towards the river. When the long-term steady state is established, the recharge to the aquifer becomes equal to baseflow into the river. The position of the phreatic water table is then also steady. The river stage at base flow h_B is set to 0.2m.

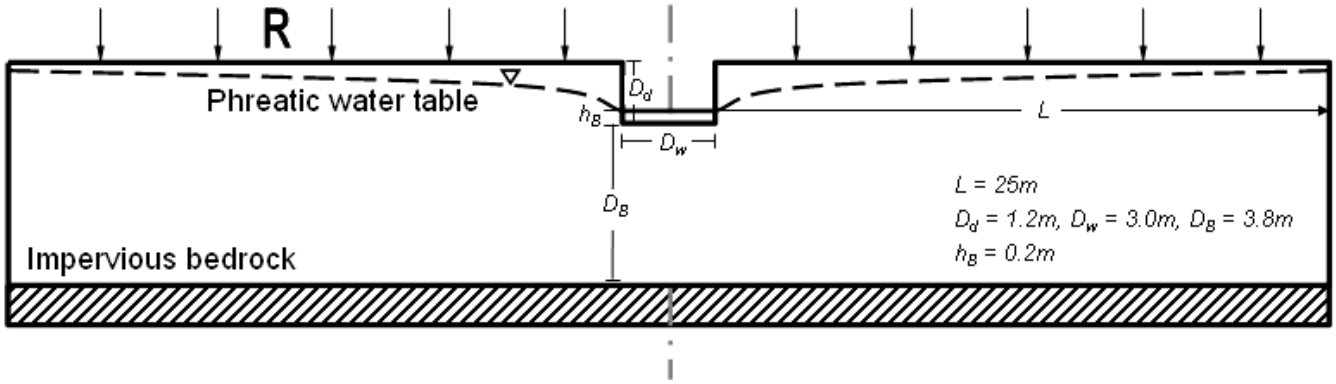


Figure 5 - 1: The schematic representation of a river–aquifer interaction model

This model is symmetrical with respect to the center of river. The distance from the side of model to the river L is set to 25m. The cross-sectional area of the river is rectangular. The bankfull depth D_d and the width D_w of the river channel are set to 1.2m and 3m respectively. The thickness of aquifer, being the distance between the bottom of the river and the impervious bedrock D_B is set to 3.8m. The soil texture for the entire geometric domain is assumed to be isotropic and homogeneous. However, this setup can be easily transformed to heterogeneous and anisotropic media as well as other geometries.

5.2.2 Analytical solution for steady-state heat transfer

The governing partial differential equation for describing one-dimensional heat transfer through the saturated sediment with vertical water flow is expressed as:

$$\frac{\partial T}{\partial t} = D_T \frac{\partial^2 T}{\partial z^2} - q_z \frac{C^*_w}{C^*_B} \frac{\partial T}{\partial z} \tag{5.1}$$

where T is temperature (K); t is time (T); z is vertical depth (L) below the riverbed surface, where defined as $z = 0$; q_z is the specific discharge ($L\,T^{-1}$) along the z direction; D_T is the effective thermal diffusivity ($L^2\,T^{-1}$); C^* is the volumetric heat capacity

($M\ L^{-1}T^{-2}\ K^{-1}$), which can also be defined as the product of density, $\boldsymbol{\rho}$ ($M\ L^{-3}$) and specific heat, $\boldsymbol{c}$ ($L^2\ T^{-2}\ K^{-1}$); the subscripts $\boldsymbol{B}$ and $\boldsymbol{w}$ denote the bulk sediment matrix and its liquid phase, respectively.

Schmidt *et al*. (2007) proposed an analytical method for solving Equation (5.1) based on the Turcotte and Schubert (1982) solution in order to estimate the water flux $\boldsymbol{q_z}$:

$$q_z = \frac{\kappa(\theta)}{C^*_w} \ln \frac{T(z) - T_L}{T_o - T_L} \tag{5.2}$$

where $\boldsymbol{\kappa}$ is the thermal conductivity ($M\ L\ T^{-3}K^{-1}$) of the porous medium; $\boldsymbol{T_o}$ is the average temperature at the uppermost position ($\boldsymbol{z} = 0$) of riverbed, $\boldsymbol{T_L}$ is the temperature at the lower boundary of the heat transfer domain below the riverbed. Equation (5.2) is considered as rather simple and less data intensive. It is assumed that the vertical temperature gradient in the riverbed is only a function of $\boldsymbol{q_z}$. This equation was used to estimate the steady upwelling water flux by observing the temperature at a single depth (Conant Jr., 2004; Schmidt *et al*., 2007; Kalbus *et al*., 2009), which has to be located at proper position to avoid the influence of diurnal river water temperature fluctuations. Consequently, the determination of the depth of temperature measurement is influential.

Previous studies defined the temperature damping depth, $\boldsymbol{Z_d}$, as the depth in the soil at which the influence of diurnal change in surface temperature is lost (Blume *et al*., 2002) or reduced by $\boldsymbol{e^{-1}}$ (0.37) (Segal *et al*., 2000; Gülser and Ekberli, 2004; Blume *et al*., 2008). $\boldsymbol{Z_d}$ is expressed by the equation (Robson, 1989):

$$Z_d = \sqrt{\frac{2D_T(\theta)}{\omega}} = \sqrt{\frac{2\kappa(\theta)}{\omega C^*_B}} \tag{5.3}$$

where $\boldsymbol{\omega}$ is the angular frequency of diurnal temperature oscillation, which equals to $2\pi/86400$. As the effective thermal diffusivity, $\boldsymbol{D_T}$, can be expressed as the ratio of thermal conductivity to volumetric heat capacity, therefore, $\boldsymbol{Z_d}$ is a function of soil bulk density and water content (Blume *et al*., 2002).

Equation (5.3) describes heat transport in the soil purely by conduction. Studies have pointed out the attenuation of surface temperature oscillations is also influenced by the magnitude of upwelling groundwater flux (Constantz and Stonestrom, 2003; Blasch *et al*., 2004; Anderson, 2005).

5.2.3 Numerical modelling approach: HYDRUS 2D/3D

A numerical model allows to solve complex cases in two or three dimensions. Anderson (2005) provided a review on some important coupled groundwater flow and heat transfer codes. The codes for the simulation of groundwater-river water exchange in shallow aquifers by temperature include VS2DH, SUTRA, and FEFLOW. The successful applications can be seen in Essaid *et al*. (2008) and Anibas *et al*. (2009); both studies applied VS2DH in one-dimensional version.

HYDRUS is a widely accepted and well tested numerical model for simulating the water, solute and heat transport in variably saturated porous media (Šimůnek *et al*., 2008). It is a finite element model solving the Richard's equation for water flow and convection-dispersion type equations for solute and heat transport. The boundary condition at the soil surface can be assigned with prescribed sinusoidal temperature variation (Šimůnek *et al*., 2006).

A 2-D vertical working domain was created in HYDRUS according to the geometric parameters for the model as shown in Figure 5-1. The model grid consisted of 20,802 two-dimensional elements (triangles). The targeted finite element (FE) mesh size for the entire model was specified to 0.5m and the mesh was refined to 0.05m near the water–sediment interface.

The constant water flux boundary was applied at the top of the model. The groundwater recharge rate $\boldsymbol{R}$ was set at 3mm/day. The bottom, left and right side of the model were defined as no-flow boundaries. The aquifer–riverbed interface was set as a time-dependent prescribed head boundary such that the scenarios of instantaneous river-stage change can be implemented during the simulation.

A fixed temperature was assigned to the aquifer (7°C) during the simulations. The mean temperature at the aquifer–riverbed interface was assigned to 10°C for the summer period and 2°C for the winter period. Neglible energy flux was assumed across the bottom, left and right side of model since they are set as no water flow boundaries. The hydraulic and thermal transfer properties of soil were kept at the default empirical parameters in HYDRUS. Table 5-1 provides the hydraulic and heat transport parameters of the soils which have been chosen for simulation in this study.

Table 5 - 1: The hydraulic and heat transport parameters of the soils for HYDRUS simulations

Soil type	K_s	n_e	κ	D_T
	m/s	m^3/m^3	*W/m·K*	m^2/s
Sand	8.25E-05	4.30E-01	2.41E-00	8.34E-07
Sandy loam	1.23E-05	4.10E-01	1.39E-00	4.79E-07
Sandy clay	3.33E-07	3.80E-01	0.99E-00	3.43E-07

K_s, saturated hydraulic conductivity (m/s) at 20°C; n_e, porosity (m^3/m^3); κ, thermal conductivity (*W/m·K*); D_T, thermal diffusivity (m^2/s)

5.2.4 Scenarios

The simulation started with the establishment of a steady-state water flowing condition for the entire model. Afterwards, certain parameters were changed. The effect of diurnal river water temperature oscillations was not considered before the achievement of steady-state. The establishment of steady-state water flow and heat transfer was, respectively, confirmed by obtaining constant pressure heads and the temperature data from the observation points placed below the riverbed.

The first stage simulations were performed under steady-state gaining conditions to study the vertical temperature gradients and the attenuation of temperature oscillations in the riverbed. Sediment textures with contrasting difference in hydraulic and thermal conductivities as provided in Table 5-1 were selected for simulation. The river stage remained constant at the base flow level, h_B (0.2m), during this simulation. The effect of diurnal river water temperature oscillations was included. The hypothetical amplitude of surface river water temperature oscillation was set as 1°C. The hydraulic properties are considered as temperature dependent. The temperature effect on hydraulic conductivity is predicted on the basis of the influence of temperature on the viscosity and density of water. The temperature-based estimates of long-term steady groundwater discharge across the side and the bottom of river channel were determined.

The simulations during the second stage were performed to evaluate the transient flow from aquifer reversing its direction as induced by the rising of the river-stage. The rise in river stage was 0.8m. The hydraulic properties were scaled for changes in viscosity in function of temperature. By using the flowing particle tracking option in HYDRUS the vertical and lateral extent of river water penetration in winter and summer period, respectively, can be quantified. In addition, the bank storage zone and the hyporheic zone can be distinguished.

5.3 Results and discussion

5.3.1 The evaluation of thermal regimes under steady state upward water flow

Figure 5-2 illustrates a simulated temperature-depth profile below the center of the sandy-loam riverbed under steady-state upward groundwater flow. The curve of average temperature versus depth (solid line) contracted upward due to the continuous recharge of upwelling water flow. The transient subsurface temperature oscillations (dashed lines) were displayed for time increments of 2.4 hours during a single day. The amplitude of temperature oscillation was damped with depth.

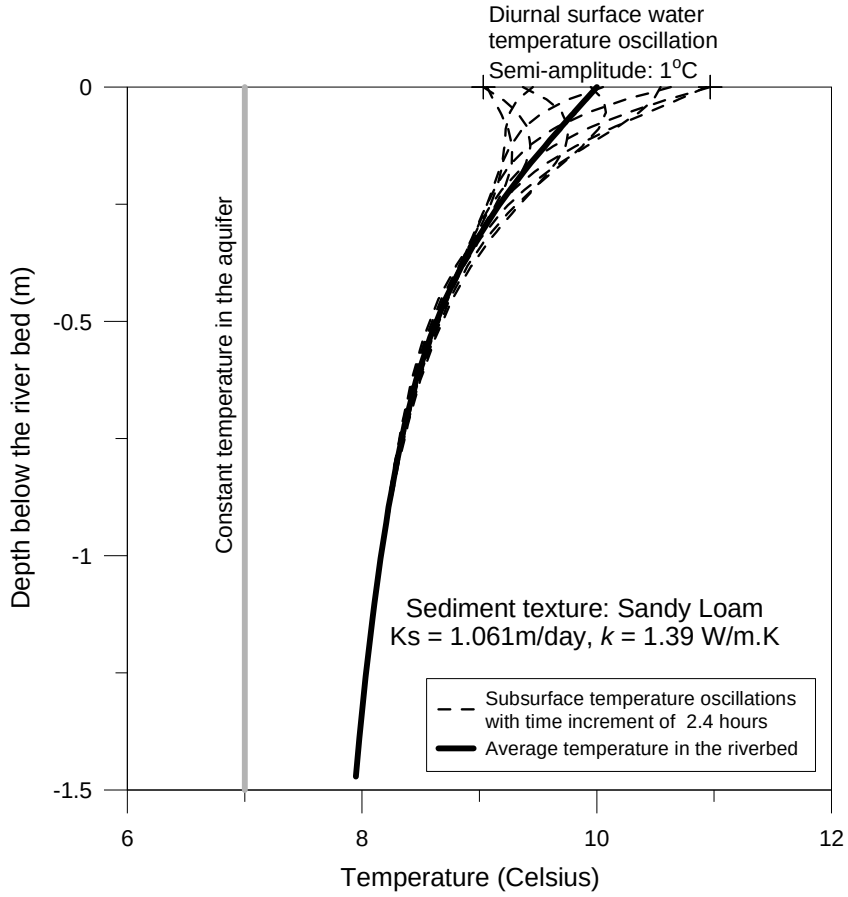


Figure 5 - 2: Simulated temperature-depth profile below the center of sandy-loam riverbed in the summer period under steady-state upward groundwater flow

The curves of average temperature within the upper 1.5m of the riverbed with different sediment textures in the winter and summer period are shown in Figure 5-3. In the winter period, heat was transported from the aquifer towards the river. The greater

temperature gradient was observed in the sandy riverbed which has a much higher thermal conductivity. On the contrary, the average temperature in the river was higher than the temperature in the aquifer during the summer period, thus heat was transported from the river towards the aquifer. The more noticeable decline in temperature was found in the riverbed consisting of sandy clay due to its lower thermal conductivity.

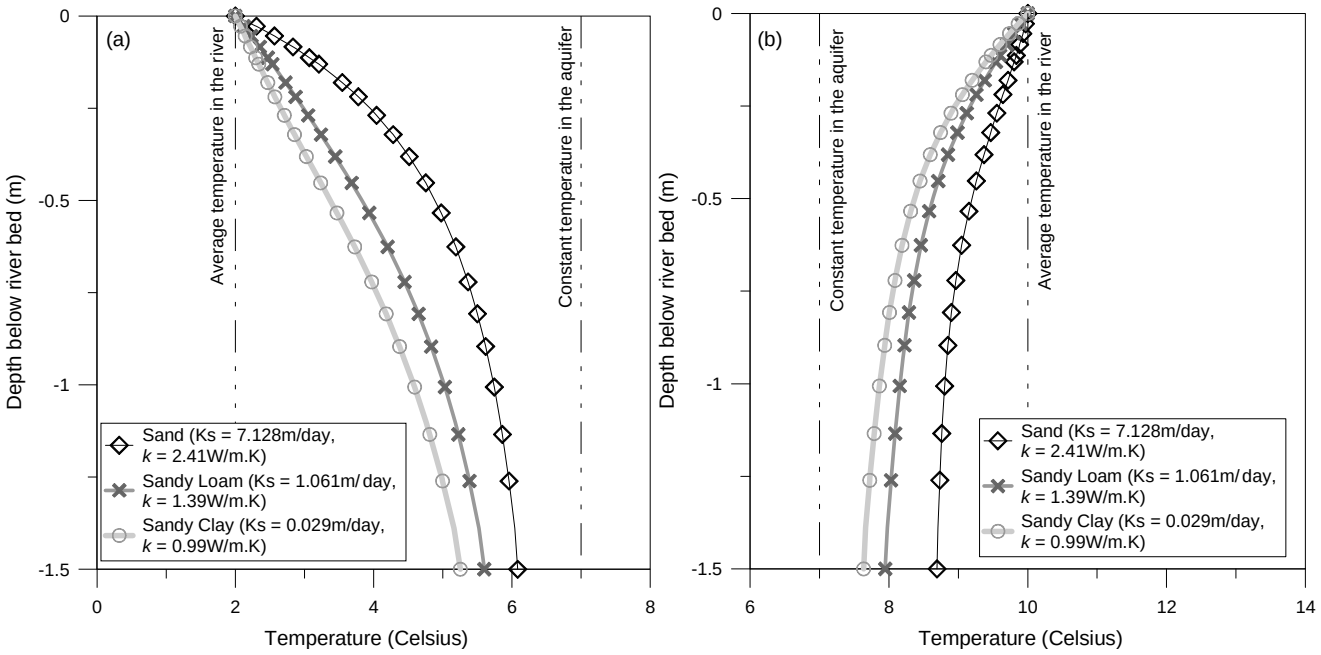


Figure 5 - 3: Comparison of the simulated average temperature-depth profiles in different sediment textures in the (a) winter period and (b) summer period

Simulations were then performed to investigate the attenuation of temperature fluctuations in the riverbed. No significant seasonal difference in $\boldsymbol{Z_d}$ (0.11m) was observed in the riverbed consisting of sandy-clay and sandy-loam. Figure 5-4(a) and 5-4(b) compare the temperature envelope below a sandy riverbed formed by diurnal variation between the minimum and maximum temperatures at different seasons. As the amplitude of surface river water temperature oscillation, $\boldsymbol{T_A(0)}$, was hypothesized to be 1°C, the damping depth $\boldsymbol{Z_d}$ was determined as the depth at which amplitude of temperature oscillation, $\boldsymbol{T_A(z)}$, equals 0.37°C. It can be seen in Figure 5-4, under steady-state groundwater flow condition, the attenuation of temperature fluctuations in summer ($\boldsymbol{Z_d}$ = 0.18m) was deeper than that in winter ($\boldsymbol{Z_d}$ = 0.11m) for the case of sandy riverbed. It was assumed that the steady upwelling groundwater flux in winter would be much larger compared to that in summer.

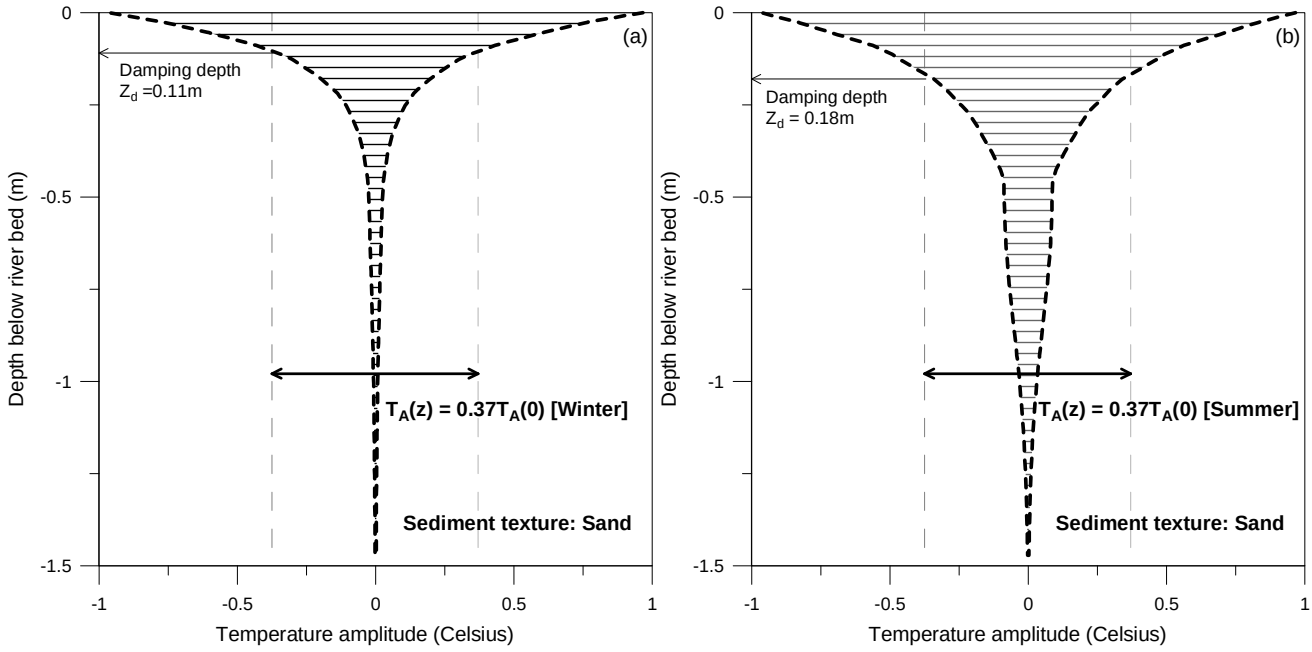


Figure 5 - 4: Comparison of the amplitude of subsurface temperature oscillations versus depth for sandy riverbed in the (a) winter period and (b) summer period

5.3.2 The temperature-based estimates of steady groundwater flux

Figure 5-5(a) to 5-5(c) illustrates the output graphics in HYDRUS of the steady groundwater flow patterns surrounding the riverbed in different seasons. The temperature in the aquifer was fixed at 7°C and the effect of different river temperatures on the model output was compared. Figure 5-6(a) to 5-6(c) compares the effect of different bank slopes (horizontal over vertical distance, H:V, of 0.00, 0.58 and 1.73) on the groundwater flow patterns with the same boundary conditions. Only half of model domain adjacent to the river is shown due to the fact that the model is symmetrical with respect to the center of river. The simulation showed that the groundwater flux at the sides of the river channel tended to be larger and more variable than the groundwater flux near the center. The study of Storey *et al*. (2003) attributed this phenomenon to the depth of permeable alluvial sediment below the riverbed. However in our study the medium is homogeneous. Therefore we have to attribute this to the length of the flow-lines which are shorter at the side of a river as compared to the bottom. The lateral groundwater flux from the sides is larger in winter than in summer, as shown in Figure 5-5(a) to 5-5 (c). There was relatively less seasonal difference in the vertical upwelling groundwater flux near the center of the river channel.

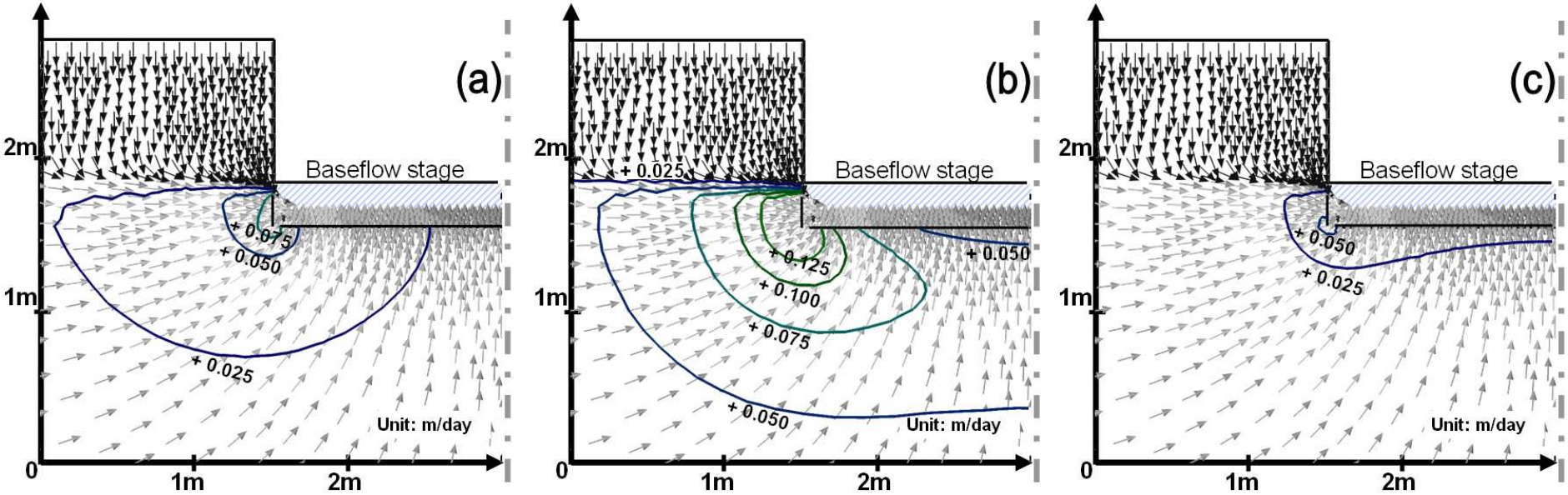


Figure 5 - 5: Graphical output of steady groundwater flow patterns surrounding the riverbed. The sediment texture is sandy-loam. Temperature in the aquifer is assigned to 7°C and temperature in the river is assigned to (a) 7°C; (b) 2°C; and (c) 10°C.

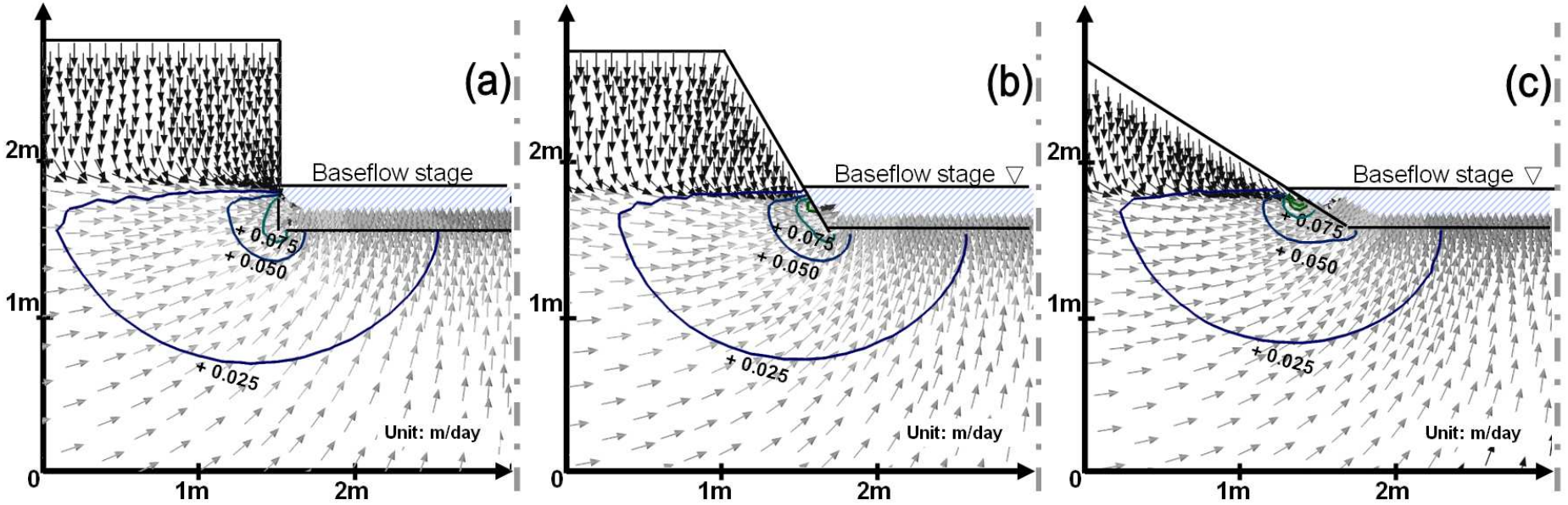


Figure 5 - 6: Graphical output of steady groundwater flow patterns surrounding the sandy-loam riverbed. The bank slope of river channel is set to H:V = (a) 0, (b) 0.58 and (c) 1.73. Temperature in the aquifer and the river is assigned to 7°C

The influence of changing temperatures on water fluxes at the sides and bottom of the river channel at aquifer–riverbed interface in function of sediment texture (sandy-loam and loamy-sand) is summarized in Figure 5-7. The lateral groundwater flux at the side of the river channel was sensitive to the change in river water temperature and the hydraulic conductivity of sediment texture. The flux at the side can be 2-3 times larger as compared to the water flux through the centre of bottom of the riverbed.

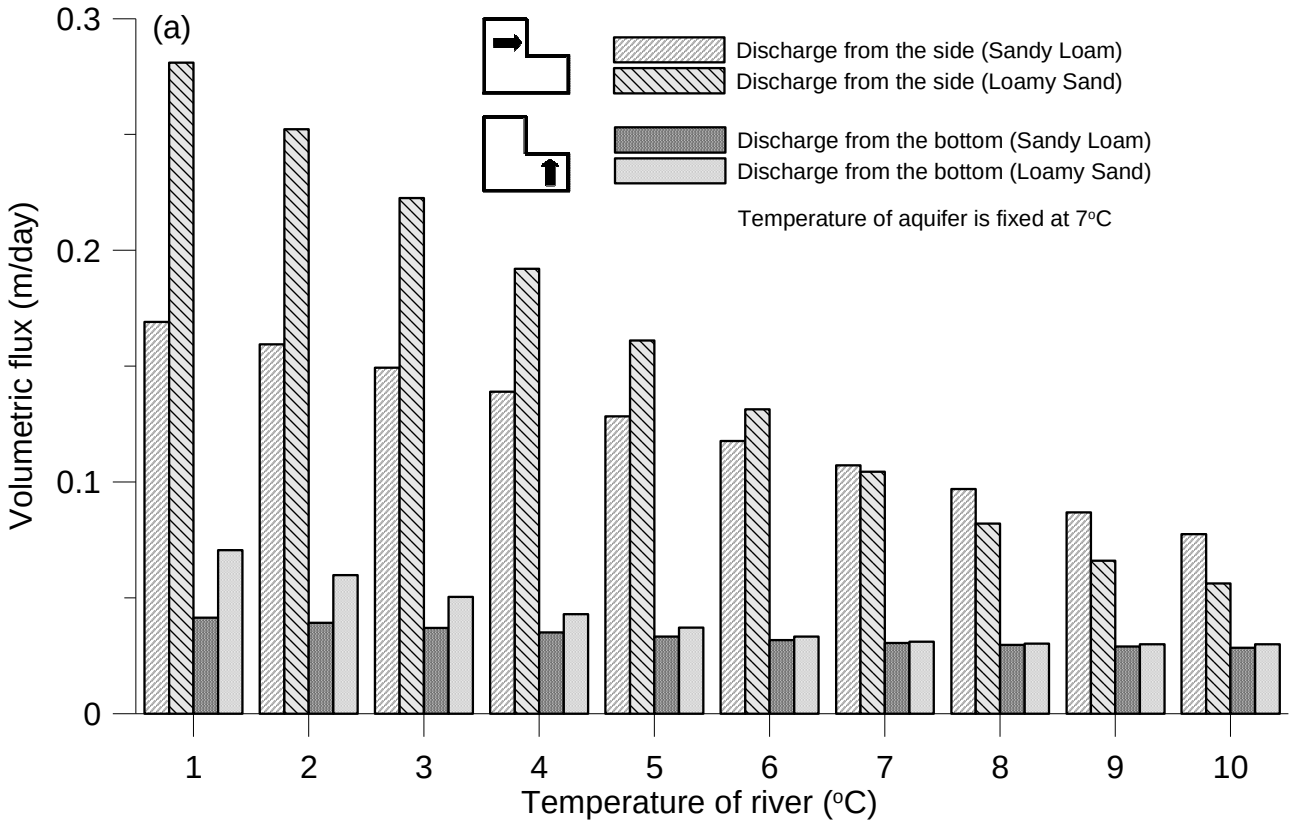


Figure 5 - 7: The estimation of steady volumetric flux at the sides and the bottom of the river channel by changing the temperature at aquifer–riverbed interface and varying the sediment texture

The groundwater flux at the sides of the river channel is more variable as influenced by temperature changes as compared to center of the river bed. It is therefore advisable to measure riverbed temperatures at the center of the river. In what follows attention was focused on the evaluation of groundwater fluxes below the center of river. Figure 5-8 shows steady upwelling groundwater fluxes simulated by HYDRUS and by 1-D an analytical solution. All are calculated for the center of the (a) sandy-clay, (b) sandy-loam and (c) sandy riverbed sediment and for at different seasons. The 1-D analytical solution (Equation 5.2) proposed by Schmidt *et al*. (2007) was used.

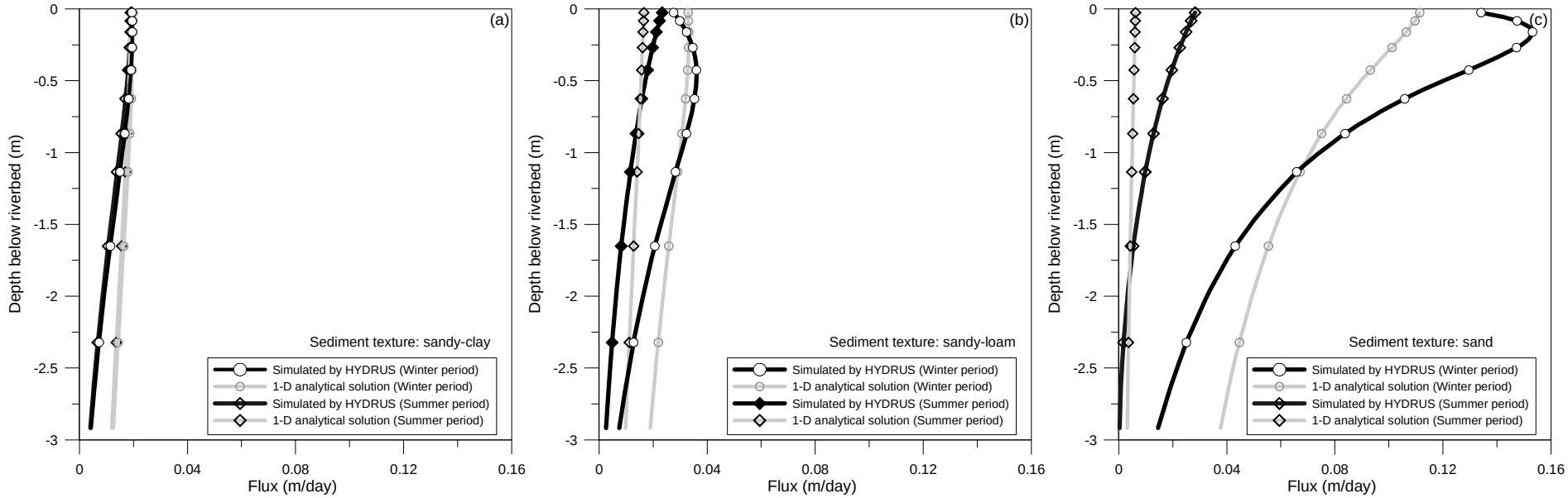


Figure 5 - 8: Comparison of the steady state groundwater fluxes simulated by HYDRUS 2D/3D and calculated by using 1-D analytical solution for sediment textures ranging from (a) sandy-clay, (b) sandy-loam to (c) sand at different seasons

It is shown in Figures 5-8(a), 5-8 (b) and 5-8 (c) that less seasonal differences in vertical distribution of groundwater fluxes were found below the fine-grained clayey sediment. For this texture the calculated groundwater fluxes using 1-D analytical solution were close to the simulated values by HYDRUS. This could be attributed to the fact that in clayey sediment the temperature dependence of the hydraulic conductivity is relatively small. In contrast, a significant seasonal difference in groundwater fluxes was found below much coarser-grained sediment; the greater upwelling groundwater flux was found in winter as compared to summer. The seasonal differences in groundwater fluxes were attributable to the change in temperature gradients between river and groundwater, as already shown in the previous section the greater temperature gradients in the riverbed were present in winter. The calculation by using the 1-D analytical solution showed a similar trend but with a slight deviation. The study of Schmidt *et al*. (2007) attributed the deviation to the uncertainty of subsurface temperature measurements and the spatial heterogeneity of riverbed, however, our simulation shows that in addition the effect of the stronger fluxes near the sides of river channel should also be considered.

5.3.3 The temperature-based estimates of transient penetration of river water

The second stage simulation was performed to evaluate the transient penetration of river water into aquifer induced by the imposed higher water level. The river stage was instantly rising to 1m and remained for 1 day. The temperature of the river water was assumed to remain constant during the rising of river stage. Additionally, the influence of diurnal surface water temperature oscillations on transient water fluxes was assumed to be negligible. Figure 5-9 illustrates the graphical output of (a) the penetration of river water into a sandy-loam riverbed right after the rise in river stage, (b) the penetration of river water into a sandy-loam riverbed after one day, and (c) the recovery of baseflow after the recession of river stage. The negative fluxes represent the transient downwelling flow (i.e. river water penetration into the surrounding aquifer), while the positive fluxes represent the groundwater discharge towards the river.

The instantaneous change in river water level caused a relatively large flux difference at shallow depth below the riverbed. The lateral penetration of river water was also found to be stronger than the downwelling flow at the bottom of the river channel. The penetration pattern of river water in the aquifer would be moderated by the steady groundwater recharge over time. After the recession of the river stage, the penetrated water during high flood stage returned from the aquifer towards the river channel.

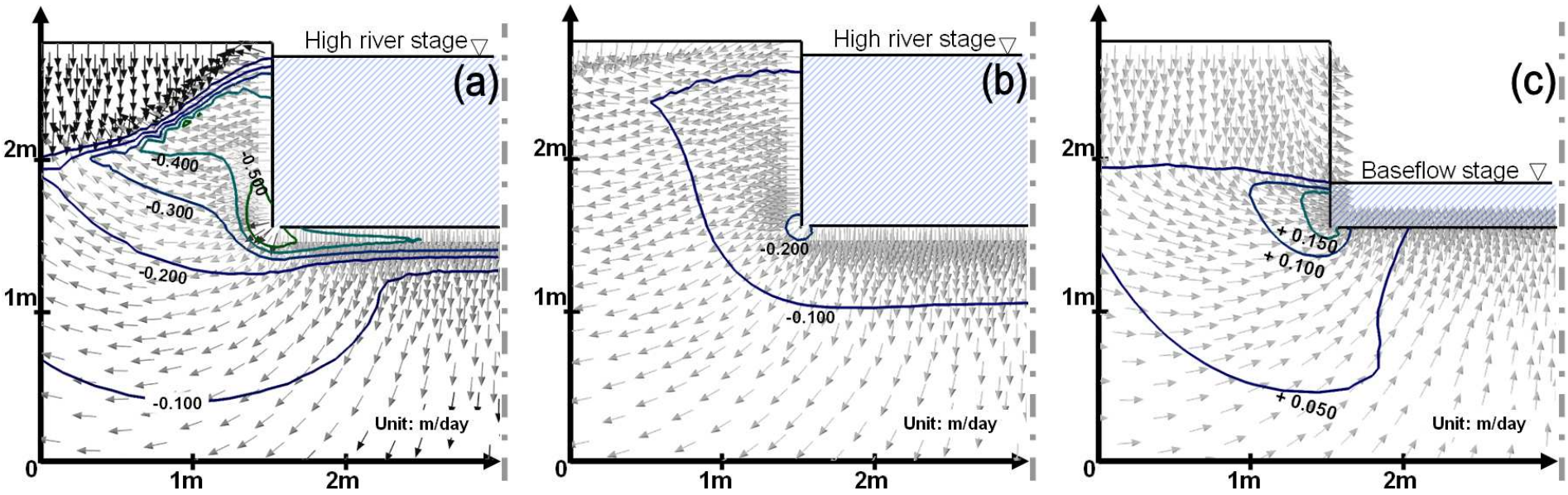


Figure 5 - 9: The graphical output of (a) the penetration of river water into a sandy-loam riverbed right after the rise in river stage, (b) the penetration of river water into a sandy-loam riverbed after 1 day and (c) the recovery of baseflow after the recession of river stage. The rise of water level was assigned to be 1m

As concluded in the study by Storey *et al*. (2003) the hyporheic exchange flows across the aquifer–riverbed interface are only possible when high-permeability sediments (saturated hydraulic conductivity, ***Ks*** > 10^{-5}m/s) were surrounding the river channel. Two types of sediment texture: (a) sandy-loam (***Ks*** = 1.23×10^{-5}m/s, ***κ*** = 1.39W/m·K) and (b) loamy-sand (***Ks*** = 4.05×10^{-5}m/s, ***κ*** = 2.41W/m·K), were selected for simulation of this stage.

The particle tracking option in HYDRUS was used for the characterization of the spatial and temporal variability of the hyporheic zone. Several flowing particles were released from the side and the bottom of the river channel during the change of river stage. Figure 5-10(a) illustrates the travelling distances of the flowing particles in the aquifer during the high river stage event after 0.1day, 0.2 day, 0.5 day and 1day. The flow trajectories of particles can be seen in Figure 5-10(b).

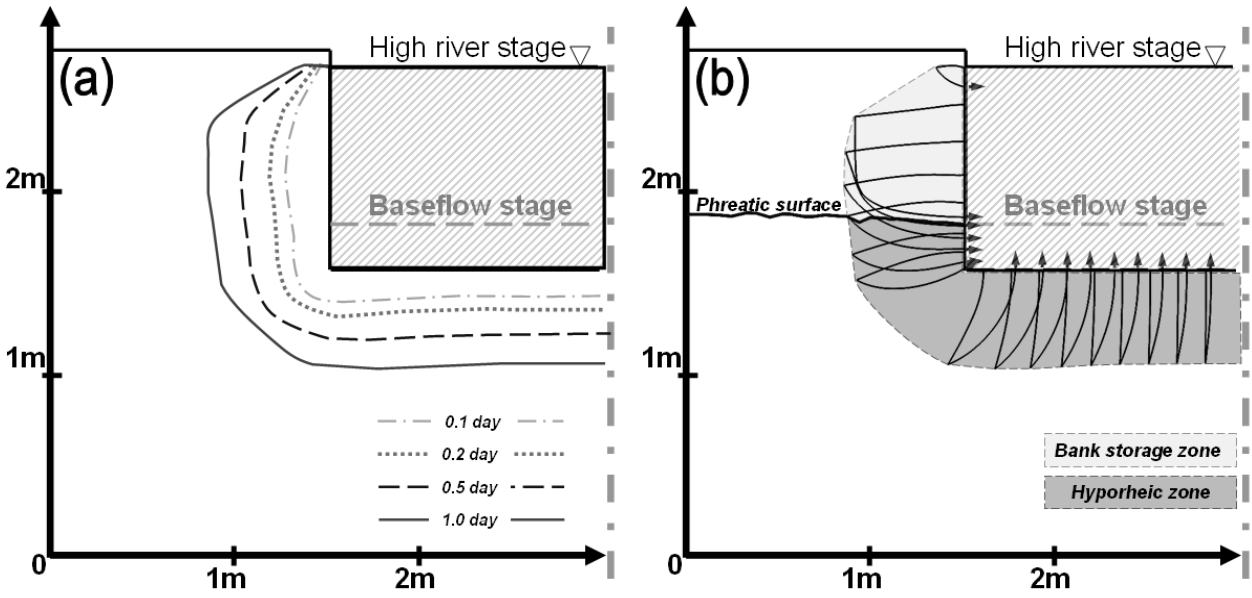


Figure 5 - 10: (a) Travelling distances of the flowing particles in the aquifer during the high river stage event after 0.1 day, 0.2 day, 0.5 day and 1 day; (b) The flow trajectories of particles and the distinction between bank storage zone and hyporheic zone

Unlike previous studies that lumped together bank storage and hyporheic exchange as a single storage zone (Bencala and Walters, 1983; Laenen and Bencala, 2001; Chen and Chen, 2003), a clear distinction can be drawn in Figure 5-10(b). The light-gray area above the phreatic surface indicates the bank storage zone. During the high river stage event, river water infiltrated into the bank storage zone. After the recession of the river stage, the infiltrated river water in the bank storage zone was not only directed back towards the river, but also mixed with shallow groundwater and released as baseflow at a later time. Correspondingly, the flow trajectory of particles in the bank storage zone was found to be relatively long, which resulted in relatively long residence times. The dark-gray area below the phreatic surface indicates the hyporheic zone, where the penetration of river water mixed with the shallow groundwater. The flow trajectories of particles were getting shorter near the center of the river channel.

Figures 5-11(a) to 5-11(d) showed the maximum distance of river water penetration in the aquifer in one day duration, the effect of changing river temperature conditions and hydraulic conductivities on the spatial variability of hyporheic zone can be quantified. The cumulative flux across the side ***QLin*** and the bottom ***QVin*** of the river channel in one day duration can also be calculated from the internal mesh-lines. The simulation reveals that the lateral extent ***DLin*** of the hyporheic zone can be 2 to 3.5 times longer than its vertical extent ***DVin*** below the riverbed. Change in the hydraulic conductivity of sediment has a great impact on the magnitude and spatial extent of hyporheic exchange flows. The ratio of cumulative groundwater flux across the side and the bottom of the river channel over 1 day (***QLin***/***QVin***) is estimated to be 1.5-1.8 for the sandy-loam sediment, and 1.2-1.3 for the loamy-sand sediment. The greater flux of river water penetration occurred during the summer period due to the increase in hydraulic conductivity, which is attributed to the decrease in viscosity of the water. Consequently, hyporheic exchange flows tend to be more intense in summer than in winter.

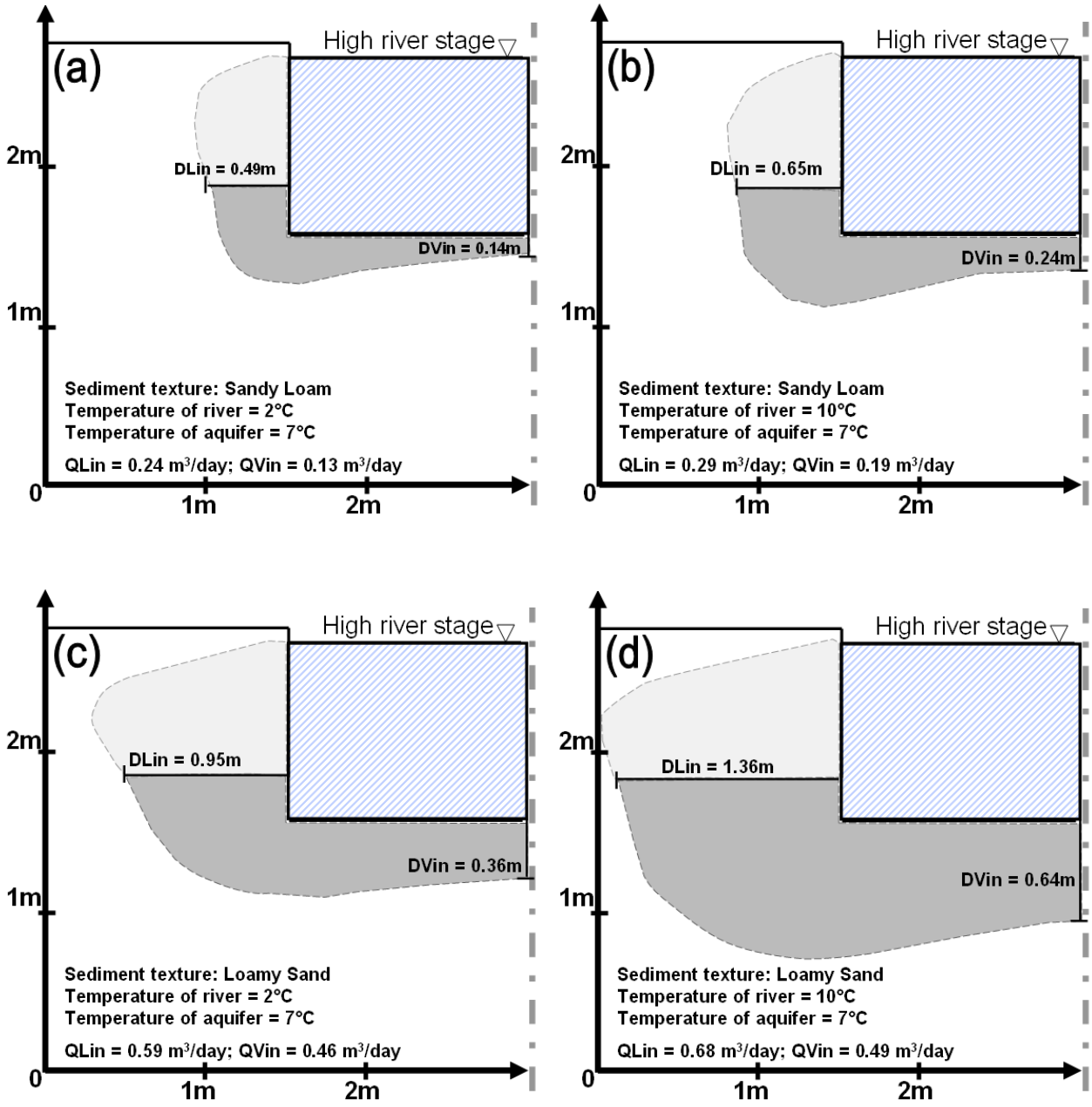


Figure 5 - 11: The estimated vertical versus lateral flow paths of hyporheic zone in (a) sandy-loam sediment during winter; (b) sandy-loam sediment during summer; (c) loamy-sand sediment during winter; (d) loamy-sand sediment during summer in 1 day duration

5.4 Conclusions and recommendations

The measurement of temperature is able to provide quantitative estimation for both long-term and transient groundwater flow regimes. This study applied HYDRUS to simulate the river–aquifer interaction in the shallow aquifer. It provides a useful and simple framework for interpreting the flux variability in the riverbed associated with the change of ambient temperature. By respectively analyzing the long-term steady discharge and the transient downwelling groundwater flow patterns surrounding the riverbed, the vertical versus lateral flow paths of the hyporheic zone can be accurately delineated. Many previous studies that considered the hyporheic zone as a fixed volume adjacent to the river channel and denoted its boundary by the discontinuity of physical or chemical properties. In contrast our study revealed that the extent of hyporheic zone varies in different seasons and sediment permeability. We also can make a distinction between the bank storage zone above the normal phreatic water table and the hyporheic zone.

The following conclusions and recommendations are obtained from this study:

1. The temperature dependence of hydraulic conductivity cannot be ignored in the field study of river-aquifer interaction. It is especially crucial for the evaluation of transient water flux in shallow aquifers. The thermal regime in the riverbed substrate is influenced not only by the thermal properties of the sediment but also the magnitude of groundwater flux through the aquifer.

2. For a river system gaining baseflow from a surrounding aquifer with a steady recharge, the groundwater flux through the side of the riverbed is larger than the flux across the bottom of the river channel. This is due to the fact that groundwater flow lines near the side of a river are relatively shorter and therefore with a stronger hydraulic gradient. The difference is more significant during winter when the temperature of the river water is lower than that of the aquifer. In addition, the groundwater discharge from the side of the river channel is more sensitive to a change in river water temperature, whereas less seasonal variability in the vertical groundwater discharge from the bottom is found.

3. The application of Schmidt *et al*. (2007) analytical solution only provides a rough estimation of the upward groundwater fluxes. In order to apply this analytical solution, the data logging of groundwater temperature is recommended to be kept a certain distance from the sides of the river channel. Consequently, the combination

of a 2-D coupled groundwater flow and heat transfer numerical model, like HYDRUS, is recommended as it can improve the reliability of estimates in the field study.

4. Hyporheic exchange flows tend to be more intense in summer than in winter. The lateral penetration of river water into the aquifer during high flood events was also found to be stronger than the downwelling flow at the bottom of the river channel. The lateral extent of the hyporheic zone is found to be 2 to 3.5 times longer than its vertical extent.

5. The current study assumes that the sediments were homogeneous and isotropic. Further numerical simulation should be performed to evaluate the influence of subsurface heterogeneity on temporal and spatial variability of riverbed-aquifer interactions. More research is required to investigate the effect of both long-term and instantaneous changes in river temperature on the patterns of fluxes exchange in the hyporheic zone.

Chapter 6
Conclusions and Recommendations for Future Research

6.1 General conclusions

The hyporheic zone is a very crucial link between river and aquifer. It is the region under and alongside the riverbed where mixing of shallow groundwater and river water occurs. The water exchange in the hyporheic zone has an important impact on the transport of contaminant, energy, and organisms within the catchment. The hyporheic zone is also an active ecotone with consequences for biodiversity and environmental quality.

It is well documented that hyporheic exchange flows are governed by transient processes closely related to the catchment rainfall-runoff dynamics. The principal controlling mechanisms of hyporheic exchange flows are flow-induced pressure-differences across the riverbed. Larger changes in vertical hydraulic gradient associated with high water-table elevation will result in more intensive mixing of groundwater and river water. The extent of the hyporheic zone thus varies in time and space, which dominates the physical, chemical and biological transitions between the river and the surrounding aquifer.

As a result, the hyporheic zone can be defined and delineated as the zone in which water fluxes are bidirectional, so that exchange and mixing between river and aquifer occurs. The fluxes reverse direction is a function of river-stage fluctuations in combination to the groundwater flow towards the river. In order to understand the exchange of river water and groundwater it is crucial to quantify these fluctuating fluxes.

However, traditional measurement techniques are usually labour-intensive, time-consuming, intrusive and difficult for interpreting of the small scale water flux variability in the riverbed. The applications of traditional chemical tracer studies are not able to measure at a short spatial and temporal resolution. They have difficulty to

distinguish the difference between lateral and vertical exchange of water across the aquifer–riverbed interface. There is certainly a need for having an improved modelling along with a measurement methodology.

In addition, according to the literature review, the importance of lateral groundwater inflow originating from the recharge was often neglected in hyporheic research. There is a big gap in our understanding of the hydrodynamic transport from the unsaturated zone, passing the surrounding aquifer into the river. Since river and aquifer are considered as a whole entity within the watershed, the conceptual integration with the focus on aquifer will contribute to a better insight of the whole hydrologic pattern in the hyporheic zone.

Consequently, this PhD research has investigated riverbed-aquifer flux interactions in a systematic way. In order to accurately identify the physical processes and characteristics in the hyporheic zone in conjunction with the adjacent aquifer, a laboratory J-shaped column experiment was developed. This J-shaped column model represents a schematic flow line in the succession of unsaturated recharge zone, saturated zone (aquifer) and river. The experimental setup was combined with various measurement techniques and equipments. The usefulness and relevance of this laboratory setup was confirmed in this research.

Two series of experiments were conducted to study the exchange of bidirectional flow between the river and the aquifer. The experimental measurements were compared with the numerical simulations by means of HYDRUS. The main tasks which have been carried out were the following:

Dispersion of lateral groundwater inflow into the river

In the first experiment, we characterized the transport of dissolved material by hydrodynamic dispersion in the hyporheic zone in conjunction with the adjacent aquifer. By analysing consecutive column segments with the application of the transfer function method proposed by Mojid *et al*. (2004), transport parameters including pore water velocity and dispersivity were determined for both unsaturated and saturated sections along the column.

The conclusions of this experiment are:

1. The observed pore velocities were much higher in the unsaturated section (i.e. in vadose zone), where the water content is lower and the water filled pore space is less. The pore-water velocity then decreased dramatically in the saturated section (i.e. in riverbed in conjunction with the adjacent aquifer), and the measured dispersion coefficients varied accordingly.

2. It was found that the classical estimation of dispersivity, i.e. by dividing the dispersion coefficient by the pore water velocity, neglecting the molecular diffusion effect and taking empirical coefficient $n = 1$ did not deliver consistent results. The calculated dispersivity was flux dependent and increased at lower flux in unsaturated section; in contrast, it was fairly constant and independent of flux variation in saturated section.

3. In order to simulate over the entire range of fluxes and water contents as present in the continuum of the unsaturated zone, aquifer and river, a more general relationship was identified. We found the longitudinal dispersion coefficient can best be related to the square of the ratio of pore-water velocity over soil water content. This relation can be used for simulating the transport of solutes and other substances in the environment which is imbedded by saturated and unsaturated zones. The testing by using HYDRUS 2D/3D also supported the use of this relation to determine dispersion coefficients as it presented a better correlation than the inverse modelling by fitting dispersivities.

4. The parameter α controlling the shape of the soil water retention curve should be given sufficient attention when evaluating the hydrodynamic dispersion transport parameters in a variably saturated environment.

Can temperature be used as a tracer for estimating transient water flux?

In this experiment, we studied the penetration of river water into the riverbed. We created a square shaped hydrograph (mimicking a simplified flood event) by instantaneously raising the water level at the river section of the J-shaped column model. This hydrograph altered the vertical hydraulic gradient and reversed the flow direction in the riverbed. Since the techniques of using dye or salt solution as a tracer were considered to be difficult to sample within a small distance in this case, we tried whether temperature can be used as an indirect tracer to estimate the fluctuating water fluxes. The numerical model HYDRUS was used to simulate water flow and heat

transfer.

During each experiment, a square shaped hydrograph accompanied with a simultaneous change in water temperature was created in the river section. The hydrograph was ended by a similar step function after 30 minutes. By using the flowing particle tracking options in HYDRUS, the simulated extent of river water penetration was found to be limited to shallow depths in the riverbed only. The corresponding temperature change measured by the thermocouple during experiments also revealed the same trend. Sharper rise in river-stage resulted in a relatively steeper gradient of temperature at shallow depth; while temperature profiles at deeper depths did not show substantial changes.

The conclusions of this experiment are:

1. It was found that the rapid change in groundwater temperature has an important effect on hydraulic conductivity. However, the simple scaling of the viscosity in function of temperature is not able to predict the hydraulic conductivity. Hydraulic conductivity is a crucial parameter which should be systematically updated by inverse modelling using heat as a tracer. This is especially important for accurately characterising the extent of the hyporheic zone.

2. We concluded that temperature can be used as an indirect tracer to assist the estimation of fluctuating water fluxes in the field. As a first step, temperature data at shallow depth below the riverbed are used in order to determine the optimal hydraulic conductivity through inverse modelling. The thermal conductivity could be taken as temperature invariant. The objective function in this step is the minimum sum of squared deviations between observed and simulated temperatures. As the most prominent temperature changes were detected at shallow depth below the riverbed the majority of sensors should consequently be placed close to the riverbed and at short distances from each other. After determination of the optimal conductivity, the fluctuating water fluxes below the riverbed can be estimated by a numerical model, such as HYDRUS.

3. As the most prominent temperature changes were detected at shallow depth below the riverbed, consequently, the majority of sensors should be placed close to the riverbed and at short distance from each other. Sensors in the river water and at a distance in the aquifer are important to measure the boundary conditions.

4. The flux fluctuations below and near the riverbed are influenced by the groundwater inflow. The influence of this lateral inflow needs to be considered in the study of the hyporheic zone. This requires data logging of water levels in piezometers and of temperature so that this inflow can also be quantified.

Numerical simulation by HYDRUS 2D/3D of long- and short-term groundwater flux in the hyporheic zone as influenced by temperature regimes and changing river stage

In the last part of the research, we investigated the influence of temperature and river stage changes on riverbed-aquifer flux interactions in the hyporheic zone by the numerical simulation using HYDRUS 2D/3D. The change in ambient temperatures is easily influenced by meteorological conditions and by human activities, which has a substantial effect on water flux variability in shallow aquifers. This model provides a useful and simple framework for interpreting the flux variability in the riverbed associated with the change of ambient temperature. By respectively analyzing the long-term steady discharge and the transient downwelling groundwater flow patterns surrounding the riverbed, the vertical versus lateral flow paths of the hyporheic zone can be accurately delineated. Unlike previous studies that considered the hyporheic zone as a fixed volume adjacent to the river channel and denoted its boundary by the discontinuity of physical or chemical properties, this study revealed that the extent of hyporheic zone varies in different seasons and sediment permeability. In this study a distinction can also be made between the bank storage zone and the hyporheic zone.

The conclusions of this numerical simulation are:

1. The temperature dependence of hydraulic conductivity should not be ignored in the field study of river-aquifer interaction. It is especially crucial for the evaluation of transient water flux in shallow aquifers. The thermal regime in the riverbed substrate is influenced not only by the thermal properties of the sediment but also the magnitude of groundwater flux through the aquifer.

2. For a gaining river system which receives constant recharge by precipitation, as shown in this study, the steady groundwater flux at the side is stronger than the flux across the bottom of the river channel. This is due to the fact that groundwater flow lines near the side of a river are relatively shorter. The difference is significant during winter when the temperature of the river is much lower than the aquifer. In

addition, the groundwater discharge from the side of the river channel is more sensitive to a change in river water temperature, whereas less seasonal variability in the vertical groundwater discharge from the bottom is found.

3. The application of Schmidt *et al*. (2007) analytical solution only provides a rough estimation of the upward groundwater fluxes. In order to apply this analytical solution, the data logging of groundwater temperature is recommended to be kept a certain distance from the sides of the river channel. Consequently, the combination of a 2-D coupled groundwater flow and heat transfer numerical model, like HYDRUS, is necessary as it would improve the reliability of estimates in the field study.

4. It was found that the hyporheic exchange flows tend to be more intense in summer than in winter. The lateral penetration of river water into the aquifer during high flood events was also found to be stronger than the downwelling flow at the bottom of the river channel. The lateral extent of the hyporheic zone is found to be 2 to 3.5 times longer than its vertical extent.

6.2 Recommendations for the future research

The recommendations for the future research are the following:

Further research with the laboratory model:

- It is recommended that the relation between longitudinal dispersion coefficient and the ratio of pore-water velocity over soil water content should be tested with different soil types and moisture status under more field-realistic conditions.
- The improvement of the experimental setup of J-shaped column model is recommended to include a horizontal section between the two bends. The evaluation of aquifer heterogeneity on spatial distribution of groundwater flow can be involved in the modelling.
- The combination of temperature measurement and conservative tracer experiments in this laboratory model could provide more insights into the mechanisms underlying the exchange of bidirectional flow in the riverbed.

Further research with the field-scale numerical model:

- The current study assumes that the sediments were homogeneous and isotropic. Investigating the hyporheic exchange flows in real rivers is expected to be much more complex. Further numerical simulation should be performed to evaluate the influence of subsurface heterogeneity on temporal and spatial variability of riverbed-aquifer interactions. More research is required to investigate the effect of both long-term and instantaneous changes in river temperature on the patterns of fluxes exchange in the hyporheic zone.
- The geometric setting of the numerical model is recommended to include irregular cross section for the river, which will be able to better approximate the existing natural topography.
- More research is required to investigate the effect of long-term or instantaneous changes in river temperature on the exchange of bidirectional flow in the riverbed.

Considerations for the fieldwork implementation:

- Thermal effects on temporal variability of hydraulic conductivity should not be ignored in the field study of river-aquifer interaction. The existing relations appear not to be valid under transient conditions because of the fact that the porous medium is composed of grains and water, which are at different and heterogeneous temperatures. Consequently, strategies in determining the most appropriate updating scheme for hydraulic conductivity under transient heat transfer in transient water flow conditions are influential. A simple and robust pragmatic optimisation of hydraulic conductivity by inverse modelling in function of temperature is required.

References

Alexander MD, Caissie D. 2003. Variability and comparison of hyporheic water temperatures and seepage fluxes in a small Atlantic salmon stream. *Ground Water* **41**: 72-82. DOI: 10.1111/j.1745-6584.2003.tb02570.x.

Anderson JK, Wondzell SM, Gooseff MN, Haggerty R. 2005. Patterns in stream longitudinal profiles and implications for hyporheic exchange flow at the H.J. Andrews Experimental Forest, Oregon, USA. *Hydrological Processes* **19**: 2931-2949. DOI: 10.1002/hyp.5791.

Anderson MP. 2005. Heat as a ground water tracer. *Ground Water* **43**: 951-968. DOI: 10.1111/j.1745-6584.2005.00052.x.

Anibas C, Fleckenstein JH, Volze N, Buis K, Verhoeven R, Meire P, Batelaan O. 2009. Transient or steady-state? Using vertical temperature profiles to quantify groundwater-surface water exchange. *Hydrological Processes*. DOI: 10.1002/hyp.7289.

Baker MA, Dahm CN, Valett HM. 2000. Anoxia, Anaerobic Metabolism, and Biogeochemistry of Stream-water-Ground-water Interface. In *Streams and Ground Waters*, Jones JB, Mulholland PJ (eds). Academic Press: New York; 259-283.

Bärlocher F, Seena S, Wilson KP, Williams DD. 2008. Raised water temperature lowers diversity of hyporheic aquatic hyphomycetes. *Freshwater Biology* **53**: 368-379. DOI: 10.1111/j.1365-2427.2007.01899.x.

Battin TJ. 1999. Hydrologic flow paths control dissolved organic carbon fluxes and metabolism in an alpine stream hyporheic zone. *Water Resources Research* **35**: 3159-3169. DOI: 10.1029/1999WR900144.

Battin TJ. 2000. Hydrodynamics is a major determinant of streambed biofilm activity: From the sediment to the reach scale. *Limnology and Oceanography* **45**: 1308-1319.

Battin TJ, Kaplan LA, Newbold JD, Hendricks SP. 2003. A mixing model analysis of stream solute dynamics and the contribution of a hyporheic zone to ecosystem function. *Freshwater Biology* **48**: 995-1014. DOI: 10.1046/j.1365-2427.2003.01062.x.

Bear J. 1972. *Dynamics of fluids in porous media*. American Elsevier: New York. 764 pp.

Becker MW, Georgian T, Ambrose H, Siniscalchi J, Fredrick K. 2004. Estimating flow and flux of ground water discharge using water temperature and velocity. *Journal of Hydrology* **296**: 221-233. DOI: 10.1016/j.jhyrol.2004.03.025.

Belaidi N, Taleb A, Gagneur J. 2004. Composition and dynamics of hyporheic and surface fauna in a semi-arid stream in relation to the management of a polluted reservoir. *Annales De Limnologie-International Journal of Limnology* **40**: 237-248. DOI: 10.1051/limn/2004020.

Bencala KE, Walters RA. 1983. Simulation of solute transport in a mountain pool-and-riffle stream - a transient storage model. *Water Resources Research* **19**: 718-724. DOI: 10.1029/WR019i003p00718.

Bencala KE. 2000. Hyporheic zone hydrological processes. *Hydrological Processes* **14**: 2797-2798. DOI: 10.1002/1099-1085(20001030)14:15<2797::AID-HYP402>3.0.CO;2-6.

Bencala KE. 2005. Hyporheic exchange flows. In *Encyclopedia of Hydrological Sciences*, Anderson MG (ed). John Wiley & Sons: New Jersey, 1733-1740.

Biksey TM, Gross ED. 2001. The hyporheic zone: linking groundwater and surface water – understanding the paradigm. *Remediation Journal* **12**: 55-62. DOI: 10.1002/rem.1025.

Blasch KW, Ferré TPA, Hoffmann JP. 2004. A statistical technique for interpreting streamflow timing using streambed sediment thermographs. *Vadose Zone Journal* **3**: 936-946. DOI: 10.2113/3.3.936.

Blume E, Bischoff M, Reichert JM, Moorman T, Konopka A, Turco RF. 2002. Surface and subsurface microbial biomass, community structure and metabolic activity as a function of soil depth and season. *Applied Soil Ecology* **20**: 171-181. DOI: 10.1016/S0929-1393(02)00025-2.

Blume T, Zehe E, Bronstert A. 2008. Investigation of runoff generation in a pristine, poorly gauged catchment in the Chilean Andes II: Qualitative and quantitative use of tracers at three spatial scales. *Hydrological Processes* **22**: 3676-3688. DOI: 10.1002/hyp.6970.

Boano F, Revelli R, Ridolfi L. 2007. Bedform-induced hyporheic exchange with unsteady flows. *Advances in Water Resources* **30**: 148-156. DOI: 10.1016/j.advwatres.2006.03.004.

Borselli L, Cassi P, Torri D. 2008. Prolegomena to sediment and flow connectivity in the landscape: A GIS and field numerical assessment. *Catena* **75**: 268-277. DOI: 10.1016/j.catena.2008.07.006.

Boulton AJ. 1993. Stream ecology and surface hyporheic hydrologic exchange - implications, techniques and limitations. *Australian Journal of Marine and Freshwater Research* **44**: 553-564. DOI: 10.1071/MF9930553.

Boulton AJ, Findlay S, Marmonier P, Stanley EH, Valett HM. 1998. The functional significance of the hyporheic zone in streams and rivers. *Annual Review of Ecology and Systematics* **29**: 59-81. DOI: 10.1146/annurev.ecolsys.29.1.59.

Boulton AJ. 2007. Hyporheic rehabilitation in rivers: restoring vertical connectivity. *Freshwater Biology* **52**: 632-650. DOI: 10.1111/j.1365-2427.2006.01710.x.

Boxall GD, Giannico GR, Li HW. 2008. Landscape topography and the distribution of Lahontan cutthroat trout (*Oncorhynchus clarki henshawi*) in a high desert stream. *Environmental biology of fishes* **82**: 71-84. DOI: 10.1007/s10641-007-9254-1.

Bracken LJ, Croke J. 2007. The concept of hydrological connectivity and its contribution to understanding runoff-dominated geomorphic systems. *Hydrological Processes* **21**: 1749-1763. DOI: 10.1002/hyp.6313.

Bredehoeft JD, Papadopulos IS. 1965. Rates of vertical groundwater movement estimated from the earth's thermal profile. *Water Resources Research* **1**: 325-328. DOI: 10.1029/WR001i002p00325.

Brown LE, Hannah DM, Milner AM. 2005. Spatial and temporal water column and streambed temperature dynamics within an alpine catchment: implications for benthic communities. *Hydrological Processes* **19**: 1585-1610. DOI: 10.1002/hyp.5590.

Brunke M, Gonser T. 1997. The ecological significance of exchange processes between rivers and groundwater. *Freshwater Biology* **37**: 1-33. DOI: 10.1046/j.1365-2427.1997.00143.x.

Burow KR, Constantz J, Fujii R. 2005. Heat as a tracer to estimate dissolved organic carbon flux from a restored wetland. *Ground Water* **43**: 545-556. DOI: 10.1111/j.1745-6584.2005.0055.x.

Butturini A, Bernal S, Sabater S, Sabater F. 2002. The influence of riparian-hyporheic zone on the hydrological responses in an intermittent stream. *Hydrology and Earth System Sciences* **6**: 515-525.

Caissie D. 2006. The thermal regime of rivers: a review. *Freshwater Biology* **51**: 1389-1406. DOI: 10.1111/j.1365-2427.2006.01597.x.

Cardenas MB, Wilson JL. 2007. Effects of current-bed form induced fluid flow on the thermal regime of sediments. *Water Resources Research* **43**. DOI: 10.1029/2006WR005343.

Chen X, Chen XH. 2003. Stream water infiltration, bank storage, and storage zone changes due to stream-stage fluctuations. *Journal of Hydrology* **280**: 246-264. DOI: 10.1016/s0022-1694(03)00232-4.

Cirmo CP, McDonnell JJ. 1997. Linking the hydrologic and biogeochemical controls of nitrogen transport in near-stream zones of temperate-forested catchments: a review. *Journal of Hydrology* **199**: 88-120. DOI: 10.1016/S0022-1694(96)03286-6.

Cleven EJ. 2004. Seasonal and spatial distribution of ciliates in the sandy hyporheic zone of a lowland stream. *European Journal of Protistology* **40**: 71-84. DOI: 10.1016/j.ejop.2003.11.002.

Conant Jr B. 2004. Delineating and quantifying ground water discharge zones using streambed temperatures. *Ground Water* **42**: 243-257. DOI: 10.1111/j.1745-6584.2004.tb02671.x.

Constantz J, Thomas CL. 1996. The use of streambed temperature profiles to estimate the depth, duration, and rate of percolation beneath arroyos. *Water Resources Research* **32**: 3597-3602. DOI: 10.1029/96WR03014.

Constantz J, Stonestrom DA. 2003. Heat as a tracer of water movement near streams. In *Heat as a tool for*

studying the movement of ground water near streams, Stonestrom DA, Constantz J (eds). U.S. Geological Survey: Reston, Virginia; 1-6.

Constantz J, Cox MH, Su GW. 2003a. Comparison of heat and bromide as ground water tracers near streams. *Ground Water* **41**: 647-656. DOI: 10.1111/j.1745-6584.2003.tb02403.x.

Constantz J, Tyler SW, Kwicklis E. 2003b. Temperature-profile methods for estimating percolation rates in arid environments. *Vadose Zone Journal* **2**: 12-24. DOI: 10.2113/2.1.12.

Costa JL, Prunty L. 2006. Solute transport in fine sandy loam soil under different flow rates. *Agricultural Water Management* **83**: 111-118. DOI: 10.1016/j.agwat.2005.10.002.

Cox MH, Su GW, Constantz J. 2007. Heat, chloride, and specific conductance as ground water tracers near streams. *Ground Water* **45**: 187-195. DOI: 10.1111/j.1745-6584.2006.00276.x.

Cozzetto K, McKnight D, Nylen T, Fountain A. 2006. Experimental investigations into processes controlling stream and hyporheic temperatures, Fryxell Basin, Antarctica. *Advances in Water Resources* **29**: 130-153. DOI: 10.1016/j.advwatres.2005.04.012.

Dahiya R, Ingwersen J, Streck T. 2007. The effect of mulching and tillage on the water and temperature regimes of a loess soil: Experimental findings and modeling. *Soil & Tillage Research* **96**: 52-63. DOI: 10.1016/j.still.2007.02.004.

Dahm CN, Grimm NB, Marmonier P, Valett HM, Vervier P. 1998. Nutrient dynamics at the interface between surface waters and groundwaters. *Freshwater Biology* **40**: 427-451. DOI: 10.1046/j.1365-2427.1998.00367.x.

Dalgaard P. 2004. *Introductory Statistics with R*. Springer-Verlag: New York. 267 pp.

Datry T, Larned ST, Scarsbrook MR. 2007. Responses of hyporheic invertebrate assemblages to large-scale variation in flow permanence and surface-subsurface exchange. *Freshwater Biology* **52**: 1452-1462. DOI: 10.1111/j.1365-2427.2007.01775.x.

De Smedt F, Wierenga PJ. 1984. Solute transfer through columns of glass-beads. *Water Resources Research* **20**: 225-232. DOI: 10.1029/WR020i002p00225.

Dent CL, Schade JD, Grimm NB, Fisher SG. 2000. Subsurface influences on surface biology. In *Streams and Ground Waters*, Jones JB, Mulholland PJ (eds). Academic Press: New York; 381-402.

Dim JR, Sakura Y, Fukami H. 2002. Heat transport analysis and three-dimensional thermo-hydraulic simulation in the Ishikari basin, Hokkaido, Japan. *Hydrological Processes* **16**: 2221-2238. DOI: 10.1002/hyp.1152.

Duff JH, Triska FJ. 2000. Nitrogen biogeochemistry and surface-subsurface exchange in streams. In *Streams and Ground Waters*, Jones JB, Mulholland PJ (eds). Academic Press: New York; 197-220.

Ebersole JL. 2003. Thermal heterogeneity, stream channel morphology, and salmonid abundance in northeastern Oregon streams. *Canadian Journal of Fisheries and Aquatic Sciences* **60**: 1266. DOI: 10.1139/f03-107.

Elliott AH, Brooks NH. 1997a. Transfer of nonsorbing solutes to a streambed with bed forms: Theory. *Water Resources Research* **33**: 123-136. DOI: 10.1029/96WR02784.

Elliott AH, Brooks NH. 1997b. Transfer of nonsorbing solutes to a streambed with bed forms: Laboratory experiments. *Water Resources Research* **33**: 137-151. DOI: 10.1029/96WR02783.

Ellis PA, Mackay R, Rivett MO. 2007. Quantifying urban river-aquifer fluid exchange processes: A multi-scale problem. *Journal of Contaminant Hydrology* **91**: 58-80. DOI: 10.1016/j.jconhyd.2006.08.014.

Essaid HI, Zamora CM, McCarthy KA, Vogel JR, Wilson JT. 2008. Using heat to characterize streambed water flux variability in four stream reaches. *Journal of Environmental Quality* **37**: 1010-1023. DOI: 10.2134/jeq2006.0448.

Evans EC, Petts GE. 1997. Hyporheic temperature patterns within riffles. *Hydrological Sciences Journal* **42**: 199-213.

Evans EC, McGregor GR, Petts GE. 1998. River energy budgets with special reference to river bed processes. *Hydrological Processes* **12**: 575-595. DOI: 10.1002/(SICI)1099-1085(19980330)12:4<575::AID-HYP595>3.3.CO;2-P.

Fesch C, Lehmann P, Haderlein SB, Hinz C, Schwarzenbach RP, Flühler H. 1998. Effect of water content on solute transport in a porous medium containing reactive micro-aggregates. *Journal of Contaminant Hydrology* **33**: 211-230. DOI: 10.1016/S0169-7722(98)00071-0.

Ferguson G, Woodbury AD. 2005. The effects of climatic variability on estimates of recharge from temperature profiles. *Ground Water* **43**: 837-842. DOI: 10.1111/j.1745-6584.2005.00088.x.

Fernald AG, Landers DH, Wigington PJ. 2006. Water quality changes in hyporheic flow paths between a large gravel bed river and off-channel alcoves in Oregon, USA. *River Research and Applications* **22**: 1111-1124. DOI: 10.1002/rra.961.

Findlay S. 1995. Importance of surface-subsurface exchange in stream ecosystems - the hyporheic zone. *Limnology and Oceanography* **40**: 159-164.

Fischer H, Kloep F, Wilzcek S, Pusch MT. 2005. A river's liver - microbial processes within the hyporheic zone of a large lowland river. *Biogeochemistry* **76**: 349-371. DOI: 10.1007/s10533-005-6896-y.

Fowler RT, Scarsbrook MR. 2002. Influence of hydrologic exchange patterns on water chemistry and hyporheic invertebrate communities in three gravel-bed rivers. *New Zealand Journal of Marine and Freshwater Research* **36**: 471-482.

Fox GA, Durnford DS. 2003. Unsaturated hyporheic zone flow in stream/aquifer conjunctive systems. *Advances in Water Resources* **26**: 989-1000. DOI: 10.1016/s0309-1708(03)00087-3.

Fraser BG, Williams DD. 1998. Seasonal boundary dynamics of a groundwater/surface-water ecotone. *Ecology* **79**: 2019-2031. DOI: 10.2307/176706.

Gandy CJ, Smith JWN, Jarvis AP. 2007. Attenuation of mining-derived pollutants in the hyporheic zone: A review. *Science of the Total Environment* **373**: 435-446. DOI: 10.1016/j.scitotenv.2006.11.004.

Gayraud S, Philippe M. 2003. Influence of bed-sediment features on the interstitial habitat available for macroinvertebrates in 15 French streams. *International Review of Hydrobiology* **88**: 77-93. DOI: 10.1002/iroh.200390007.

Ge SM. 1998. Estimation of groundwater velocity in localized fracture zones from well temperature profiles. *Journal of Volcanology and Geothermal Research* **84**: 93-101. DOI: 10.1016/S0377-0273(98)00032-8.

Ge Y, Boufadel MC. 2006. Solute transport in multiple-reach experiments: Evaluation of parameters and reliability of prediction. *Journal of Hydrology* **323**: 106-119. DOI: 10.1016/j.jhydrol.2005.08.021.

Gibert J, Stanford JA, Dole-Olivier MJ, Ward JV. 1994. Basic attributes of groundwater ecosystems and prospects for research. In *Groundwater Ecology*, Gibert J, Danielopol DL, Stanford JA (eds). Academic Press: San Diego; 7-40.

Gibert J, Fournier F, Mathieu J. 1997. The groundwater/surface water ecotone perspective: state of the art. In *Groundwater/Surface Water Ecotones: Biological and Hydrological Interactions and Management Options*, Gibert J, Mathieu J, Fournier F (eds). Cambridge University Press: Cambridge, UK; 3-8.

Gooseff MN, Wondzell SM, Haggerty R, Anderson J. 2003a. Comparing transient storage modeling and residence time distribution (RTD) analysis in geomorphically varied reaches in the Lookout Creek basin, Oregon, USA. *Advances in Water Resources* **26**: 925-937. DOI: 10.1016/S0309-1708(03)00105-2.

Gooseff MN, McKnight DM, Runke RL, Vaughn BH. 2003b. Determining long time-scale hyporheic zone flow paths in Antarctic streams. *Hydrological Processes* **17**: 1691-1710. DOI: 10.1002/hyp.1210.

Gooseff MN, LaNier J, Haggerty R, Kokkeler K. 2005. Determining in-channel (dead zone) transient storage by comparing solute transport in a bedrock channel-alluvial channel sequence, Oregon. *Water Resources Research* **41**. DOI: 10.1029/2004WR003513.

Greig SM, Sear DA, Carling PA. 2007. A review of factors influencing the availability of dissolved oxygen to incubating salmonid embryos. *Hydrological Processes* **21**: 323-334. DOI: 10.1002/hyp.6188.

Gülser C, Ekberli I. 2004. A comparison of estimated and measured diurnal soil temperature through a clay soil depth. *Journal of Applied Science* **4**: 418-423. DOI: 10.3923/jas.2004.418.423.

Hahn HJ. 2006. The GW-Fauna-Index: A first approach to a quantitative ecological assessment of groundwater habitats. *Limnologica* **36**: 119-137. DOI: 10.1016/j.limno.2006.02.001.

Hancock PJ. 2002. Human impacts on the stream-groundwater exchange zone. *Environmental Management* **29**: 763-781. DOI: 10.1007/s00267-001-0064-5.

Hancock PJ, Boulton AJ, Humphreys WF. 2005. Aquifers and hyporheic zones: Towards an ecological understanding of groundwater. *Hydrogeology Journal* **13**: 98-111. DOI: 10.1007/s10040-004-0421-6.

Hannah DM, Malcolm IA, Soulsby C, Youngson AF. 2004. Heat exchanges and temperatures within a salmon spawning stream in the cairngorms, Scotland: Seasonal and sub-seasonal dynamics. *River Research and Applications* **20**: 635-652. DOI: 10.1002/rra.771.

Harvey JW, Bencala KE. 1993. The effect of streambed topography on surface-subsurface water exchange in mountain catchments. *Water Resources Research* **29**: 89-98. DOI: 10.1029/92WR01960.

Harvey JW, Wagner BJ. 2000. Quantifying hydrologic interactions between streams and their subsurface hyporheic zones. In *Streams and Ground Waters*, Jones JB, Mulholland PJ (eds). Academic Press: New York; 3-44.

Harvey JW, Conklin MH, Koelsch RS. 2003. Predicting changes in hydrologic retention in an evolving semi-arid alluvial stream. *Advances in Water Resources* **26**: 939-950. DOI: 10.1016/S0309-1708(03)00085-X.

Hayashi M, Rosenberry DO. 2002. Effects of ground water exchange on the hydrology and ecology of surface water. *Ground Water* **40**: 309-316. DOI: 10.1111/j.1745-6584.2002.tb02659.x.

Hein T, Baranyi C, Herndl GJ, Wanek W, Schiemer F. 2003. Allochthonous and autochthonous particulate organic matter in floodplains of the River Danube: the importance of hydrological connectivity. *Freshwater Biology* **48**: 220-232. DOI: 10.1046/j.1365-2427.2003.00981.x.

Hendricks SP, White DS. 2000. Stream and groundwater influences on phosphorus biogeochemistry. In *Streams and Ground Waters*, Jones JB, Mulholland PJ (eds). Academic Press: New York; 221-235.

Hester ET, Doyle MW. 2008. In-stream geomorphic structures as drivers of hyporheic exchange. *Water Resources Research* **44**: W03417. DOI: 10.1029/2006wr005810.

Hinkle SR, Duff JH, Triska FJ, Laenen A, Gates EB, Bencala KE, Wentz DA, Silva SR. 2001. Linking hyporheic flow and nitrogen cycling near the Willamette River - a large river in Oregon, USA. *Journal of Hydrology* **244**: 157-180. DOI: 10.1016/S0022-1694(01)00335-3.

Hoehn E, Cirpka OA. 2006. Assessing residence times of hyporheic ground water in two alluvial flood plains of the Southern Alps using water temperature and tracers. *Hydrology and Earth System Sciences* **10**: 553-563.

Holmes RM. 2000. The importance of ground water to stream ecosystem function. In *Streams and Ground Waters*, Jones JB, Mulholland PJ (eds). Academic Press: New York, 137-148.

Hopmans JW, Simunek J, Bristow KL. 2002. Indirect estimation of soil thermal properties and water flux using heat pulse probe measurements: Geometry and dispersion effects. *Water Resources Research* **38**: 14. DOI: 10.1029/2000wr000071.

Howard KWF, Maier HS, Mattson SL. 2006. Ground-surface water interactions and the role of the hyporheic zone. In *Groundwater and Ecosystems*, Baba A, Howard KWF, Gunduz O (eds). Springer131-143.

Hutchison JM, Seaman JC, Aburime SA, Radcliffe DE. 2003. Chromate Transport and Retention in Variably Saturated Soil Columns. *Vadose Zone Journal* **2**: 702-714. DOI: 10.2113/2.4.702.

Hunt RJ, Strand M, Walker JF. 2006. Measuring groundwater-surface water interaction and its effect on wetland stream benthic productivity, Trout Lake watershed, northern Wisconsin, USA. *Journal of Hydrology* **320**: 370-384. DOI: 10.1016/j.jhydrol.2005.07.029.

Javaux M, Vanclooster M. 2003. Scale- and rate-dependent solute transport within an unsaturated sandy monolith. *Soil Science Society of America Journal* **67**: 1334-1343.

Johnson SL. 2003. Stream temperature: scaling of observations and issues for modelling. *Hydrological Processes* **17**: 497-499. DOI: 10.1002/hyp.5091.

Jones SB, Wraith JM, Or D. 2002. Time domain reflectometry measurement principles and applications. *Hydrological Processes* **16**: 141-153. DOI: 10.1002/hyp.513.

Jonsson K, Johansson H, Worman A. 2003. Hyporheic exchange of reactive and conservative solutes in streams - tracer methodology and model interpretation. *Journal of Hydrology* **278**: 153-171. DOI: 10.1016/S0022-1694(03)00140-9.

Kalbus E, Reinstorf F, Schirmer M. 2006. Measuring methods for groundwater – surface water interactions: a review. *Hydrology and Earth System Sciences* **10**: 873-887.

Kalbus E, Schmidt C, Molson JW, Reinstorf F, Schirmer M. 2009. Influence of aquifer and streambed heterogeneity on the distribution of groundwater discharge. *Hydrology and Earth System Sciences* **13**: 69-77.

Kaplan LA, Newbold JD. 2000. Surface and subsurface dissolved organic carbon. In *Streams and Ground Waters*, Jones JB, Mulholland PJ (eds). Academic Press: New York; 237-258.

Kazezyilmaz-Alhan CM, Medina MA. 2006. Stream solute transport incorporating hyporheic zone processes. *Journal of Hydrology* **329**: 26-38. DOI: 10.1016/j.jhydrol.2006.02.003.

Keery J, Binley A, Crook N, Smith JWN. 2007. Temporal and spatial variability of groundwater-surface water fluxes: Development and application of an analytical method using temperature time series. *Journal of Hydrology* **336**: 1-16. DOI: 10.1016/j.jhydrol.2006.12.003.

Kincanon R, McAnally AS. 2004. Enhancing commonly used model predictions for constructed wetland performance: as-built design considerations. *Ecological Modelling* **174**: 309-322. DOI: 10.1016/j.ecolmodel.2003.09.030.

Kollet SJ, Zlotnik VA. 2007. Evaluation of the streambed leakage concept in analytical models using data from three pumping tests. *Hydrogeology Journal* **15**: 1051-1062. DOI: 10.1007/s10040-006-0156-7.

Krause S, Hannah DM, Fleckenstein JH. 2009. Hyporheic hydrology: interactions at the groundwater-surface water interface Preface. *Hydrological Processes* **23**: 2103-2107. DOI: 10.1002/hyp.7366.

Laenen A, Bencala KE. 2001. Transient storage assessments of dye-tracer injections in rivers of the Willamette Basin, Oregon. *Journal of the American Water Resources Association* **37**: 367-377. DOI: 10.1111/j.1752-1688.2001.tb00975.x.

Landon MK, Rus DL, Harvey FE. 2001. Comparison of instream methods for measuring hydraulic conductivity in sandy streambeds. *Ground Water* **39**: 870-885. DOI: 10.1111/j.1745-6584.2001.tb02475.x.

Lin YC, Medina MA. 2003. Incorporating transient storage in conjunctive stream-aquifer modeling. *Advances in Water Resources* **26**: 1001-1019. DOI: 10.1016/S0309-1708(03)00081-2.

Lindstrom FT. 1976. Pulsed dispersion of trace chemical concentrations in a saturated sorbing porous-medium. *Water Resources Research* **12**: 229-238. DOI: 10.1029/WR012i002p00229.

Lu N, Ge SM. 1996. Effect of horizontal heat and fluid flow on the vertical temperature distribution in a semiconfining layer. *Water Resources Research* **32**: 1449-1453. DOI: 10.1029/95WR03095.

Malard F, Mangin A, Uehlinger U, Ward JV. 2001. Thermal heterogeneity in the hyporheic zone of a glacial floodplain. *Canadian Journal of Fisheries and Aquatic Sciences* **58**: 1319-1335. DOI: 10.1139/cjfas-58-7-1319.

Malard F, Tockner K, Dole-Olivier MJ, Ward JV. 2002. A landscape perspective of surface-subsurface hydrological exchanges in river corridors. *Freshwater Biology* **47**: 621-640. DOI: 10.1046/j.1365-2427.2002.00906.x.

Malcolm IA, Soulsby C, Youngson AF. 2002. Thermal regime in the hyporheic zone of two contrasting salmonid spawning streams: ecological and hydrological implications. *Fisheries Management and Ecology* **9**: 1-10. DOI: 10.1046/j.1365-2400.2002.00276.x.

Malcolm IA, Soulsby C, Youngson AF, Hannah DM, McLaren IS, Thorne A. 2004. Hydrological influences on hyporheic water quality: implications for salmon egg survival. *Hydrological Processes* **18**: 1543-1560. DOI: 10.1002/hyp.1405.

Maraqa MA, Wallace RB, Voice TC. 1997. Effects of degree of water saturation on dispersivity and immobile water in sandy soil columns. *Journal of Contaminant Hydrology* **25**: 199-218. DOI: 10.1016/S0169-7722(96)00032-0.

Marion A, Zaramella M, Packman AI. 2003. Parameter estimation of the transient storage model for stream-subsurface exchange. *Journal of Environmental Engineering-Asce* **129**: 456-463. DOI: 10.1061/(ASCE)0733-9372(2003)129:5(456).

Marion A. 2005. Models of hyporheic contamination by non reactive solutes, metals and colloids. In *Water Quality Hazards and Dispersion of Pollutants*, Czernuszenko W, Rowinski PM (eds). Springer US215-230.

McClain ME, Boyer EW, Dent CL, Gergel SE, Grimm NB, Groffman PM, Hart SC, Harvey JW, Johnston CA, Mayorga E, McDowell WH, Pinay G. 2003. Biogeochemical hot spots and hot moments at the interface of terrestrial and aquatic ecosystems. *Ecosystems* **6**: 301-312. DOI: 10.1007/s10021-003-0161-9.

Mermillod-Blondin F, Mauclaire L, Montuelle B. 2005. Use of slow filtration columns to assess oxygen respiration, consumption of dissolved organic carbon, nitrogen transformations, and microbial parameters in hyporheic sediments. *Water Research* **39**: 1687-1698. DOI: 10.1016/j.watres.2005.02.003.

Mojid MA, Rose DA, Wyseure GCL. 2004. A transfer-function method for analysing breakthrough data in the time domain of the transport process. *European Journal of Soil Science* **55**: 699-711. DOI: 10.1111/j.1365-2389.2004.00636.x.

Mojid MA, Rose DA, Wyseure GCL. 2006. Analysis of partial breakthrough data by a transfer-function method. *Australian Journal of Soil Research* **44**: 175-182. DOI: 10.1071/sr04127.

Mojid MA, Rose DA, Wyseure GCL. 2007. A model incorporating the diffuse double layer to predict the electrical conductivity of bulk soil. *European Journal of Soil Science* **58**: 560-572. DOI: 10.1111/j.1365-2389.2006.00831.x.

Moore RD, Sutherland P, Gomi T, Dhakal A. 2005. Thermal regime of a headwater stream within a clear-cut, coastal British Columbia, Canada. *Hydrological Processes* **19**: 2591-2608. DOI: 10.1002/hyp.5733.

Mortensen AP, Hopmans JW, Mori Y, Simunek J. 2006. Multi-functional heat pulse probe measurements of coupled vadose zone flow and transport. *Advances in Water Resources* **29**: 250-267. DOI: 10.1016/j.advwatres.2005.03.017.

Mualem Y. 1976. A new model for predicting hydraulic conductivity of unsaturated porous-media. *Water Resources Research* **12**: 513-522. DOI: 10.1029/WR012i003p00513.

Mutz M, Rohde A. 2003. Processes of surface-subsurface water exchange in a low energy sand-bed stream. *International Review of Hydrobiology* **88**: 290-303. DOI: 10.1002/iroh.200390026.

Nadeau TL, Rains MC. 2007. Hydrological connectivity between headwater streams and downstream waters: How science can inform policy. *Journal of the American Water Resources Association* **43**: 118-133. DOI: 10.1111/j.1752-1688.2007.00010.x.

Newman BD, Vivoni ER, Groffman AR. 2006. Surface water-groundwater interactions in semiarid drainages of the American southwest. *Hydrological Processes* **20**: 3371-3394. DOI: 10.1002/hyp.6336.

Nützmann G, Maciejewski S, Joswig K. 2002. Estimation of water saturation dependence of dispersion in unsaturated porous media: experiments and modelling analysis. *Advances in Water Resources* **25**: 565-576. DOI: 10.1016/S0309-1708(02)00018-0.

Ocampo CJ, Sivapalan M, Oldham C. 2006. Hydrological connectivity of upland-riparian zones in agricultural catchments: Implications for runoff generation and nitrate transport. *Journal of Hydrology* **331**: 643-658. DOI: 10.1016/j.jhydrol.2006.06.010.

Or, D., Jones, S. B., VanShaar, J. R., Humphries, S., and Koberstein, L.: WinTDR, Users guide, Version 6.1, available at: http://soilphysics.usu.edu/wintdr/index.htm, access: Feb 2005, Utah State university/ Soil Physics group, Utah, USA, 2004.

Ozaki N, Fukushima T, Kojiri T. 2008. Simulation of the effects of the alteration of the river basin land use

on river water temperature using the multi-layer mesh-typed runoff model. *Ecological Modelling* **215**: 159-169. DOI: 10.1016/j.ecolmodel.2008.02.030.

Packman AI, Bencala KE. 2000. Modeling surface - subsurface hydrologic interactions. In *Streams and Ground Waters*, Jones JB, Mulholland PJ (eds). Academic Press: New York; 45-80.

Packman AI, MacKay JS. 2003. Interplay of stream-subsurface exchange, clay particle deposition, and streambed evolution. *Water Resources Research* **39**. DOI: 10.1029/2002wr001432.

Padilla IY, Yeh TCJ, Conklin MH. 1999. The effect of water content on solute transport in unsaturated porous media. *Water Resources Research* **35**: 3303-3313. DOI: 10.1029/1999WR900171.

Pang LP, Close M. 1999. Field-scale physical non-equilibrium transport in an alluvial gravel aquifer. *Journal of Contaminant Hydrology* **38**: 447-464. DOI: 10.1016/S0169-7722(99)00022-4.

Patgiri DK, Baruah TC. 1995. Spatial variability of total porosity, air entry potential and saturation water-content in a cultivated inceptisol. I. Semivariance analysis. *Agricultural Water Management* **27**: 1-9. DOI: 10.1016/0378-3774(95)01132-3.

Perfect E, Sukop MC, Haszler GR. 2002. Prediction of dispersivity for undisturbed soil columns from water retention parameters. *Soil Science Society of America Journal* **66**: 696-701.

Poole GC, Berman CH. 2001. An ecological perspective on in-stream temperature: Natural heat dynamics and mechanisms of human-caused thermal degradation. *Environmental Management* **27**: 787-802. DOI: 10.1007/s002670010188.

Pretty JL, Hildrew AG, Trimmer M. 2006. Nutrient dynamics in relation to surface-subsurface hydrological exchange in a groundwater fed chalk stream. *Journal of Hydrology* **330**: 84-100. DOI: 10.1016/j.jhydrol.2006.04.013.

Pusch M, Fiebig D, Brettar I, Eisenmann H, Ellis BK, Kaplan LA, Lock MA, Naegeli MW, Traunspurger W. 1998. The role of micro-organisms in the ecological connectivity of running waters. *Freshwater Biology* **40**: 453-495. DOI: 10.1046/j.1365-2427.1998.00372.x.

Rehg KJ, Packman AI, Ren JH. 2005. Effects of suspended sediment characteristics and bed sediment transport on streambed clogging. *Hydrological Processes* **19**: 413-427. DOI: 10.1002/hyp.5540.

Ricci C, Balsamo M. 2000. The biology and ecology of lotic rotifers and gastrotrichs. *Freshwater Biology* **44**: 15-28. DOI: 10.1046/j.1365-2427.2000.00584.x.

Roach KA, Thorp JH, Delong MD. 2009. Influence of lateral gradients of hydrologic connectivity on trophic positions of fishes in the Upper Mississippi River. *Freshwater Biology* **54**: 607-620. DOI: 10.1111/j.1365-2427.2008.02137.x.

Rodgers P, Soulsby C, Petry J, Malcolm I, Gibbins C, Dunn S. 2004. Groundwater-surface-water interactions in a braided river: a tracer-based assessment. *Hydrological Processes* **18**: 1315-1332. DOI: 10.1002/hyp.1404.

Ronan AD, Prudic DE, Thodal CE, Constantz J. 1998. Field study and simulation of diurnal temperature effects on infiltration and variably saturated flow beneath an ephemeral stream. *Water Resources Research* **34**: 2137-2153. DOI: 10.1029/98WR01572.

Rulík M, Spáčil R. 2004. Extracellular enzyme activity within hyporheic sediments of a small lowland stream. *Soil Biology & Biochemistry* **36**: 1653-1662. DOI: 10.1016/j.soilbio.2004.07.005.

Runkel RL. 1998. *One-dimensional transport with inflow and storage (OTIS): A solute transport model for small streams*. U.S. Geological Survey, Water-Resources Investigations Report 98-4018. 73 pp.

Runkel RL, McKnight DM, Rajaram H. 2003. Modeling hyporheic zone processes - Preface. *Advances in Water Resources* **26**: 901-905. DOI: 10.1016/S0309-1708(03)00079-4.

Saito H, Simunek J, Mohanty BP. 2006. Numerical analysis of coupled water, vapor, and heat transport in the vadose zone. *Vadose Zone Journal* **5**: 784-800. DOI: 10.2136/vzj2006.0007.

Schilling KE, Li ZW, Zhang YK. 2006. Groundwater - surface water interaction in the riparian zone-of an incised channel, Walnut Creek, Iowa. *Journal of Hydrology* **327**: 140-150. DOI: 10.1016/j.jhydrol.2005.11.014.

Schindler JE, Krabbenhoft DP. 1998. The hyporheic zone as a source of dissolved organic carbon and

carbon gases to a temperate forested stream. *Biogeochemistry* **43**: 157-174. DOI: 10.1023/A:1006005311257.

Schmidt C, Conant B, Bayer-Raich M, Schirmer M. 2007. Evaluation and field-scale application of an analytical method to quantify groundwater discharge using mapped streambed temperatures. *Journal of Hydrology* **347**: 292-307. DOI: 10.1016/j.jhydrol.2007.08.022.

Sear DA, Armitage PD, Dawson FH. 1999. Groundwater dominated rivers. *Hydrological Processes* **13**: 255-276.

Segal M, Pan Z, Gutowski WJ. 2000. Some conceptual and scaling evaluations of snowmelt events forced by warm soil. *Journal of Hydrometeorology* **1**: 364-369. DOI: 10.1175/1525-7541(2000)001.

Silliman SE, Ramirez J, McCabe RL. 1995. Quantifying downflow through creek sediments using temperature time-series: one-dimensional solution incorporating measured surface-temperature. *Journal of Hydrology* **167**: 99-119. DOI: 10.1016/0022-1694(94)02613-G.

Šimůnek J, Jarvis NJ, van Genuchten MT, Gardenas A. 2003. Review and comparison of models for describing non-equilibrium and preferential flow and transport in the vadose zone. *Journal of Hydrology* **272**: 14-35. DOI: 10.1016/S0022-1694(02)00252-4.

Šimůnek J, Sejna M, van Genuchten MT. 2006. *The HYDRUS Software package for simulating two- and three-dimensional movement of water, heat, and multiple solutes in variably-saturated media*, User manual, Version 1.0. PC Progress: Prague, Czech Republic. 173 pp.

Šimůnek J, van Genuchten MT, Sejna M. 2008. Development and applications of the HYDRUS and STANMOD software packages and related codes. *Vadose Zone Journal* **7**: 587-600. DOI: 10.2136/vzj2007.0077.

Smith JWN, Bonell M, Gibert J, McDowell WH, Sudicky EA, Turner JV, Harris RC. 2008. Groundwater-surface water interactions, nutrient fluxes and ecological response in river corridors: Translating science into effective environmental management. *Hydrological Processes* **22**: 151-157. DOI: 10.1002/hyp.6902.

Sophocleous M. 2002. Interactions between groundwater and surface water: the state of the science. *Hydrogeology Journal* **10**: 52-67. DOI: 10.1007/s10040-001-0170-8.

Soulsby C, Malcolm IA, Youngson AF. 2001. Hydrochemistry of the hyporheic zone in salmon spawning gravels: A preliminary assessment in a degraded agricultural stream. *Regulated Rivers: Research & Management* **17**: 651-665. DOI: 10.1002/rrr.625.

Stallman RW. 1965. Steady one-dimensional fluid flow in a semi-infinite porous medium with sinusoidal surface temperature. *Journal of Geophysical Research* **70**: 2821-2827. DOI: 10.1029/JZ070i012p02821.

Stanford JA, Ward JV. 1988. The hyporheic habitat of river ecosystems. *Nature* **335**: 64-66. DOI: 10.1038/335064a0.

Stanley EH, Jones JB. 2000. Surface-Subsurface Interactions: Past. Present, and Future. In *Streams and Ground Waters*, Jones JB, Mulholland PJ (eds). Academic Press: New York, 405-417.

Stofleth JM, Shields FD, Fox GA. 2008. Hyporheic and total transient storage in small, sand-bed streams. *Hydrological Processes* **22**: 1885-1894. DOI: 10.1002/hyp.6773.

Storey RG, Howard KWF, Williams DD. 2003. Factors controlling riffle-scale hyporheic exchange flows and their seasonal changes in a gaining stream: A three-dimensional groundwater flow model. *Water Resources Research* **39**: 1034. DOI: 10.1029/2002WR001367.

Storey RG, Williams DD. 2004. Spatial responses of hyporheic invertebrates to seasonal changes in environmental parameters. *Freshwater Biology* **49**: 1468-1486. DOI: 10.1111/j.1365-2427.2004.01284.x.

Swan CM, Palmer MA. 2000. What drives small-scale spatial patterns in lotic meiofauna communities? *Freshwater Biology* **44**: 109-121. DOI: 10.1046/j.1365-2427.2000.00587.x.

Taniguchi M. 1993. Evaluation of vertical groundwater fluxes and thermal-properties of aquifers based on transient temperature-depth profiles. *Water Resources Research* **29**: 2021-2026. DOI: 10.1029/93WR00541.

Taniguchi M, Shimada J, Uemura T. 2003a. Transient effects of surface temperature and groundwater flow on subsurface temperature in Kumamoto Plain, Japan. *Physics and Chemistry of the Earth* **28**: 477-486. DOI: 10.1016/s1474-7065(03)00067-6.

Taniguchi M, Turner JV, Smith AJ. 2003b. Evaluations of groundwater discharge rates from subsurface temperature in Cockburn Sound, Western Australia. *Biogeochemistry* **66**: 111-124. DOI: 10.1023/B:BIOG.0000006099.50469.b3.

Tetzlaff D, Soulsby C, Bacon PJ, Youngson AF, Gibbins C, Malcolm IA. 2007. Connectivity between landscapes and riverscapes - a unifying theme in integrating hydrology and ecology in catchment science? *Hydrological Processes* **21**: 1385-1389. DOI: 10.1002/hyp.6701.

Thorp JH, Thoms MC, Delong MD. 2006. The riverine ecosystem synthesis: Biocomplexity in river networks across space and time. *River Research and Applications* **22**: 123-147. DOI: 10.1002/rra.901.

Tockner K, Malard F, Ward JV. 2000. An extension of the flood pulse concept. *Hydrological Processes* **14**: 2861-2883. DOI: 10.1002/1099-1085(200011/12)14:16/17.

Tonina D, Buffington JM. 2007. Hyporheic exchange in gravel bed rivers with pool-riffle morphology: Laboratory experiments and three-dimensional modeling. *Water Resources Research* **43**. DOI: 10.1029/2005wr004328.

Toride N, Inoue M, Leij FJ. 2003. Hydrodynamic dispersion in an unsaturated dune sand. *Soil Science Society of America Journal* **67**: 703-712.

Triska FJ, Duff JH, Avanzino RJ. 1993. The role of water exchange between a stream channel and its hyporheic zone in nitrogen cycling at the terrestrial aquatic interface. *Hydrobiologia* **251**: 167-184. DOI: 10.1007/BF00007177.

Turcotte DL, Schubert G. 1982. *Geodynamics: Application of Continuum Physics to Geological Problems*. John Wiley & Sons: New York. 464 pp.

Valett HM, Fisher SG, Grimm NB, Camill P. 1994. Vertical hydrologic exchange and ecological stability of a desert stream ecosystem. *Ecology* **75**: 548-560. DOI: 10.2307/1939557.

van Genuchten MT. 1980. A closed-form equation for predicting the hydraulic conductivity of unsaturated soils. *Soil Science Society of America Journal* **44**: 892-898.

van Genuchten MT, Parker JC. 1984. Boundary-conditions for displacement experiments through short laboratory soil columns. *Soil Science Society of America Journal* **48**: 703-708.

Vanderborght J, Vanclooster M, Timmerman A, Seuntjens P, Mallants D, Kim DJ, Jacques D, Hubrechts L, Gonzalez C, Feyen J, Diels J, Deckers J. 2001. Overview of inert tracer experiments in key Belgian soil types: Relation between transport and soil morphological and hydraulic properties. *Water Resources Research* **37**: 2873-2888. DOI: 10.1029/2000WR000110.

Vanderborght J, Vereecken H. 2007. Review of dispersivities for transport modeling in soils. *Vadose Zone Journal* **6**: 29-52. DOI: 10.2136/vzj2006.0096.

Wakao NS, Kaguei S. 1982. *Heat and Mass Transfer in Packed Beds*. Gordon and Breach: New York. 350 pp.

Ward JV, Tockner K, Schiemer F. 1999. Biodiversity of floodplain river ecosystems: Ecotones and connectivity. *Regulated Rivers-Research & Management* **15**: 125-139.

Webb BW, Hannah DM, Moore RD, Brown LE, Nobilis F. 2008. Recent advances in stream and river temperature research. *Hydrological Processes* **22**: 902-918. DOI: 10.1002/hyp.6994.

Weeks EP. 2006. R.W. Stallman (1924-1977) - An underappreciated contributor to hydrogeology. *Ground Water* **44**: 618-621. DOI: 10.1111/j.1745-6584.2006.00218.x.

Weigelhofer G, Waringer J. 2003. Vertical distribution of benthic macroinvertebrates in riffles versus deep runs with differing contents of fine sediments (Weidlingbach, Austria). *International Review of Hydrobiology* **88**: 304-313. DOI: 10.1002/iroh.200390027.

Winkelmann C, Koop JHE, Benndorf J. 2003. Abiotic features and macroinvertebrate colonization of the hyporheic zones of two tributaries of the river Elbe (Germany). *Limnologica* **33**: 112-121. DOI: 10.1016/S0075-9511(03)80040-3.

Woessner WW. 2000. Stream and fluvial plain ground water interactions: Rescaling hydrogeologic thought. *Ground Water* **38**: 423-429. DOI: 10.1111/j.1745-6584.2000.tb00228.x.

Wondzell SM. 2006. Effect of morphology and discharge on hyporheic exchange flows in two small streams in the Cascade Mountains of Oregon, USA. *Hydrological Processes* **20**: 267-287. DOI: 10.1002/hyp.5902.

Wörman A, Packman AI, Johansson H, Jonsson K. 2002. Effect of flow-induced exchange in hyporheic zones on longitudinal transport of solutes in streams and rivers. *Water Resources Research* **38**. DOI: 10.1029/2001WR000769.

Wroblicky GJ, Campana ME, Valett HM, Dahm CN. 1998. Seasonal variation in surface-subsurface water exchange and lateral hyporheic area of two stream-aquifer systems. *Water Resources Research* **34**: 317-328. DOI: 10.1029/97WR03385.

Wyseure GCL, Mojid MA, Malik MA. 1997. Measurement of volumetric water content by TDR in saline soils. *European Journal of Soil Science* **48**: 347-354. DOI: 10.1111/j.1365-2389.1997.tb00555.x.

Zaramella M, Packman AI, Marion A. 2003. Application of the transient storage model to analyze advective hyporheic exchange with deep and shallow sediment beds. *Water Resources Research* **39**. DOI: 10.1029/2002WR001344.

Zaramella M, Marion A, Packman AI. 2006. Applicability of the Transient Storage Model to the hyporheic exchange of metals. *Journal of Contaminant Hydrology* **84**: 21-35. DOI: 10.1016/j.jconhyd.2005.12.002.

Appendix 1: The transfer-function method (Mojid *et al*., 2004)

The input-output relation of a system can be described by a differential equation. For a linear differential equation a Laplace transform, ***F*(*s*)** with as argument the complex variable ***s***, is a common step in a solution-strategy. Linearity requires that the coefficients in the differential equation are constants in time so that superposition of effects and analytical solutions are possible. As a consequence in our experiment we apply a constant water flux which results in constant coefficients ***V*** and ***D*** in Equation (3.1) leading to a linear CDE. The transfer-function for this CDE in the Laplace domain (Wakao and Kaguei, 1982) can be expressed as the proportion of the Laplace transforms of time-dependent measured response over input concentration of the solute (***C*$_r$** , ***C*$_{in}$**), respectively. This is written as:

$$L[f(t)] = F(s) = \frac{C_r(s)}{C_{in}(s)} = \frac{\int_0^\infty C_r(t)e^{-st}dt}{\int_0^\infty C_{in}(t)e^{-st}dt} \qquad \text{(A.1)}$$

By Laplace inversion of ***F*(*s*)** we obtain a transfer-function ***f*(*t*)** in the time-domain, which has been given in Equation (3.9). The response concentration can be estimated in the time domain by convoluting the transfer function ***f*(*t*)** with the time function of the input concentration:

$$C_{r.est(t)} = \int_0^\infty C_{in}(\beta)\, f(t-\beta)\, d\beta \qquad \text{(A.2)}$$

where ***β*** is the time integration variable; ***f*(*t*)**, the transfer-function in the time domain (Equation 3.9).

The estimated response concentration of solute, **C*$_{r.est}$***, can be compared to the measured response concentration. The accuracy of fitting can be evaluated by the root-mean-square error (RMSE) between the measured and estimated concentrations:

$$RMSE = \left[\frac{\int_0^\infty \left(C_{r(t)} - C_{r.est(t)}\right)^2 dt}{\int_0^\infty \left(C_{r(t)}\right)^2 dt} \right]^{0.5} \qquad \text{(A.3)}$$

The coefficients ***V*** and ***D*** are found by minimizing RMSE by an appropriate optimization procedure. The package R (Dalgaard, 2004) contains several standard procedures in the base function "optim".

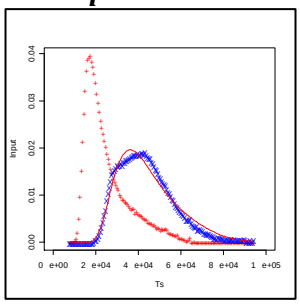
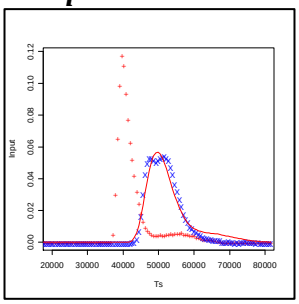
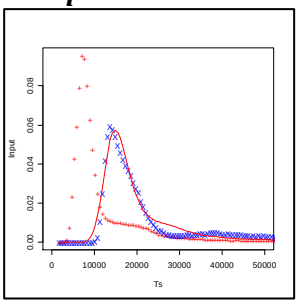
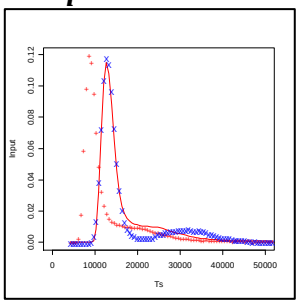
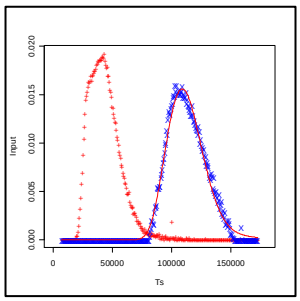
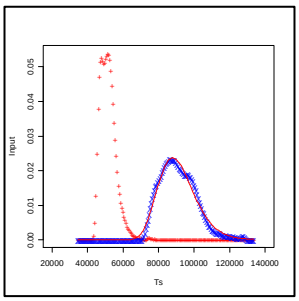
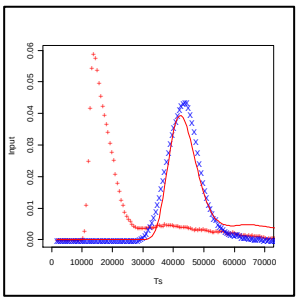
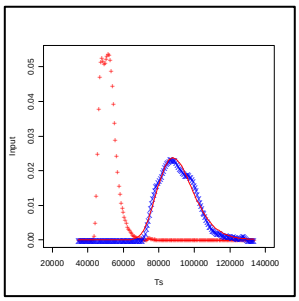
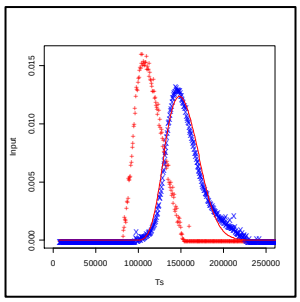
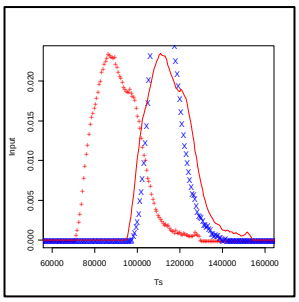
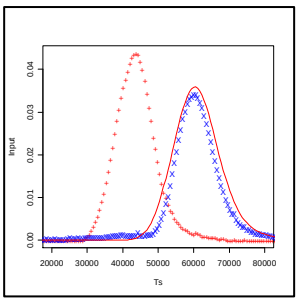
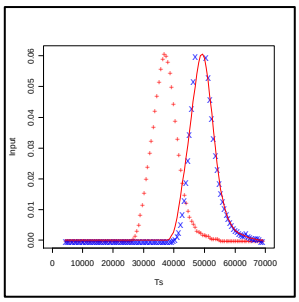
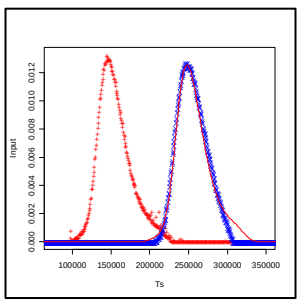
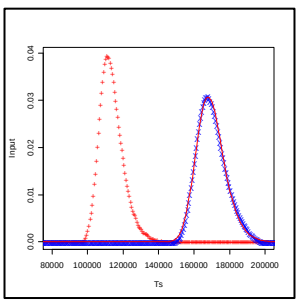
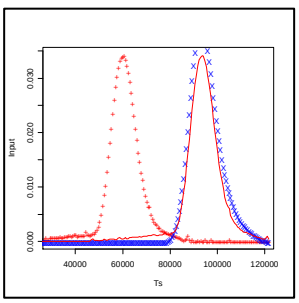
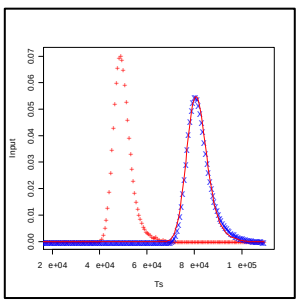
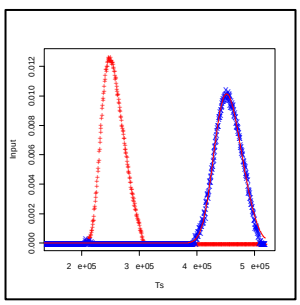
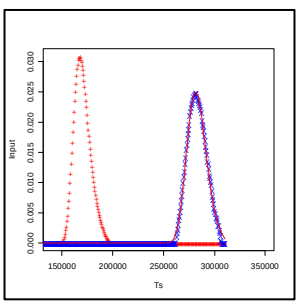
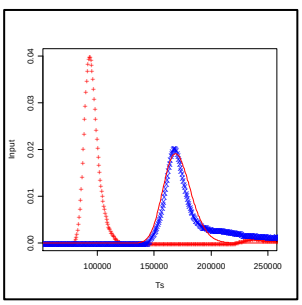
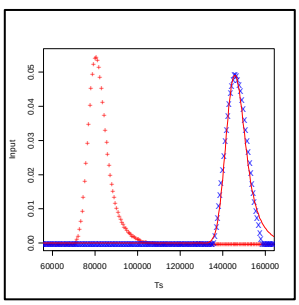
Appendix 2: R-code used for BTC analysis

```
# Path to the working directory WD to be adjusted to the computer
WD = "D:/PhDResearch/JModel/TDR/BTC"
# set a working directory
if (!is.null(WD)) setwd(WD)
# read in the data from the TDR with multiplexer
ColumnData= read.table (file.choose(),header=TRUE)
# check on the data-frame by asking the names of the variables
names(ColumnData)
# should answer:    [1] "ti"        "ProNu" "EC"        "ECN"
# check in the data to find the suitable timesteps
StartInput        =    0.09 # (day) check in the data to find the start
EndResponse      =    6    # (day) check in the data to find the end
DTmeasurement =    10/60/24    # (day) check in the data; time to return to the probe 1
Time=seq(StartInput,EndResponse, by= DTmeasurement)
xout=Time
# Subset to Probes
Pos1<-subset(ColumnData,ProNu==1)
Pos2<-subset(ColumnData,ProNu==2)
Pos3<-subset(ColumnData,ProNu==3)
Pos4<-subset(ColumnData,ProNu==4)
Pos5<-subset(ColumnData,ProNu==5)
Pos6<-subset(ColumnData,ProNu==6)
#
# Probe1
names(Pos1)=c("Ti1","Pro1","ECo1","ECN1")
attach(Pos1)
plot( ECN1~Ti1)
Probe1=approx(Ti1,ECN1,xout)
lines(Probe1$y~Probe1$x)
detach(Pos1)
###########send script up to this line#############
# probe2
names(Pos2)=c("Ti2","Pro2","ECo2","ECN2")
attach(Pos2)
plot( ECN2~Ti2)
Probe2=approx(Ti2,ECN2,xout)
lines(Probe2$y~Probe2$x)
detach(Pos2)
###########send script up to this line#############
# probe3
names(Pos3)=c("Ti3","Pro3","ECo3","ECN3")
attach(Pos3)
plot( ECN3~Ti3)
Probe3=approx(Ti3,ECN3,xout)
lines(Probe3$y~Probe3$x)
detach(Pos3)
###########send script up to this line#############
# probe4
names(Pos4)=c("Ti4","Pro4","ECo4","ECN4")
attach(Pos4)
plot( ECN4~Ti4)
Probe4=approx(Ti4,ECN4,xout)
lines(Probe4$y~Probe4$x)
detach(Pos4)
###########send script up to this line#############
# probe5
names(Pos5)=c("Ti5","Pro5","ECo5","ECN5")
attach(Pos5)
plot( ECN5~Ti5)
Probe5=approx(Ti5,ECN5,xout)
lines(Probe5$y~Probe5$x)
detach(Pos5)
###########send script up to this line#############
# probe6
```

```
names(Pos6)=c("Ti6","Pro6","ECo6","ECN6")
attach(Pos6)
plot( ECN6~Ti6)
Probe6=approx(Ti6,ECN6,xout)
lines(Probe6$y~Probe6$x)
detach(Pos6)
###########send script up to this line#############
# make new data-frame and attach
# change Time to seconds ; was days
Ts= Time*86400
BTCdata=cbind(Ts,Probe1$y,Probe2$y,Probe3$y,Probe4$y,Probe5$y,Probe6$y)
BTCdata= as.data.frame(BTCdata)
names(BTCdata)=c("Ts","EC1","EC2","EC3","EC4","EC5","EC6")
attach(BTCdata)
plot(EC1~Ts)
lines(EC2~Ts, col= "BLUE")
lines(EC3~Ts, col= "RED")
lines(EC4~Ts, col= "GREEN")
lines(EC5~Ts, col= "YELLOW")
lines(EC6~Ts, col= "PINK")
###########send script up to this line##############
# Analysis can start (all in SI-units from here one)
# Example of parameter estimation between sensor 4 and 5
# Next three lines need to be adjusted according to the case
Input= EC4
Response= EC5
RR=1      # dimensionless (Retardation factors)
VV= 0.15/0.10/0.10/3.14/1000/60/60/0.43; VV # m/s (pore water velocity)
DD= VV*0.01; DD    # m*m/s (Dispersion coefficient) check units
xx= 0.3
# Beware not all distances between probes are the same according to experimental setup
nLenLog=length(Response) ;nLenLog
Deltat=round( (Ts[5]-Ts[4]),0); Deltat # in seconds
# Analytical solutions for response and BTC of the CDE (one region -equilibrium )
# Test values; initial guesses before optimization
# for efficiency reasons it is good to limit the length of the useful system memory
LenMem= 250      # no of time steps for i-r; change if necessary
dti= Deltat
Pe= VV*xx/DD;Pe
tvec=seq(dti,dti*LenMem,by=dti)
# Auxiliary functions
# Wakao Kaguei
## mean residence time
tou=xx/VV ; tou
## Mass dispersion number
Nmd=DD/(VV*xx) ;Nmd
Wakao = function ( VV, DD, tt, RR=1, x=xx)
# Wakao function for response
# see Mojid et al. (2004)
{ Nmd=DD/(VV*xx)
   tou=xx/VV
   Wak =0
if ( tt>0 )    {
part1 = exp( - (1-tt/(tou*RR) ) ^2/(4*Nmd*tt/(tou*RR)) )
part2 = 2*tou*RR*sqrt(pi*Nmd*(tt/(tou*RR)^3) )
  Wak = part1/part2
}
Wak
}
# Wak = Wakao-Kaguei Response Function
respWak = array (LenMem)
for(i in 1:LenMem) {respWak[i]=Wakao( VV, DD, tvec[i]-dti/2)}
  sum(respWak)
respWak=respWak/sum(respWak) ; sum(respWak) # it has to be equal to 1
plot(respWak~tvec,col="blue")
###########send script up to this line###############
#convolution summation
```

```
RespCalc= array(1:nLenLog)
#
respF=respWak
for (ii in 1 : nLenLog) {
RespCalc[ii] = 0 ;
for (iii in 1 : ii) RespCalc[ii]=RespCalc[ii]
   + Input[iii]*ifelse (is.na(respF[ii-iii+1 ]),0,respF[ii-iii+1 ]) }
plot(Input~Ts,pch='+',col='red',xlim=c(50000,350000))
points(Response~Ts,pch='X',col='blue')
lines(RespCalc~Ts,col='red')
##########send script up to this line##############
####above showing the relationship between input and response#######
# Wakao Kaguei
# average residence time
      tou=xx/VV ; tou
#    mass dispersion number
      Nmd=DD/(VV*xx) ;Nmd
fModelW=function (x=xpara[1:2]) # initialisation of parameters
  {
VV =x[1]
DD =x[2]
RR=1
# prepare impulse response function
respWak = array (LenMem)
for(i in 1:LenMem) {respWak[i]=Wakao( VV, DD, tvec[i]-dti/2) }
  respF <<-respWak/sum(respWak)
RespCalc= array(1:nLenLog)
for (ii in 1 : nLenLog) {RespCalc[ii] = 0 ;
for (iii in 1 : ii) {RespCalc[ii]=RespCalc[ii] +
     Input[iii]*ifelse (is.na(respF[ii-iii+1 ]),0,respF[ii-iii+1 ]) }}
RespCalc<<-RespCalc
SSE <<- sum( (Response[1:nLenLog] -RespCalc[1:nLenLog])^2)
  }
#
xpar=c    (VV,DD)
fModelW (x=xpar)
# next line can take some longer time ( iteration for inverse modelling)
# if too long      press ESC to interrupt and try with a better choice of
# initial parameters
res1=optim (xpar,fModelW)
res1        # results
RespMean=mean(Response)
SSTO=sum((Response-RespMean)^2);SSTO
SSE1=res1$value
Codet1=1-SSE1/SSTO;Codet1
# position 1
plot(Input~Ts,pch='+',col='red',xlim=c(50000,350000))
points(Response~Ts,pch='X',col='blue')
lines(RespCalc~Ts,col='red')
##
SSR<<- sum( (Response[1:nLenLog])^2)
RMSE = sqrt(SSE/SSR); RMSE
#
```

Appendix 3: Results of the pulse-response BTCs fitting

q = 0.5cm/hr	***q*** = 1.0cm/hr	***q*** = 1.5cm/hr	***q*** = 2.0cm/hr
			
Probe No. 1 to 2	Probe No. 1 to 2	Probe No. 1 to 2	Probe No. 1 to 2
			
Probe No. 2 to 3	Probe No. 2 to 3	Probe No. 2 to 3	Probe No. 2 to 3
			
Probe No. 3 to 4	Probe No. 3 to 4	Probe No. 3 to 4	Probe No. 3 to 4
			
Probe No. 4 to 5	Probe No. 4 to 5	Probe No. 4 to 5	Probe No. 4 to 5
			
Probe No. 5 to 6	Probe No. 5 to 6	Probe No. 5 to 6	Probe No. 5 to 6

Publications list by Chou Po-Yi (2006-2009)*

A. Articles in internationally reviewed journals

Chou, P.Y., Wyseure, G. (2009). Hydrodynamic dispersion characteristics of lateral inflow into a river tested by a laboratory model. *Hydrology and Earth System Sciences*, **13**, 217-228.

Chou, P.Y., Van Nieuwenhuyse, B.H.J. Wyseure, G. (2009). Can temperature be used as a tracer to estimate fluctuating water fluxes in the riverbed? A laboratory study. Submitted to *Hydrological Processes*.

Chou, P.Y., Cuppens A, Wyseure G. (2009). Numerical simulation by HYDRUS 2D/3D of long- and short-term groundwater flux in the hyporheic zone influenced by temperature regimes and changing river stage. In preparation to be submitted to *Ground Water*

B. Papers at international conferences and symposia, published in full in proceedings

Chou, P.Y., Wyseure, G. (2008). Riparian groundwater inflow through the hyporheic zone to the river studied by an indoor experiment and by a numerical model HYDRUS 2D/3D. In: AgEng2008, International Conference on Agricultural Engineering & Industry Exhibition. Crete, Greece, 23-25 July, 2008.

Chou, P.Y., Wyseure, G. (2007). Delineation of the interface between the hyporheic and vadose zone using TDR measurements. In: International Congress on Development, Environment and Natural Resources: Multi-level and Multi-scale Sustainability. Cochabamba, Bolivia, 11-13 July, 2007.

Chou, P.Y., Wyseure, G. (2006). Indoor Simulation of Hyporheic Saturated-Unsaturated Boundary. In: HydroEco2006, International Multidisciplinary Conference on Hydrology and Ecology: The Groundwater/Ecology Connection. Karlovy Vary (Carlsbad), Czech Republic, 11-14 September, 2006.

C. Meeting abstracts, presented at international conferences and symposia, published in proceedings or journals

Chou, P.Y., Wyseure, G. (2007). An innovative experiment for modelling hydraulic connectivity of hyporheic zone. In: European Geosciences Union General Assembly 2007. Vienna, Austria, 15-20 April, 2007.

D. Miscellaneous publications

Chou, P.Y., Wyseure, G. (2008). Lateral inflow into the hyporheic zone tested by a laboratory model. *Hydrology and earth system sciences & discussions*, 5, 1567-1601.

* Contact: poyi.chou@ees.kuleuven.be or poyi.chou@gmail.com